Université d'Ottawa · University of Ottawa

Université d'Ottawa · University of Ottawa

FACULTÉ DES ÉTUDES SUPÉRIEURES
ET POSTDOCTORALES

FACULTY OF GRADUATE AND
POSTDOCTORAL STUDIES

Jinkai WANG
AUTEUR DE LA THÈSE - AUTHOR OF THESIS

M. A. Sc. (Mechanical Engineering)
GRADE - DEGREE

Department of Mechanical Engineering
FACULTÉ, ÉCOLE, DÉPARTEMENT - FACULTY, SCHOOL, DEPARTMENT

TITRE DE LA THÈSE - TITLE OF THE THESIS

Large Eddy Stimulation (2D) of Spatially Developing Mixing Layer Using
Vortex-in-Cell for Flow Field and Filtered Density Function dor Scalar Field

R. Milane
DIRECTEUR DE LA THÈSE - THESIS SUPERVISOR

CO-DIRECTEUR DE LA THÈSE - THESIS CO-SUPERVISOR

EXAMINATEURS DE LA THÈSE - THESIS EXAMINERS

B. Jodoin

E. Matida

J.-M. De Koninck, Ph.D.

LE DOYEN DE LA FACULTÉ DES ÉTUDES
SUPÉRIEURES ET POSTDOCTORALES

DEAN OF THE FACULTY OF GRADUATE
AND POSTDOCTORAL STUDIES

LARGE EDDY SIMULATION (2D) OF SPATIALLY DEVELOPING MIXING LAYER USING VORTEX-IN-CELL FOR FLOW FIELD AND FILTERED DENSITY FUNCTION FOR SCALAR FIELD

Jinkai Wang

A thesis submitted to the Faculty of Graduate and Postdoctoral Studies
in partial fulfilment of the requirements for the degree of

MASTER OF APPLIED SCIENCE
in Mechanical Engineering

Ottawa-Carleton Institute for Mechanical and Aerospace Engineering

University of Ottawa

Ottawa, Canada

Library and
Archives Canada

Published Heritage
Branch

395 Wellington Street
Ottawa ON K1A 0N4
Canada

Bibliothèque et
Archives Canada

Direction du
Patrimoine de l'édition

395, rue Wellington
Ottawa ON K1A 0N4
Canada

Your file Votre référence
ISBN: 0-494-01631-0
Our file Notre référence
ISBN: 0-494-01631-0

NOTICE:
The author has granted a non-exclusive license allowing Library and Archives Canada to reproduce, publish, archive, preserve, conserve, communicate to the public by telecommunication or on the Internet, loan, distribute and sell theses worldwide, for commercial or non-commercial purposes, in microform, paper, electronic and/or any other formats.

The author retains copyright ownership and moral rights in this thesis. Neither the thesis nor substantial extracts from it may be printed or otherwise reproduced without the author's permission.

AVIS:
L'auteur a accordé une licence non exclusive permettant à la Bibliothèque et Archives Canada de reproduire, publier, archiver, sauvegarder, conserver, transmettre au public par télécommunication ou par l'Internet, prêter, distribuer et vendre des thèses partout dans le monde, à des fins commerciales ou autres, sur support microforme, papier, électronique et/ou autres formats.

L'auteur conserve la propriété du droit d'auteur et des droits moraux qui protège cette thèse. Ni la thèse ni des extraits substantiels de celle-ci ne doivent être imprimés ou autrement reproduits sans son autorisation.

In compliance with the Canadian Privacy Act some supporting forms may have been removed from this thesis.

While these forms may be included in the document page count, their removal does not represent any loss of content from the thesis.

Conformément à la loi canadienne sur la protection de la vie privée, quelques formulaires secondaires ont été enlevés de cette thèse.

Bien que ces formulaires aient inclus dans la pagination, il n'y aura aucun contenu manquant.

Canada

Abstract

A Large Eddy Simulation (LES) based on filtered vorticity transport equation formulated using diffusion-velocity method and discrete vortex method has been coupled to filtered density function (FDF) equation for scalar, to predict the velocity and passive scalar field of a spatially developing mixing layer. In the vortex method, the vorticity-based and eddy-viscosity type subgrid scale (SGS) model simulating the enstrophy transfer between the large and small scale appears as a convective term in the diffusion-velocity formulation. The methodology has been tested on a spatially growing mixing layer using the two-dimensional vortex-in-cell method with both Smagorinsky and Dynamic Eddy Viscosity subgrid scale models for an anisotropic flow. The effects on the vorticity contours, momentum thickness, streamwise mean velocity profiles, root-mean-square velocity and vorticity fluctuations and negative cross-stream correlation are discussed. Comparison is made with experimental and numerical works where diffusion is simulated using random walk.

The transport equation for FDF is solved using the Lagrangian Monte Carlo method scheme. The unsolved subgrid scale convective term in FDF equation is modeled using the conventional gradient diffusion model for an anisotropic flow. The subgrid scalar mixing term is modelled using the Modified Curl model. The characteristics of the passive scalar, i.e., mean concentration, root-mean-square concentration fluctuation profiles and probability density function (PDF) are presented and compared with previous numerical and experimental works. The sensitivity of results to SGS model, Schmidt number, constant in mixing frequency and inlet boundary condition is discussed.

Acknowledgements

I would like to express my appreciation to my supervisor, Dr. Roger Milane, for his guidance, ideas, experience and encouragement that he supplied throughout my graduate studies.

I wish to express my gratitude to the academic members and staff of the department of mechanical engineering, especially Mrs. Solange Lamontagne for her help. I would also like to thank my friends for their suggestions and encouragement.

Finally, I would like to thank my family for their continual support and encouragement and devote the thesis to them.

Table of Contents

Chapter 1. Introduction

Chapter 2. Literature Survey

Chapter 3. Governing Equations

Chapter 4. Vortex-In-Cell

Chapter 5. Large Scale Scalar Field

Chapter 6. Flow Field

Chapter 7. Scalar Field

Chapter 8. Summary and Recommendations

List of Figures

List of Tables

Nomenclature

C	Concentration
C_U, C_L	Concentration of the free stream above and below the splitter plate
C_c	Average concentration
C_r	Constant in SGS model
d	Distance between point vortices
L	Length of the computational domain
M_x, M_y	Subgrid mass fluxes
n	Number of particles
NP	Number of particles in a box centered at node
N_v	Number of vortices
PDF	Probability density function
r	Velocity ratio
Re	Reynolds number
S_{ij}	Modulus of the strain rate
S_{cT}	Turbulent Schmidt number
t	Time
$\mathbf{u}$	Velocity vector
u,v	Cartesian velocity components

$\overline{U}, \overline{V}$	Streamwise and lateral filtered velocities
u', v'	Turbulent velocity fluctuations
U_n, V_n	Velocity components of the vortices
U	Mean velocity in stream-wise direction
U_H, U_L	Fast upper and slow lower free stream velocities
U_c	Arithmetic average of the free stream velocities
x_v, x_c	Virtual origins for velocity and concentration
x, y	Cartesian coordinates
x_n, y_n	Coordinates of the vortices
y_0	Y-coordinate of the centerline
Δ	Physical filter size
Δ'	Test filter size
Δt	Time step
$\Delta x, \Delta y$	Filter sizes in x- and y-direction

Greek Symbols

α	Random variable for Modified Curl model
β	Coefficient for Modified Curl model
Γ	Circulation
Γ_n	Circulation of the vortex element number n
Γ_x, Γ_y	Components of circulation vector of vortex elements

$\mathit{\Gamma}_{Tx}$, $\mathit{\Gamma}_{Ty}$	Components of diffusion coefficient
γ_T	Scalar diffusion
δ_x, δ_y	Grid sizes of x-direction and y-direction
$\delta_{laminar}$	Laminar boundary layer thickness
η_v	Similarity variable for velocity
η_c	Similarity variable for concentration
μ	Viscosity
ν	Kinematic viscosity
ν_T	Eddy viscosity, turbulent diffusion
ξ	Mixture fraction, or normalized concentration
σ	Core radius
ρ	Density
ϕ	Mixture fraction
$\overline{\phi}$	Mass fraction
ψ	Stream function
ω_f	Mixing frequency
ω	Vorticity vector
ω_x,ω_y	Components of vorticity vector
$\overline{\omega}_\alpha$	Filtered reaction rate (large scale)
C_ϕ	Mixing frequency constant
χ	Trajectories of vortices

ξ_{rms}	Root-mean-square of concentration
$\bar{\xi}$	Mean concentration

Chapter 1

Introduction

1.1 Mixing Layer

Turbulent flows are highly irregular fluid motions in which random motions of parts are superimposed on a mean stream whose detailed configuration is neither reproducible from one experiment to the other nor predictable theoretically, but whose statistical dynamic properties are significant. Turbulence stirs fluids across many scales simultaneously and accelerates fluid mixing which occurs much faster than simple molecular diffusion. So turbulent flows are very efficient at mixing fluids in which the chemical mixing or heat transfer is needed. In engineering turbulence it is important to investigate flow around car, aircraft and ship, flow in a propulsion engine and the atmosphere.

In the view of the energy cascade, the turbulence can be considered to be composed of eddies of different sizes, loosely termed as vortices. The forces driving the flow produce the largest eddies which move laterally or longitudinally in the flow field. With these motions, a large eddy changes its shape, rotates or breaks into two or smaller eddies which continue to break down into yet smaller eddies, and so on. The cascade transfer energy from large eddies to successively smaller and smaller eddies is terminated by viscosity. In real fluids the action of the viscosity causes the dissipation of the kinetic energy and the turbulent motion will decay without an external source.

The plane mixing layer is one of the simplest conceivable free shear flows to maintain turbulence. Two initially separated parallel flows come into contact and mix. Due to their apparent simplicity, the fundamentals of plane mixing layers have been the subject of extensive theoretical and experimental investigations. In general, information about the characteristics of turbulent flows is obtained from experiments because of the complexity of turbulent flows. Recently due to the development in computer technology, it is feasible to numerically simulate turbulent flows by solving the governing equations of turbulent flows, i.e., conservation of mass, momentum and energy with various methods of computing turbulent flows has been developed and will be briefly introduced in the following.

1.2 Direct Numerical Simulation

Direct numerical simulation (DNS) solves the Navier-Stokes equations without averaging or approximation and resolves all the scales of motion. The scales include everything from the large energy-containing or integral scales to the smallest scales which are responsible for the dissipation of turbulence kinetic energy. DNS requires that the solution domain will be large enough to encompass all the large scale motions containing energy, while the computational grid must be fine enough to resolve the smallest dissipative scales. In homogeneous turbulence, the computer requirements increase rapidly with increasing Reynolds number (*Re*), because the ratio of a solution domain to a computational grid is proportional to $Re^{3/4}$ and the computational cost increases approximately to Re^3.

Due to the limitation of computational resource, DNS can be carried out only at relatively low or moderate Reynolds numbers.

1.3 Reynolds Averaged Navier-Stokes

Reynolds Averaged Navier-Stokes (RANS) are based on averaging the Navier-Stokes equations over the scales of turbulent fluctuations. The nonlinear terms in the Navier-Stokes equations give rise to the Reynolds stress term in RANS, but the set of equations can never be closed without modelling the Reynolds stress term. Empirical models, i.e., eddy viscosity model and k-ϵ model, have been constructed to solve the problem. Because all turbulent scales are modelled and velocity fluctuations are not calculated, the Reynolds Averaged Navier-Stokes (RANS) method is one of the most affordable methods of computing turbulent flows. The major weakness of RANS is its poor or uncertain accuracy by averaging out all of the unsteadiness of turbulence.

1.4 Large Eddy Simulation

Large Eddy Simulation (LES) occupies an intermediate position between DNS and RANS. Large eddy simulation can be defined as the simulation of a turbulent flow in which the unsteady large-scale motions are resolved explicitly while the small-scale motions are represented approximately by a model (Smagorinsky, 1963; Lilly, 1967).

In LES, the Navier-Stokes equations are filtered, so that the terms representing the large scale structures are separated from those representing the effect of the small scales on the large one (Leonard, 1974). In other words, the large eddy motions of the resolved scales are simulated by solving the filtered Navier-Stokes equations. Because the unsteady large-scale motions are resolved explicitly, LES is more accurate and reliable than RANS in which the unsteadiness of the large scale is significant. In LES, the effect of the small scales or subgrid scale (SGS) must be modelled so that the computational cost of explicitly resolving the small-scale motion can be saved comparing with DNS. That means that LES allows to compute flows at much higher Reynolds numbers than those in DNS. The core of LES is to choose the appropriate subgrid scale terms to match the particular flow and numerical scheme, which is also known as subgrid scale modelling.

1.5 Vortex Methods

Vortex methods offer an alternative numerical solutions to finite difference methods for high resolution of the Navier-Stokes equations. Vortex methods are based on the discretization of the vorticity field into a finite number of vortex points or blobs which are tagged and traced at each time(Lagrangian approach). Rosenhead (1931) introduced the point vortex method to trace the path line of fluid particles with concentrated vorticity (vortex points or blobs) and at each time-step the vorticity transport equation control the change of vorticity distribution within a blob. The point vortex method was used by Abernathy and Kronauer(1962) to simulate vortex streets. Chorin(1973) solved the two-dimensional problem using vortex blobs. Chorin's method was used by Ashurst(1979) to a two-dimensional mixing layer and there was good agreement between simulation results of the downstream evolution of the large scale structures and experiment of Brown and Roshko(1974)

In order to reduce the computational time of the full Lagrangian method, Vortex-in-cell(VIC) or cloud-in-cell(CIC) method has been developed to solve the vorticity equation. In this method, Eulerian Scheme is used to calculate the velocity field by solving Poisson's equation and the Lagrangian scheme is used to track the vortices obtained from the Laplacian of the stream function. Baker(1979), Aref and Siggia(1980) had applied the VIC method for their research.

The direct numerical simulation (DNS) using vortex methods can be found in Leonard (1980), Inoue and Leonard(1987). The Reynolds Averaged Navier-Stokes (RANS) simulation with vortex methods can be found in Baig and Milane(2004). Examples of Large eddy simulation (LES) using vortex methods are found in Lin and Pratt (1987), Milane and Nourazar(1995, 1997) and Mansfield *et al.*(1998).

1.6 Probability Density Function Method

One method used to solve the problem of turbulent flows is the probability density function method (PDF) and has been widely used for many years. The conservation equation for the joint PDF of velocity was derived, modelled and solved by Lundgren(1969) and Bray(1973). Furthermore, Pope (1976) and Dopazo and O'Brien (1976) derived, modelled and solved the transport equation for the composition joint PDF. In contrast with conventional turbulence models in which the mean reaction rate can be determined only when the reaction rate is linear or when it is either very fast or slow compared with the turbulent time scales, this equation treated the complicated reactions without an approximation. The modelled composition joint PDF equation overcomes the closure problem associated with nonlinear reaction rates. The PDF equations can be solved by either Eulerian or Lagrangian methods. Because of a high dimensionality, Pope (1980) devised a Monte Carlo method to solve the composition joint PDF equation. Monte Carlo methods provide a feasible alternative mean of obtaining numerical solutions for problems with large number of independent variables. As compared to conventional turbulence models, the PDF methods derive their advantage from their more complete representation of the turbulent flow field (Pope, 1985).

Chapter 2

Literature Survey

2.1 Large Eddy Simulation-Vortex Method

In recent works, the vortex method in a pure Lagrangian frame (particle representation) has been developed in the context of large eddy simulation (LES) using the eddy viscosity subgrid scale (SGS) model (Mansfield *et al.*, 1998). By filtering the vorticity transport equation and modelling the subgrid scale (SGS) velocity and vorticity fluctuations, a Lagrangian large eddy simulation was developed. Both the Smagorinsky and Dynamic Eddy Viscosity SGS models were implemented and the constants were obtained specifically for the vorticity equation. Comparison of the results obtained from LES of a homogeneous and isotropic turbulence flow field with those obtained by filtering DNS results indicated good agreement.

In the particle representation, the effect of eddy viscosity model was implemented by modifying the strength of the particles using the integral approximation for the solution of the diffusion equation (Degond and Mas-Gallic, 1989), also denoted as the particle strength exchange (PSE). In other development, Milane and Nourazar(1995, 1997) used the core-spreading technique to simulate the diffusion equation in the context of LES where the eddy viscosity SGS vorticity model (Mansour *et al.*, 1979) and the SGS turbulent kinetic energy model (Bardina, 1980) were tested, respectively. The core-spreading technique is valid in the limit of vanishing viscosity (Greengard *et al.*, 1985; Cottet and Koumoutsakos, 2000). Cottet (1996) presented subgrid scale model based on a rigorous analysis of truncation error of the filtered vorticity equation. The author developed a scheme based on the PSE method for small scale contribution. The method was tested by removing all the back scatters produced by the flow strain.

2.2 Diffusion-Velocity Method

The diffusion-velocity method is an alternative way for simulating the diffusion equation and can be extended to an eddy-viscosity-based LES formulation. Originally, Ogami and Akamatsu (1991) introduced the method as an alternative to the random walk solution of the diffusion equation in order to extend the solution to Reynolds number values below the lower limit of applicability of the random walk. In diffusion-velocity method, the viscous diffusion is produced by the vortices' movement induced by the diffusion velocities which can be regarded as the summary of the contribution from each vortex and are added to the velocities at which the vortices are carried following the procedure of vortex method. Ogami and Akamatsu (1991) suggested that the diffusion velocity method can solve problems such as separation and reattachment of the boundary layer without the boundary layer theory. The results for one-dimensional diffusion equation are found to be in close agreement with analytical solution.

For an incompressible Newtonian fluid, Clarke and Tutty(1994) applied the discrete vortex method to solve the two-dimensional Navier-Stokes equations in which the viscous effects are modelled using a combination of the random walk and diffusion velocity techniques with few arbitrary parameters. The discrete vortex method can produce worthwhile solutions for the two-dimensional Navier-Stokes equations but the diffusion is limited to regions where the circulation of a single vortex is much larger than a region of low vorticity. The results were validated in the flow translating circular cylinder and rotating translating circular cylinder. In the context of diffusion velocity method, Ogami(1999) introduced a remeshing technique in the region where vortices are sparse and do not overlap as encountered by Clarke and Tutty(1994).

Lacombe and Mas-Gallic(1999) proved the existence and uniqueness result from diffusion velocity method by solving the one-dimensional, two-dimensional and three-dimensional Navier-Stokes equations. Recently, Beaudoin *et al.*(2003), using the diffusion-velocity method as an alternative to PSE method, concluded that for anisotropic diffusion problems it is by far easier to derive than that of the PSE method. The present study is concerned with a LES study using the diffusion-velocity method. The feasibility of the method will be illustrated using the two-dimensional mixed Lagrangian-Eulerian vortex-in-cell(VIC) method applied to a spatially growing mixing layer and using both the Smagorinsky and Dynamic Eddy Viscosity SGS models. The VIC method is used because it combines the best features of Lagrangian and Eulerian methods, i.e., the numerical dissipation is reduced relative to the pure Eulerian method (Sarpkaya, 1994; Ghoneim and Givi, 1987; Leonard, 1980; Chorin and Marsden, 1979) and the computational time is reduced relative to the Lagrangian method. In the VIC method, an Eulerian scheme is used to calculate the velocity field and a Lagrangian scheme is used to track the vortices. The vortices that represent fluid particles with concentrated vorticity (vortex points or blobs) are tagged and traced in time. As time proceeds, the change of vorticity distribution within a blob is governed by the vorticity transport equation. The justification for this method stem from the fact that, in turbulent flows, vorticity is often very large in thin thread like fluid, while the remaining fluid is virtual without vorticity. Therefore, the vorticity can be lumped into concentrated vortex blobs around which the fluid spins.

2.3 Large Eddy Simulation-Filtered Density Function method

Recently Gao and O'Brien(1993) first introduced the transport equation for the large eddy PDF for a chemically reacting flow. Colucci *et al.*(1998) developed LES based on PDF, termed the filtered density function (FDF) for a chemically reacting turbulent flow. The FDF method is developed for isothermal, constant density, reacting flows with a simple kinetics scheme. The effect of chemical reactions appears in a closed form in the transport equation for the FDF and the influences of subgrid scale(SGS) mixing and convection is modeled. The FDF transport equation is solved using Langrangian Monte Carlo Scheme together with the Navier-Stokes equation for flow field. The methodology is assessed using a temporally developing mixing layer and a spatially developing planar jet under both non-reacting and reacting conditions. In non-reacting flows, authors proved that the result is similar between the Monte Carlo solution of the FDF and finite difference LES, and in reacting flows with the absence of a closure for the SGS scalar fluctuations, the result of FDF is in agreement with that of filtered DNS (*a priori test*).

Jaberi *et al.* (1999) developed a methodology named "Filtered Mass Density Function" (FMDF) by extending filtered density function (FDF)(Colucci *et al.*, 1998) to variable density and reacting flows at low Mach numbers. In FMDF a transport equation is developed by modelling SGS mixing via the linear mean-square estimation (LMSE) and the influence of SGS convection flux via the gradient diffusion model. Then the modelled FMDF transport equation is solved by a Lagrangian Monte Carlo scheme where the solutions are obtained using the equivalent stochastic differential equations(SDEs).

In reacting shear flows with non-premixed reactants, the FMDF results show closer agreement with the data of experimental measurements and direct numerical simulation (DNS). In non-reacting flows, without the influence of the SGS fluctuations on the reaction rate, the FMDF results are closer agreement with the DNS results of two-dimensional temporally developing mixing layers, spatially developing jet and three-dimensional temporally developing mixing layers.

Zhou and Pereira (2000) implemented FDF developed by Colucci *et al.*(1998) to investigate the two-dimensional, gas phase, spatially developing, reacting and non-reacting, constant-density, plane mixing layer in a flow regime prior to the mixing transition similar to the experiment of Masutani and Bowman(1986)(M&B). The FDF results showed satisfactory agreement with experimental measurements.

2.4 Objectives

The objective of this study is concerned to apply a large eddy simulation(LES) scheme based on the filtered vorticity transport equation formulated using the diffusion-velocity method in conjunction with FDF transport equation for scalar to predict the velocity and passive scalar field. The methodology will be tested on a spatially developing mixing layer. Both the Smagorinsky and Dynamic Eddy Viscosity SGS models are used to model the effects of subgrid scale fluctuations. For the flow field, the mean velocity, Reynolds stress, turbulent diffusivity, mixing frequency and momentum thickness are predicted.

For scalar field, the filtered density function (FDF) is solved using a Lagrangian Monte-Carlo scheme. The diffusion of the unresolved scalar fluctuations is modeled following the eddy diffusivity concept and the mixing of unresolved scalar fluctuations is modeled using the Modified Curl model.

Comparison is made with two-dimensional experiment of Masutani and Bowman(1986) and numerical simulation results of Zhou and Pereira(2000). The mean scalar concentrations, root-mean-square (rms) scalar fluctuations and probability density function(PDF) of scalar are presented. The effect of mixing frequency, Schmidt number, constant in mixing frequency and inlet boundary conditions on scalar field development is discussed.

Chapter 3

Governing Equations

3.1 Vorticity Equation

The continuity and vorticity transport equations for an incompressible and viscous fluid flow are respectively,

$$\frac{\partial u_i}{\partial x_i}=0 \tag{1}$$

$$\frac{\partial \omega_i}{\partial t} + u_j\frac{\partial \omega_i}{\partial x_j} = \omega_j \frac{\partial u_i}{\partial x_j} + \nu\frac{\partial^2 \omega_i}{\partial x_j \partial x_j} \tag{2}$$

where ω_i represents the component of the vorticity vector **ω**, u_i and u_j represent the components of the velocity vector **u**, and ν is the kinematic viscosity. The left-hand side (L.H.S.) of Eq.(2) includes the rate of change of vorticity in time and the rate of change due to convection respectively. On the right-hand side (R.H.S.), the first term is the vortex stretching term and the second term is the viscous diffusion.

For a two-dimensional flow parallel to (x,y)-plane, the velocity vector is **u**=**u**(x,y,t), the vorticity vector **ω** is reduced to one component in the z-direction (ω_z) perpendicular to the (x,y)-plane, and the stretching term vanishes. Therefore Eq.(2) reduces to

$$\frac{\partial \omega_z}{\partial t} + u_j \frac{\partial \omega_z}{\partial x_j} = \nu \frac{\partial^2 \omega_z}{\partial x_j \partial x_j} \tag{3}$$

A different form of vorticity equation can be written if the continuity Eq.(1) is combined with the vorticity Eq.(3) assuming constant viscosity as

$$\frac{\partial \omega_i}{\partial t} + \frac{\partial u_j \omega_i}{\partial x_j} = \frac{\partial}{\partial x_j}\left\{\nu \frac{\partial \omega_i}{\partial x_j}\right\} \tag{4a}$$

which can also be rewritten as

$$\frac{\partial \omega_i}{\partial t} + \frac{\partial}{\partial x_j}\left\{u_j \omega_i - \nu \frac{\partial \omega_i}{\partial x_j}\right\} = 0 \tag{4b}$$

Eq.(4b) is identical to the equation used by Ogami and Akamatsu(1991) in the development of the diffusion-velocity method.

3.2 Filtered Vorticity Equations

For any time- and space-dependent variable $\phi(x,y,t)$, the spatial filtered value $\overline{\phi}$ is

$$\overline{\phi}(x,y,t) = \int \int \phi(\zeta,\eta,t)\, G(\,x-\zeta\,,\, y-\eta\,)\, d\zeta\, d\eta \tag{5}$$

where G(x,y) is the spatial filter shape. For a two-dimensional flow, the velocity and vorticity fields are decomposed in the filtered field (overline), and the sub-grid scale field (superscript $'$) as:

$$\omega_x = \omega'_x(x,y;t)$$

$$\omega_y = \omega'_y(x,y;t)$$

$$\omega_z = \bar{\omega}_z(x,y;t) + \omega'_z(x,y;t)$$

$$U = \bar{U}(x,y;t) + u'(x,y;t)$$

$$V = \bar{V}(x,y;t) + v'(x,y;t)$$

$$w = w'(x,y;t)$$

In the above decompositions, $\bar{w} = \bar{\omega}_x = \bar{\omega}_y = 0$ are nil in the two-dimensional formulation. The filtered continuity Eq.(1) and the filtered transport equation [Eq.(3)] for the spanwise component $\bar{\omega}_z$ are (Cottet, 1996)

$$\frac{\partial \bar{U}}{\partial x} + \frac{\partial \bar{V}}{\partial y} = 0 \tag{6}$$

$$\frac{\partial \bar{\omega}_z}{\partial t} + \bar{U}\frac{\partial \bar{\omega}_z}{\partial x} + \bar{V}\frac{\partial \bar{\omega}_z}{\partial y} = \nu\frac{\partial^2 \bar{\omega}_z}{\partial x^2} + \nu\frac{\partial^2 \bar{\omega}_z}{\partial y^2} - \frac{\partial Y}{\partial x} - \frac{\partial Z}{\partial y} \tag{7}$$

where the subgrid scale terms being responsible for the transfer of enstrophy between large and small scales are

$$\begin{gathered} \frac{\partial Y}{\partial x} = \frac{\partial}{\partial x}\left(\overline{U\omega_z} - \bar{U}\,\bar{\omega}_z \right) \\ and \\ \frac{\partial Z}{\partial y} = \frac{\partial}{\partial y}\left(\overline{V\omega_z} - \bar{V}\,\bar{\omega}_z \right) \end{gathered} \tag{8}$$

Another form for Eq.(7) can be obtained by using the continuity Eq.(6) and rearranging the SGS terms

$$\frac{\partial \bar{\omega}_z}{\partial t} + \frac{\partial\left\{ \bar{U} - \frac{Y}{\bar{\omega}_z}\right\}\bar{\omega}_z}{\partial x} + \frac{\partial\left\{ \bar{V} - \frac{Z}{\bar{\omega}_z}\right\}\bar{\omega}_z}{\partial y} = \nu\frac{\partial^2 \bar{\omega}_z}{\partial x^2} + \nu\frac{\partial^2 \bar{\omega}_z}{\partial y^2} \tag{9}$$

In Eq.(9), the SGS terms are treated as convective terms. This is similar to the procedure followed by Ogami and Akamatsu(1991) in the development of the diffusion-velocity method. The third form for

Eq.(7) can be obtained by inserting the diffusion terms in the convective terms as

$$\frac{\partial \bar{\omega}_z}{\partial t}+\frac{\partial \left\{ \bar{U}+\frac{Y}{\bar{\omega}_z}-\frac{\nu}{\bar{\omega}_z}\frac{\partial \bar{\omega}_z}{\partial x}\right\} \bar{\omega}_z}{\partial x}+\frac{\partial \left\{ \bar{V}+\frac{Z}{\bar{\omega}_z}-\frac{\nu}{\bar{\omega}_z}\frac{\partial \bar{\omega}_z}{\partial y}\right\} \bar{\omega}_z}{\partial y}=0 \tag{10}$$

Eq.(10) is a convective equation and is similar to the equation solved in the diffusion-velocity method.

3.2.1 SGS Eddy Viscosity Model

The two groups of term (*-Y*) and (*-Z*) are the SGS vorticity stress. Their net effect is to transfer energy from the large scales to the small scales. By analogy with the SGS Reynolds stress in the filtered momentum, the SGS vorticity stress are modeled using the eddy viscosity concept for an anisotropic flow as $-Y = \nu_{Tx} \partial\bar{\omega}_z/\partial x$ and $-Z = \nu_{Ty} \partial\bar{\omega}_z/\partial y$. Substituting into Eq.(7), developing and rearranging

$$\frac{\partial \overline{\omega_z}}{\partial t}+\left(\bar{U}-\frac{\partial \nu_{Tx}}{\partial x}\right)\frac{\partial \overline{\omega_z}}{\partial x}+\left(\bar{V}-\frac{\partial \nu_{Ty}}{\partial y}\right)\frac{\partial \overline{\omega_z}}{\partial y}=(\nu+\nu_{Tx})\frac{\partial^2 \overline{\omega_z}}{\partial x^2}+(\nu+\nu_{Ty})\frac{\partial^2 \overline{\omega_z}}{\partial y^2} \tag{11}$$

The convective terms in Eq.(11) may be rearranged using continuity Eq.(6) and the following expression

$$-\frac{\partial \nu_{Ty}}{\partial y}\frac{\partial \overline{\omega_z}}{\partial y} = -\frac{\partial}{\partial y}\left\{\overline{\omega_z}\frac{\partial \nu_{Ty}}{\partial y}\right\}+\overline{\omega_z}\frac{\partial^2 \nu_{Ty}}{\partial y^2}$$

which will result in

$$\frac{\partial \bar{\omega}_z}{\partial t}+\frac{\partial \left\{ \bar{U}-\frac{\partial \nu_{Tx}}{\partial x}\right\} \bar{\omega}_z}{\partial x}+\frac{\partial \left\{ \bar{V}-\frac{\partial \nu_{Ty}}{\partial y}\right\} \bar{\omega}_z}{\partial y}=$$

$$(\nu+\nu_{Tx})\frac{\partial^2 \overline{\omega_z}}{\partial x^2}+(\nu+\nu_{Ty})\frac{\partial^2 \overline{\omega_z}}{\partial y^2}-\overline{\omega_z}\frac{\partial^2 \nu_{Tx}}{\partial x^2}-\overline{\omega_z}\frac{\partial^2 \nu_{Ty}}{\partial y^2} \tag{12}$$

Eq.(12) should be used rather than Eq.(11) because of the adequate form of convective terms. In order to treat the convective terms properly (within the context of vortex method), the convective terms shall be modified. By doing so, source term (the last two terms on R.H.S. of Eq.(12)), disappeared in the following equations.

Another form can be obtained by substituting the SGS terms, $-Y = \nu_{Tx}\partial\bar{\omega}_z/\partial x$ and $-Z = \nu_{Ty}\partial\bar{\omega}_z/\partial y$, into Eq.(9)

$$\frac{\partial\bar{\omega}_z}{\partial t}+\frac{\partial\left\{\bar{U}-\frac{\nu_{Tx}}{\bar{\omega}_z}\frac{\partial\bar{\omega}_z}{\partial x}\right\}\bar{\omega}_z}{\partial x}+\frac{\partial\left\{\bar{V}-\frac{\nu_{Ty}}{\bar{\omega}_z}\frac{\partial\bar{\omega}_z}{\partial y}\right\}\bar{\omega}_z}{\partial y}=\nu\frac{\partial^2\bar{\omega}_z}{\partial x^2}+\nu\frac{\partial^2\bar{\omega}_z}{\partial y^2} \tag{13}$$

Also Eq.(13) may be rearranged by moving the diffusion terms to the L.H.S. as

$$\frac{\partial\bar{\omega}_z}{\partial t}+\frac{\partial\left\{\bar{U}-\frac{(\nu+\nu_{Tx})}{\bar{\omega}_z}\frac{\partial\bar{\omega}_z}{\partial x}\right\}\bar{\omega}_z}{\partial x}+\frac{\partial\left\{\bar{V}-\frac{(\nu+\nu_{Ty})}{\bar{\omega}_z}\frac{\partial\bar{\omega}_z}{\partial y}\right\}\bar{\omega}_z}{\partial y}=0 \tag{14}$$

Eqs.(12), (13) and (14) are equivalent. However the equation forms are different because the forms of the terms are different. Eq.(12) contains convection, diffusion and source terms. Eq.(13) contains convection and diffusion terms, and Eq.(14) contains only convection terms. Therefore the solution techniques are different and the results may be different. This aspect will not be investigated in this study and Eq.(14) is chosen as the governing equation for the study. The terms added to the convective velocity are called diffusion velocities in analogy with the derivation in Ogami and Akamatsu(1991).

Another equation used in the VIC method is derived using the definition of vorticity vector,

$$\bar{\omega}_z=\frac{\partial\bar{V}}{\partial x}-\frac{\partial\bar{U}}{\partial y} \tag{15}$$

Since the divergence of the velocity is zero because of the continuity equation Eq.(6),i.e.

$$\frac{\partial\bar{U}}{\partial x}+\frac{\partial\bar{V}}{\partial y}=0$$

therefore the components of the velocity **u** can be expressed as the gradients of the stream function ψ,

$$\bar{U} = \frac{\partial \psi}{\partial y} \quad , \quad \bar{V} = -\frac{\partial \psi}{\partial x} \tag{16}$$

Combining Eqs.(15) and (16), Poisson's equation is obtained as,

$$\nabla^2 \psi = -\bar{\omega}_z \tag{17}$$

The solution obtained by the Poisson's equation [Eq.(17)] is equivalent to the solution obtained by the convective part of Eqs.(12), (13) and (14), i.e. the contribution of ***u***= ($\bar{U}$,$\bar{V}$) in the vorticity transport equation. The solution of Poisson's equation is given by the Green's function or the Biot-Savart (Batchelor, 1967).

3.2.2 Subgrid Scale Models

The constant in SGS model is a function of the type of governing equations (vorticity or momentum) and of SGS model used. Mansfield *et al.* (1998) obtained the constant in the Smagorinsky model and also derived the expression for the constant in the dynamic case. In this study, both the constant for Smagorinsky SGS model and the expression of the constant for dynamic SGS model have been adopted. In the Smagorinsky SGS model, the eddy viscosities ν_{Tx} and ν_{Ty} in x- and y-direction, respectively, are expressed for an anisotropic flow as (Sagaut 2002, p.168).

$$\begin{gathered} \nu_{Tx} = C_r^2 (\Delta^3)^{2/9} \Delta_x^{4/3} (2 S_{ij} S_{ij})^{1/2} \\ \textit{and} \\ \nu_{Ty} = C_r^2 (\Delta^3)^{2/9} \Delta_y^{4/3} (2 S_{ij} S_{ij})^{1/2} \end{gathered} \tag{18}$$

where Δ_x and Δ_y are the filter sizes in x- and y-direction, respectively, with $\Delta = (\Delta_x \Delta_y)^{1/2}$ or $\Delta = \max(\Delta_x, \Delta_y)$ (Sagaut, 2002 p.165), and the modulus of the strain rate for 2D flow $|\bar{S}| \equiv (2 S_{ij} S_{ij})^{1/2}$ is

$$(2S_{ij}S_{ij})^{1/2} = [\ 2(\frac{\partial \bar{U}}{\partial y})^2 + \frac{1}{2}(\frac{\partial \bar{U}}{\partial y}+\frac{\partial \bar{V}}{\partial x})^2\ ]^{\frac{1}{2}} \quad [\ 2(\frac{\partial \bar{V}}{\partial x})^2 + \frac{1}{2}(\frac{\partial \bar{U}}{\partial y}+\frac{\partial \bar{V}}{\partial x})^2\ ]^{\frac{1}{2}} \tag{19a}$$

Eq.(18) has been extended to anisotropic flow by simply using different filter sizes Δ_x and Δ_y, in x- and y-direction, respectively. The filter sizes, $\Delta = (\Delta_x\ \Delta_y)^{1/2}$, are a multiple (>1) of grid sizes. The Smagorinsky subgrid model was used even though it is too dissipative (see for example Vreman *et al.*,1997) because the one of the objectives of this study is to show that the diffusion-velocity method can simulate the dissipative effect of a SGS model. If so, it is expected that any other eddy viscosity based SGS model (non-dynamic or dynamic) would behave qualitatively in the same fashion. The constant $C_r = 0.12$ in Smagorinsky SGS model has been obtained by balancing enstrophy production and dissipation for homogeneous, isotropic flow (Mansfield *et al.*, 1998). The derivatives of velocities are calculated at the nodes at each time-step and the modulus Eq.(19a) is calculated as well. Note that Eq.(19a) can be expressed in terms of stream function using Eq.(16) as

$$(2S_{ij}S_{ij})^{1/2} = [\ 2(\frac{\partial^2\psi}{\partial x\partial y})^2 + \frac{1}{2}(\frac{\partial^2\psi}{\partial y^2} - \frac{\partial^2\psi}{\partial x^2})^2\ ]^{\frac{1}{2}} \quad [\ 2(\frac{\partial^2\psi}{\partial y\partial x})^2 + \frac{1}{2}(\frac{\partial^2\psi}{\partial y^2} - \frac{\partial^2\psi}{\partial x^2})^2\ ]^{\frac{1}{2}} \tag{19b}$$

The dynamic implementation requires calculating C_r at each node and at each time-step. As shown in Mansfield *et al.* (1998), two equations are generated. The first one is the "filtered vorticity equation" using the physical filter size Δ and the second one is the filtered "filtered vorticity equation" using an additional test filter $\Delta' > \Delta$, in such a way that $\Delta' = 2\ \Delta$. Then the first equation is filtered again using the test filter and subtracted from the second equation assuming the same subgrid scale model in both equations. This yields an expression for the constant as

$$l = C_r^2 m \tag{20}$$

where

$$l = l^c + l^s \tag{21}$$

$$m = m^D + m^Z \tag{22}$$

For a 2D simulation

$$l^s = 0 \tag{23}$$

$$l^c = e_z \left\{ \overline{\bar{u} \frac{\partial \overline{\omega}_z}{\partial x}} + \overline{\bar{v} \frac{\partial \overline{\omega}_z}{\partial y}} - \bar{\bar{u}} \frac{\partial \bar{\bar{\omega}}_z}{\partial x} - \bar{\bar{v}} \frac{\partial \bar{\bar{\omega}}_z}{\partial y} \right\} \tag{24}$$

$$m^Z = 0 \tag{25}$$

$$\begin{aligned} m^D = & e_z \ \Delta^2 \frac{\partial}{\partial x} \overline{\left\{ \left| \bar{S} \right| \frac{\partial \overline{\omega}_z}{\partial x} \right\}} + e_z \ \Delta^2 \frac{\partial}{\partial y} \overline{\left\{ \left| \bar{S} \right| \frac{\partial \overline{\omega}_z}{\partial y} \right\}} \\ & - e_z \Delta'^2 \frac{\partial}{\partial x} \left\{ \left| \bar{\bar{S}} \right| \frac{\partial \bar{\bar{\omega}}_z}{\partial x} \right\} - e_z \Delta'^2 \frac{\partial}{\partial y} \left\{ \left| \bar{\bar{S}} \right| \frac{\partial \bar{\bar{\omega}}_z}{\partial y} \right\} \end{aligned} \tag{26}$$

The constant C_r is uniquely specified in 2D simulation, unlike 3D simulation where the constant is overspecified and error minimization is invoked. For any variable $\bar{\phi}$ ccalculated at the nodes, double filtering is calculated using the differential interpretation of the filter in which the second order terms are neglected (Sagaut, 2002, pp. 23-25), For both the tope hat filter and the Gaussian filter $\bar{\bar{\phi}}$ is given as:

$$\bar{\bar{\phi}} = \bar{\phi} + \frac{\Delta^2}{24} \left\{ \frac{\partial^2 \bar{\phi}}{\partial x^2} + \frac{\partial^2 \bar{\phi}}{\partial y^2} \right\} \tag{27}$$

and the product of two double filtered terms as

$$\begin{aligned} \bar{\bar{\phi}} \ \bar{\bar{\eta}} = & \bar{\phi} \ \bar{\eta} + \frac{\Delta^2}{24} \bar{\eta} \left\{ \frac{\partial^2 \bar{\phi}}{\partial x^2} + \frac{\partial^2 \bar{\phi}}{\partial y^2} \right\} + \frac{\Delta^2}{24} \bar{\phi} \left\{ \frac{\partial^2 \bar{\eta}}{\partial x^2} + \frac{\partial^2 \bar{\eta}}{\partial y^2} \right\} \\ & + \left(\frac{\Delta^2}{24}\right)^2 \left\{ \frac{\partial^2 \bar{\phi}}{\partial x^2} + \frac{\partial^2 \bar{\phi}}{\partial y^2} \right\} \left\{ \frac{\partial^2 \bar{\eta}}{\partial x^2} + \frac{\partial^2 \bar{\eta}}{\partial y^2} \right\} \end{aligned} \tag{28}$$

Chapter 4

Vortex-In-Cell

The vorticity field is discretized into a set of vortex particles. The motion of the vortex particles is governed by the vorticity transport equation [Eq.(14)]. The discretization of the field into vortex particles will be discussed in section 4.1. In the vortex-in-cell method, the vorticity is transferred from the vortex particles to the nodes of a grid, using an interpolation technique which will be discussed in section 4.2. The motion of the vortex particles is traced by splitting the vorticity transport equation into several substeps. In the first substep, the convection of the interacting vortex particles is obtained by first calculating the components of the velocity $\boldsymbol{u}=(\bar{U}, \bar{V})$ at the nodes by solving the Poisson's equation Eq.(17). Then the components of the diffusion velocities are calculated at the nodes as $\left(-\frac{(\nu + \nu_{Tx})}{\bar{\omega}_z}\frac{\partial \bar{\omega}_z}{\partial x}, -\frac{(\nu + \nu_{Ty})}{\bar{\omega}_z}\frac{\partial \bar{\omega}_z}{\partial y}\right)$. The velocity components $\boldsymbol{u}=(\bar{U}, \bar{V})$ and the diffusion velocities at the nodes are transferred to the location of each vortex particle, using an interpolation technique. Then the vortex particles are convected using the equation of motion of a material point with a two-step viscous splitting algorithm. This step will be discussed in section 4.3.

For the diffusion-velocity method, no additional substep is needed. However in this study, a second substep, in which the diffusion velocity term is replaced by the random walk, has been considered in simulating the molecular diffusion term without SGS model. A comparison between the two methods is made in section 6.3.

Whenever the distance between two neighbouring vortex blobs is outside a range specified by a criteria, a regridding procedure used to improve the accuracy of the calculations by inserting or removing vortex particles was implemented (Ghoneim *et al.*, 1988). The procedure was tested on runs without SGS model and the effect on the mixing layer flow characteristics was small. It was small probable because the number of vortex particles used was high. Therefore, the regridding procedure was not used in the runs presented in this study in order to reduce the computational time.

4.1. Vortex Particles

In vortex methods, the vorticity field is discretized into N_p point vortices with circulation Γ_i for each, the vorticity field is given as

$$\omega(x) = \sum_{i=1}^{N_p} \Gamma_i \, \delta(x-x_i) \tag{29}$$

where $\delta(x)$ is the Dirac delta function, $\boldsymbol{x}$ represents the coordinates at which the vorticity is calculated and x_i is the coordinates position of the vortex points. The point vortices are vortex blobs rather than vortex points because the Biot-Savard law, i.e., the Green's function, has a singularity at the origin. It creates large velocities in its neighbourhood, which causes numerical as well as theoretical instabilities. To remove this difficulty, finite core size vortices or blob vortices may be used instead of point vortices (Chorin, 1973). Thus inside the core, velocity is smooth and finite at the centre of the core. Although this trick creates some errors, it is very effective in removing the singularities from the flow field. With this technique, the velocity field induced by each vortex is quantitatively correct, only away from the centre of the vortices. In the vortex blob approach, the particles have a core radius σ (in VIC σ is equal the grid size), a volume $\delta\upsilon_i$ and a vorticity vector of magnitude ω_i smoothened within the volume $\delta\upsilon_i$.

For a given vortex particle, the circulation Γ_i is identical to the product of the vorticity and the volume of the vortex particle, $\omega_i\ \delta v_i$, which also represents the contribution of the vortex particle to the vorticity field. Therefore each vortex particles, is completely characterized by (x, Γ_i) and the vorticity field is given as

$$\omega(x) = \sum_{i=1}^{N_p} \Gamma_i\ \zeta_\sigma(x-x_i) \tag{30}$$

where the smoothing function $\zeta_\sigma(x-x_i)$ is expressed as

$$\zeta_\sigma(x-x_i) = \frac{1}{\sigma^2}\ \zeta(\frac{x-x_i}{\sigma}) \tag{31}$$

with $\int\zeta(x)\ dx = 1$. For the present 2D formulation, the vorticity field is given as

$$\omega(x) = \frac{1}{\sigma^2} \sum_{i=1}^{N_p} \Gamma_i\ \zeta(\frac{x-x_i}{\sigma})\ \zeta(\frac{y-y_i}{\sigma}) \tag{32}$$

where [$(x-x_i)/\sigma$, $(y-y_i)/\sigma$)] are the coordinates distance in units of core size.

4.2 Interpolation Scheme

The smoothing functions used are the area-weighing scheme (Baker, 1979),

$$\zeta(\eta) = (\ 1 - |\eta|\ ) \qquad |\eta|<1 \tag{33a}$$

and the M_4' scheme, a higher order scheme (Cottet and Koumoutsakos, 2000),

$$\zeta(\eta) = \begin{cases} 1 - \frac{5}{2}|\eta|^2 + \frac{3}{2}|\eta|^3 & |\eta|<1 \\ \frac{1}{2}(\ 2-|\eta|)^2\ (\ 1-|\eta|) & 1 < |\eta| < 2 \\ 0 & |\eta|>2 \end{cases} \tag{33b}$$

Results obtained from the two schemes will be compared in section 6.2. The interpolation scheme [either Eqs.(32) and (33a) or Eqs.(32) and (33b)] is used to transfer the vorticity from the vortex blobs to the nodes of the grid. A vortex blob contributes to the nearest 4 nodes as shown in Figure (1a) in the area-weighting scheme and 16 nodes for the M_4' scheme, respectively. The total vorticity at each node is obtained by summing the vorticity contributions of all the vortex particles which are within one grid or two grids from that node for the area-weighing scheme and the M_4'scheme, respectively. Also since there is at least one vortex blob per grid, therefore the vortex blobs will always overlap. The position vector of the vortex blob center is determined by (x_i, y_i) and is discussed in the next section.

4.3. Convection and diffusion velocity

The Poisson's equation Eq.(17) is solved in order to obtain the velocity components at each node, by using the successive-over-relaxation method with a central difference approximation for the derivatives, the method is also called the extrapolated Liebmann's method (Abdolhosseini and Milane, 2000). Once the components of the velocity at the nodes $\boldsymbol{u}_n = (\bar{U}_n, \bar{V}_n)$ are calculated, the components of the velocity $\boldsymbol{u}_i = (\bar{U}_i, \bar{V}_i)$ acting on the center of the vortex blob can be calculated with the interpolation technique as,

$$U_i = \sum_n U_n \, \zeta\left(\frac{x_i - x_n}{\sigma}\right) \zeta\left(\frac{y_i - y_n}{\sigma}\right) \tag{34a}$$

$$V_i = \sum_n V_n \, \zeta\left(\frac{x_i - x_n}{\sigma}\right) \zeta\left(\frac{y_i - y_n}{\sigma}\right) \tag{34b}$$

where n is the representation of the nearest 4 nodes or 16 nodes surrounding the vortex blob in the area-weighing scheme or the M_4'scheme, respectively. The position vector of the vortex blob centre $\chi = (x_i, y_i)$ is calculated by integrating the equation of motion of a material point

$$d\chi/dt = \mathbf{u}\,(\chi(x,y,z,t)) \tag{35}$$

using the improved Euler's method where the predictor is

$$\chi^*(t+\Delta t) = \chi(t) + \mathbf{u}\,\Delta t \tag{36a}$$

and the corrector is

$$\chi(t+\Delta t)=\chi(t)+(\mathbf{u}+\mathbf{u}^{*})\Delta t/2 \qquad (36b)$$

Δt is the time-step and the velocity $\mathbf{u} = \boldsymbol{u}_i$. To implement Eqs.(36a) and (36b), the calculations are carried out in two steps within each time step. In the first step, the algorithm is executed using the predictor Eq.(36a). At the end of this step, the values are denoted by the superscript (*). Then in the second step, the algorithm is repeated using the corrector Eq.(36b). Two values of each variables are stored at each time-step, i.e. the old value at time t and the predicted value denoted by (*). At the end of the calculations, the old value is replaced by an updated value at time $t+\Delta t$.

After completing the above operation, the components of the diffusion velocities are calculated at the nodes, ($U_{di} = -\frac{(\nu+\nu_{Tx})}{\bar{\omega}_z}\frac{\partial\bar{\omega}_z}{\partial x}$, $V_{di} = -\frac{(\nu+\nu_{Ty})}{\bar{\omega}_z}\frac{\partial\bar{\omega}_z}{\partial y}$) , and transferred to the centre of the vortex blob using Eqs.(34a) and (34b). The position vector of the vortex blob is calculated using Eqs.(36a) and (36b) in which $\mathbf{u} = \boldsymbol{u}_{di}$. The diffusion velocity could be unreasonably high in regions of small vorticity and non-zero vorticity gradient because it is inversely proportional to the vorticity. This problem is remedied by setting the components of the diffusion velocity to zero whenever the vorticity at the nodes is less than 0.1% of the vorticity associated with vortex particles.

Here it is noted that the solution of the Poisson's equations together with the Lagrangian movement of the vortex particles is equivalent to the solution of the convective term $\boldsymbol{u} = (\bar{U}_n, \bar{V}_n)$ in Eq.(14).

4.4. Random walk

For the case without SGS model, the diffusion term in Eq.(7) is $\nu\left(\frac{\partial^2\overline{\omega_z}}{\partial x^2}+\frac{\partial^2\overline{\omega_z}}{\partial y^2}\right)$, This term can be simulated using random walk for high Reynolds number (Chorin, 1973). This is handled by superimposing on the motion due to the convection of the vortices(without the contribution of the diffusion velocity), the random walk using first the predictor Eq.(36a),

$$\chi^*(t+\Delta t) = \chi(t) + \mathbf{u}\,\Delta t + \eta_1 \tag{37a}$$

then the corrector [Eq.(36b)] as

$$\chi(t+\Delta t) = \chi(t) + (\mathbf{u} + \mathbf{u}^*)\Delta t/2 + \eta_2 \tag{37b}$$

where $\mathbf{u} = u_i$, η_1 and η_2 are obtained from a Gaussian distribution with zero mean and standard deviation $(2\nu\,\Delta t)^{1/2}$.

4.5. Boundary and Initial Conditions

The computational domain in Figure 1 consists of a rectangular grid with uniform grid size in each direction and in general ($\delta_x \neq \delta_y$). The lower left corner of the grid is located at $x=1$ and $y=1$. The boundary conditions for LES are the same as for the unfiltered case because they are assumed to be governed by the large scale. The Neumann conditions apply to the inflow and outflow boundaries with $\psi=0$ at $y=0$. At inflow, two laminar boundary layers, which develop on high speed side and low speed side of splitter plate, are represented by third-order polynomials and another third-order polynomial is used to patch the two boundary layers to avoid the accumulation of particles in the box used in the FDF approach (see section 5.1.2). The velocity profile also reflects the development of the wake at some distance from the edge of the splitter. Here assuming a third-order profile, $u = ay + by^2 + cy^3$. Using boundary condition y=0, $u=0$; $u=U$,

$$(\partial u/\partial y)=0, \quad \text{at } y=\delta_{laminar}$$

$$(\partial^2 u/\partial y^2)=0, \quad \text{at } y=0$$

it gives laminar velocity profile:

$$\frac{u}{U} = \frac{3}{2}\frac{y}{\delta_{laminar}} - \frac{1}{2}\frac{y^3}{\delta^3_{laminar}}$$

where $\delta_{laminar}$ can be calculated using $(\delta_{laminar}/x)=5.0/Re_x^{1/2}$ and x=0.5 for this study. So the laminar velocity profile in y-direction are

$$(\partial\psi/\partial y)_{1j} = [\frac{3}{2}\frac{y}{\delta_{laminar}} - \frac{1}{2}\frac{y^3}{\delta^3_{laminar}}]U \qquad U=U_H,\ at\quad y>y_{SP} \tag{38a}$$

$$(\partial\psi/\partial y)_{1j} = [\frac{3}{2}\frac{y}{\delta_{laminar}} - \frac{1}{2}\frac{y^3}{\delta^3_{laminar}}]U \qquad U=U_L,\ at\quad y\leq y_{SP} \tag{38b}$$

Where subscript j corresponds to the node in the y-direction, U_H and U_L are the velocities of the high-speed side and the low-speed side, respectively, y_{sp} is the splitter plate y location. The outflow stream function profile correspond to profile of velocity that is error functions in such a way that

$$(\partial\psi/\partial y)_{N,j} = (\Delta U/2)\ \mathrm{erf}\,\{\sigma\,(y-y_{ov})\,/(x-x_v)\} + U_c \tag{39}$$

where subscript N=M correspond to the node in x-direction at the outflow, j corresponds to the node in the y-direction, $\Delta U=U_H - U_L$ is the velocity difference across the layer, U_H and U_L are the velocities of the high-speed side and the low-speed side, respectively, y_{ov} is the ordinate of centerline, x_v is the virtual origin, σ is the spreading parameter and $U_c=(U_H+U_L)/2$ is the average velocity. In addition in order to simulate the Kelvin-Helmholtz instability mechanism, the profile may be augmented by a perturbation based on linear stability analysis(Monkewitz,1982). Another approach that does not rely on stability analysis may be used as discussed in Inoue(1992). In vortex method, the Kelvin-Helmholtz instability may be simulated by moving vertically the vortex closest to the edge of the splitter plate by a small distance (perturbation) given by a sinusoidal function of time operating at the fundamental frequency (f) of the unforced mixing layer as

$$y(t) = A\,x\,\sin(2\pi f t) \tag{40}$$

where $A=0.5U_c\Delta t$ is the amplitude and x represents a small percentage of A (x= 3.0 % in this study).

The fundamental frequency (f) is calculated using $f\theta_i/(2U_c)\approx 0.02$ (Oster and Wygnanski, 1982) where θ_i is the momentum thickness at the beginning of the region of linear growth. The factor A has been used by Inoue(1992) where a forced mixing layer was investigated. In this study the small value of x=3.0 % introduced ensures that the mixing layer is in the unforced mode.

The error function outflow boundary condition has been adopted because it constrains the growth rate of the momentum thickness and yields a slope for the linear growth region in close agreement with the experiment (Abdolhosseini and Milane, 2000).

Furthermore, slip conditions are assumed for the top and bottom boundaries. The Dirichlet condition is used for the bottom boundary at $y_L = 1$, consistent with $\psi_{i,0}=0$ at $y=0$, as

$$\psi_{i,1} = y_L \times U_L \tag{41}$$

and for the top boundary

$$\psi_{i,N} = U_L\, y_{sp} + U_H(y_{i,N} - y_{sp}) \tag{42}$$

where y_{sp} is the splitter plate y location and N corresponds to the nodes at the top boundary.

Initially, the velocity discontinuity across the splitter plate is simulated using a vortex sheet, which is discretized into a row of point vortices as shown in Figure (1b). At time $t=0$, the point vortices are equidistant, and separated by a distance $d = L/N_v$, where N_v is the number of vortices and $L= \delta_x M$ is the computational domain length. The vortex closest to the edge of the splitter plate is moved vertically using Eq.(40) to initialize the Kelvin-Helmholtz instability. The unfiltered total circulation in the computational domain is $L(U_H - U_L)$. The circulation is equally distributed among the N_v vortices as $\Gamma_i = L(U_H - U_L)/N_v = d(U_H - U_L)$. Furthermore, if at the end of each time step Δt, defined as the characteristic time $\Delta t = d/U_c$, a vortex with circulation Γ_i is introduced at the trailing edge of the splitter plate, the vorticity generation rate is $\Gamma_i/\Delta t = (U_H - U_L)U_c$ and therefore the Kutta condition is satisfied. The oldest vortex, i.e., the vortex with the largest residence time, is discarded from the calculations when a new vortex is introduced at the edge of the splitter plate. Furthermore, the vortices can move freely in and out through the outflow boundary to avoid the collection of vortices at the end of the computational domain. The motion of the vortices outside the computational domain is assumed to be governed by the velocity at the outflow boundary.

In the LES, the initial circulation of the vortices should be filtered. However approximating the vorticity field using Eq.(30) corresponds to filtering the circulation of each vortex Γ_i using the smoothing function $\zeta\,(x-x_i)$ (Mansfield *et al.*, 1998; Cottet, 1996). As noted earlier, in vortex method, smoothing or filtering has been used in order to remove the singularity in Biot-Savard Law. Therefore the vorticity field given by Eq.(30) is interpreted as the filtered vorticity field used in LES. Two questions remain to be addressed, the correspondence between the smoothing function and the LES filter shape and between the core size used in the smoothing function and the filter size Δ. Regarding the former issue, it is noted that for the Smagorinsky model no filter shape is invoked explicitly, therefore the smoothing function could be any of the ones used in VIC, such as either area-weighing scheme or the M_4' scheme. Regarding the latter issue, the filter size is proportional to the core size since both are proportional to the grid size (the core size=grid size in VIC).

4.6. Solution Procedure for Diffusion-Velocity Method

The solution procedure to solve the velocity and vorticity fields consists in the following steps:

(a) Initializing by placing the equidistant vortices at the level of the splitter plate and by assuming arbitrary values for ψ at the internal nodes together with the boundary conditions [Eqs.(38)-(42)].

(b) Distributing the vorticity from the vortex particles to the nodes using the interpolation scheme [either Eqs.(32) and (33a) or Eqs.(32) and (33b)].

(c) Solving the Poisson's equation [Eq.(17)], using a Gauss-Seidel iteration with a left-to-right sweep of the nodes and bottom-to-top sweep of the lines. Iteration convergence is obtained when the percent difference between consecutive ψ is less than 0.001%.

(d) Computing the velocities $\bar{U}$ and $\bar{V}$ at the nodes using Eq.(16).

(e) Calculating the velocities at the location of each vortex ($\bar{U}_n$, $\bar{V}_n$) using the interpolation scheme [Eqs.(34a) and (34b)].

(f) Updating the co-ordinates of the vortices using Eqs.(36a) and (36b).

(g) Computing the SGS eddy viscosity using Eqs.(18) and (19b) either with constant C_r=0.12 or with dynamic calculating C_r at each node [Eqs.(20)-(28)].

(h) Computing the component of diffusion velocity $\left(- \frac{(\nu + \nu_{Tx})}{\bar{\omega}_z}\frac{\partial \bar{\omega}_z}{\partial x} , - \frac{(\nu + \nu_{Ty})}{\bar{\omega}_z}\frac{\partial \bar{\omega}_z}{\partial y}\right)$ at the nodes.

(i) Calculating the diffusion velocity at the location of each vortex using the interpolation scheme [Eqs.(34a) and (34b)] where ($\bar{U}_n$, $\bar{V}_n$) is replaced by the component of diffusion velocity .

(j) Updating the coordinates of the vortices using Eqs.(36a) and (36b).

(k) Introducing a new vortex at the edge of the splitter plate and discarding the oldest one.

(l) Marching in time by repeating the calculations from step b through k.

The first and second derivatives are calculated using fourth-order central difference formulas.

Chapter 5

Large Scale Scalar Field

5.1 Governing Equations

Consider a reactive flow governed by a single step chemical reaction, A + B → C + D, in which the mass fraction of each species is governed by rate equations. Assuming that the species mass fraction depend on one of them denoted by ϕ. The filtered species conservation equation for mass fraction $\overline{\phi}$ is (Colucci *et al.*, 1998)

$$\frac{\partial \overline{\phi}}{\partial t} + \frac{\partial (\overline{U}\,\overline{\phi})}{\partial x} + \frac{\partial (\overline{V}\,\overline{\phi})}{\partial y} = \frac{\partial}{\partial x}(\Gamma \frac{\partial \overline{\phi}}{\partial x}) + \frac{\partial}{\partial y}(\Gamma \frac{\partial \overline{\phi}}{\partial y}) - \frac{\partial M_x}{\partial x} - \frac{\partial M_y}{\partial y} + \overline{\omega}_\alpha \tag{43}$$

where $M_x = \overline{U\,\phi} - \overline{U}\,\overline{\phi}$ *and* $M_y = \overline{V\,\phi} - \overline{V}\,\overline{\phi}$ are the unresolved subgrid mass fluxes in x- and y-directions, respectively; $\overline{\omega}_\alpha$ is the filtered reaction rate (large scale); Γ is the molecular diffusion coefficient related to the eddy viscosity ν via the turbulent Schmidt number S_{c_T}, as $\Gamma = \nu \,/\, S_{c_T}$. By analogy with the SGS in the filtered momentum equation, the subgrid mass fluxes are modelled using the eddy diffusion concept for an anisotropic flow as $-M_x = \Gamma_{Tx}\, \partial\overline{\phi}/\partial x$ and $-M_y = \Gamma_{Ty}\, \partial\overline{\phi}/\partial y$, Substituting in Eq.(43) and rearranging as

$$\frac{\partial\overline{\Phi}}{\partial t} + \frac{\partial(\overline{U}\,\overline{\Phi})}{\partial x} + \frac{\partial(\overline{V}\,\overline{\Phi})}{\partial y} = \frac{\partial}{\partial x}[(\Gamma+\Gamma_{Tx})\frac{\partial\overline{\Phi}}{\partial x}] + \frac{\partial}{\partial y}[(\Gamma+\Gamma_{Ty})\frac{\partial\overline{\Phi}}{\partial y}] + \overline{\omega}_{\alpha} \tag{44}$$

where Γ_{Tx} *and* Γ_{Ty} are related to ν_{Tx} *and* ν_{Ty} defined by Eq.(18) via the turbulent Schmidt number S_{c_T}, as $\Gamma_{Tx} = \nu_{Tx} / S_{c_T}$; $\Gamma_{Ty} = \nu_{Ty} / S_{c_T}$. For an isothermal flow of constant density considered in this study, the flow field solution is decoupled from the scalar field solution.

The FDF is the relative frequency density of a realization over an ensemble. A large eddy probability density function (LEPDF)(Gao and O'Brien, 1993) similar to the filtered probability density function (FDF)(Colucci *et al.*, 1998) has been introduced. A transport equation for the FDF of a reactive scalar (P_L), has been derived by filtering the fine-grained PDF, that is the delta-function $\delta(\xi-\phi)$, to yield

$$\begin{aligned}\frac{\partial(P_L)}{\partial t}+\frac{\partial(\overline{U}P_L)}{\partial x}+\frac{\partial(\overline{V}P_L)}{\partial y} &= -\frac{\partial}{\partial x}(\overline{U|\xi}-\overline{U})P_L-\frac{\partial}{\partial y}(\overline{V|\xi}-\overline{V})P_L \\ &+\frac{\partial}{\partial x}[\Gamma\frac{\partial P_L}{\partial x}]+\frac{\partial}{\partial y}[\Gamma\frac{\partial P_L}{\partial y}]-\frac{\partial^2}{\partial\xi^2}[\overline{\Gamma(|\frac{\partial\phi}{\partial x}|^2+|\frac{\partial\phi}{\partial y}|^2)|\xi}P_L]-\frac{\partial}{\partial\xi}(\omega P_L)\end{aligned} \tag{45}$$

where $\overline{U}$ and $\overline{V}$ are the streamwise and lateral filtered velocities, respectively, and ω is the chemical reaction term which filtered value is used in Eq.(44). The symbol $\overline{U|\xi}$ indicates the expected value of u conditional on the satisfaction of the constraint ξ. The mixture fraction ξ is defined as $\xi = \frac{c - c_U}{c_L - c_U}$, where c is the concentration of passive scalar, $c_L = 1$ and $c_U = 0$ are the concentrations of upper and lower bounds of the variable c. In FDF method, the quantities that have to be modelled are one point one time conditional expectation, i.e., terms including the constraint ξ in Eq.(45).

The three terms on the L.H.S. of Eq.(45) are in closed form. The first term is the transient term, the second and third terms are the convection terms. On the R.H.S., the first two terms represent the subgrid convective flux. They are not closed and need to be modelled similar to M_x *and* M_y in Eq.(43) or the SGS terms Y and Z in Eq.(7). The model for subgrid convective flux will be discussed in section 5.1.1. The third and fourth terms on the R.H.S. represent molecular diffusion and are closed. The fifth term representing molecular dissipation or molecular mixing, is not closed. In this study, the mixing model used to close the molecular mixing term is the Modified Curl model and will be discussed in section 5.1.2. The sixth term corresponding to the chemical reaction term is closed. In this study, a non-reactive flow is considered and will be introduced in section 5.1.3.

5.1.1 Subgrid Convective Flux

The closure of the subgrid convective flux requires knowledge of the expected value of the velocity fluctuation conditioned to ξ. This term is known when the joint statistics of the velocity and mixture fraction ξ are known, i.e. when P_L is their joint FDF. In this study the velocity is not included in P_L, and the subgrid convective term is modelled using the gradient diffusion model as,

$$\begin{gathered} [\overline{U|\xi}-\overline{U}]\; P_L = -\Gamma_{Tx}\,\frac{\partial P_L}{\partial x} \\ \textit{and} \\ [\overline{V|\xi}-\overline{V}]\; P_L = -\Gamma_{Ty}\,\frac{\partial P_L}{\partial y} \end{gathered} \tag{46}$$

where Γ_{Tx} *and* Γ_{Ty} is related to the eddy viscosity ν_{Tx} *and* ν_{Ty} defined by Eq.(18) via the turbulent Schmidt number S_{c_T}, as $\Gamma_{Tx} = \nu_{Tx} / S_{c_T}$; $\Gamma_{Ty} = \nu_{Ty} / S_{c_T}$.

5.1.2 Molecular Mixing Models

The closure of the mixing term requires the joint statistics of ξ and its gradients, for which several models have been proposed by Dopazo (1994) and Pope (2000). Every mixing model must satisfy several requirements during mixing. A satisfactory model fulfilling these requirements has not yet been developed. In the particle implementation, i.e. the Monte-Carlo technique, the coalescence and dispersion models (the Modified Curl model) and the linear mean square estimation (LMSE) or the interaction by exchange with mean (IEM) satisfy the conservation of the mean values of scalar, the exponential decay in time of the scalar variance and the boundedness condition upon mixing. In this study the Modified Curl model is adopted.

Modified Curl Model

In the Modified Curl model the mixing term, $\frac{\partial^2}{\partial \xi^2}\,[\overline{\Gamma(|\frac{\partial \phi}{\partial x}|^2 + |\frac{\partial \phi}{\partial y}|^2)|\xi}\; P_L]$, is modelled by selecting pairs of particles randomly as

$$n_m = \beta\ \overline{\omega}_f\ N\ \Delta t \tag{47}$$

where n_m denotes number of pairs of particles that will mix in grid, $\overline{\omega}_f$ is the mean mixing frequency in grid and the coefficient β is a function of the mixing model. After mixing, the concentrations of the two particles in a mixing pair are given as

$$\xi_1^* = [(1-\alpha)\xi_1 + \frac{\alpha(\xi_1+\xi_2)}{2}] \tag{48a}$$

$$\xi_2^* = [(1-\alpha)\xi_2 + \frac{\alpha(\xi_1+\xi_2)}{2}] \tag{48b}$$

where ξ_1 and ξ_2 denotes the concentrations of the two particles before mixing, and ξ_1^* and ξ_2^* denotes the concentrations after mixing. The variable α is specified by a distribution function describing the mixing model. For the Modified Curl model, β=3 and α is a uniform random number between 0 and 1.

The mixing model requires an externally supplied mixing frequency. In the context of Filtered density function (FDF), Colucci *et al.*(1998) have assumed that the unsteady mixing frequency is given as $\omega_f = C_\Phi(\Gamma+\Gamma_T) \,/\, \Delta^2$ in analogy with the procedure used in Reynolds averaged methods where the governing equation for the fluctuations variance obtained from the conservation equation is compared with the one obtained from the PDF equation. The constant $C_\Phi \approx 3$ was also suggested by Colucci *et al.*(1998). For the anisotropic flow considered in this study, the mixing frequency is calculated at the nodes as $\omega_f = C_\Phi \dfrac{[(\Gamma+\Gamma_{Tx}) \,/\, \Delta_x^2 + (\Gamma+\Gamma_{Ty}) \,/\, \Delta_y^2\,]}{2}$, where Δ_x and Δ_y are the filter sizes in x- and y-direction used in SGS models. The mean mixing frequency ($\overline{\omega}_f$), which is used in the Modified Curl model [Eq. (47)], is obtained by arithmetical averaging the mixing frequencies at particle locations in grid. The mixing frequencies at particle locations are calculated by transferring the mixing frequency (ω_f) from nodes using interpolation scheme [Eq. (33a)].

5.1.3 Reacting flow

In non-reacting flow, the reaction is nil and only species A is entrained, *i.e.* an inert gas is introduced in the low speed stream. While for reacting flow, species B is introduced into high speed stream. The reaction rate is assumed to be at constant rate and without heat release describing the depletion of A is $\omega_A = \kappa\, X_A X_B$, where X_A and X_B are concentrations in p.p.m.V. The unit of ω_A is in p.p.m.V/s. Note that $\omega_A = \omega_B$. In this study, a non-reacting flow is considered.

5.1.4 Modelled FDF Equation

For reacting flow, the governing equation for the FDF is obtaining by substituting Eq.(46) into Eq.(45) to yield

$$\begin{aligned}\frac{\partial(P_L)}{\partial t}+\frac{\partial(\overline{U}P_L)}{\partial x}+\frac{\partial(\overline{V}P_L)}{\partial y}&=\frac{\partial}{\partial x}[(\Gamma+\Gamma_{Tx})\frac{\partial P_L}{\partial x}]+\frac{\partial}{\partial y}[(\Gamma+\Gamma_{Ty})\frac{\partial P_L}{\partial y}]\\&-\frac{\partial^2}{\partial \xi^2}[\overline{\Gamma(|\frac{\partial\phi}{\partial x}|^2+|\frac{\partial\phi}{\partial y}|^2)}|\xi P_L]-\frac{\partial}{\partial\xi}(\omega P_L)\end{aligned}\tag{49}$$

The solution of Eq.(49) gives all the statistical information concerning the scalar field. For non-reacting flow, $\frac{\partial}{\partial\xi}(\omega P_L) = 0$.

5.2 Monte-Carlo Simulation

The scalar FDF transport equation [Eq.(49)] is solved using the Monte Carlo method. Two approaches may be used for the Monte Carlo solution, an Eulerian(Pope, 1981) or a Lagrangian (Pope, 1985, 1994). The Eulerian approach is a first order approximation because particles motion between nodes is based on an upwind approach. It has been shown to be adequate to solve low-Mach numbers, variable density flows (BRITE-EURAM project, 1993-1996) and compressible flows (Hsu *et al.*, 1994), and is less expensive than Lagrangian approach (Möbus *et al.*, 2001). In the context of an LES simulation, Colucci *et al.*(1998) pointed out that the Eulerian approach produces numerical diffusion which degrade the results whereas the Lagrangian approach produces better results. Therefore in this study the Lagrangian approach is used.

In the Lagrangian approach, the ensemble of particles are initially spread uniformly in grids in the computational domain of Figure 2. Each particle is viewed as being sampled from different realizations of the mixing layer and identified by a representative value of the scalar concentration ξ. As an approximation, the ensemble mean at node is calculated as the arithmetic average of the particles' concentration in the box (Figure 2) centred at node. The approximation is more accurate as the box size is decreased and as the number of particles is increased. The particles are subjected to convection, turbulent transport and molecular mixing as discussed below.

Convection / Turbulent Transport

The time evolution of the particle position $X_i(t) = [x_i(t), y_i(t)]$ with property ξ is governed by a continuous Markov process. For this process, the governing equation describing the time, space and concentration evolutions for the probability density of ξ is given by the forward Fokker Plank equation, and also identically in a stochastic manner by the Langevin equation which describes the time evolution equation for the continuous Markov process. The form of the Langevin equation used in the Lagrangian approach, is given as

$$dX_i(t) = D_i(X(t),t)dt + E(X(t),t)dW_i(t) \tag{50}$$

where X_i is the Lagrangian position of a stochastic particle, D_i and E are the drift and diffusion coefficients, respectively, and W_i denotes the Wiener-Levy process (Pope, 1985). These coefficients appearing also in the Fokker Plank equation are obtained by comparing it with the governing equation [Eq.(49)]. This results in

$$\begin{gathered} D_i = (\overline{u_i}, \overline{v_i}) + \left(\frac{\partial(\Gamma + \Gamma_{Tx})}{\partial x_i}, \frac{\partial(\Gamma + \Gamma_{Ty})}{\partial y_i} \right) \\ \textit{and} \\ E = \left(\sqrt{2(\Gamma+\Gamma_{Tx})}, \sqrt{2(\Gamma+\Gamma_{Ty})} \right) \end{gathered} \tag{51}$$

The Wiener-Levy process is identical to the random walk used in Eq.(37) which are obtained from a Gaussian distribution with zero mean and standard deviation $[2(\Gamma + \Gamma_{Tx})dt]^{1/2}$ in x-direction and $[2(\Gamma + \Gamma_{Ty})dt]^{1/2}$ in y-direction, respectively. Eq.(50) is also denoted the stochastic differential equation (SDE) which represent the general diffusion process in a stochastic manner.

Molecular Mixing

For this study, molecular mixing is handled by the Modified Curl model which requires to select particles in the ensemble to mix them and has been discussed in section 5.1.2.

5.3 Boundary and Initial Conditions

The computational domain (Figure 2b) for the Monte Carlo simulation consists of a rectangular grid, with uniform grid sizes in each direction similar to the flow field (Figure 1b). For non-reactive mixing layer, the faster stream above the splitter plate has an initial concentration of $c_U = 0.0$, while the slower stream below the splitter plate has an initial concentration of $c_L = 1.0$. Two inlet boundary conditions, stepwise profile and error function, will be tested. The error function is given as,

$$c(y)_{1,j} = (\Delta c/2)\ \mathrm{erf}\ \{\sigma(y-y_{oc}) / x_v\} + c_c \tag{52}$$

where subscript 1 corresponds to the inflow x-location and subscript j corresponds to the nodes in the y-direction, $\Delta c = c_L - c_U$ is the concentration difference across the layer, $c_c = (c_L + c_U)/2$ is the average concentration, σ is the spreading rate and y_{oc} is different from y_{ov}, the ordinate of centerline of velocity field [Eq.(39)], The relation $y_{oc} \neq y_{ov}$ is similar to the cross-stream adjustment length used in the "wake-modified" inlet conditions by Soteriou and Ghoniem(1998), and also the relation $y_{oc} \neq y_{ov}$ is necessary to obtain predict that fit the experimental data and previous numerical simulations. The outflow boundary condition is not specified (Eq.(49) is parabolic) because the displacement of concentration due to streamwise convection is very high, as compared to the displacement of concentration due to backward diffusion. Therefore, the concentration values in the downstream flow do not have any significant upstream effect.

Particles are allowed to exit the top, bottom, and the outflow domain boundaries. The domain is replenished at the corresponding nodes of the boundary opposing the boundary of the particle exit.

At inflow, the replenished concentrations are defined by the inlet boundary condition.

5.4 Solution Procedure

The flow field and scalar field are determined by the VIC solution and the solution of the transport equation [Eq.(49)]. For the FDF, the solution procedure consists of the following steps:

(a) Initializing the number of particles in the computational domain by prescribing particles to grids.

(b) Assigning initial concentration to each particle, using either a stepwise profile with 0 above and 1 below the splitter plate, respectively, or the error function [Eq.(52)].

(c) Calculating D_i and E using Eq. (51) and the mixing frequency at the nodes.

(d) Transferring D_i and E from the nodes to particle locations using interpolation scheme and displacing the particles using Eq.(50).

(e) Updating the number of particles in grid and renumbering them consecutively.

(f) Transferring mixing frequency from the nodes to particle locations using interpolation technique, and calculating the arithmetic average mixing frequency in grid, then using the Modified Curl model to calculate the number of mixing pairs [Eq. (47)]. The pairs are selected and new concentrations are calculated following Eqs. (48a) and (48b).

(g) Marching in time by repeating steps (c) to (f) is performed only within the defined range of time steps.

The first and second derivatives are calculated using fourth-order central difference formulas.

Chapter 6

Flow Field

Several numerical experiments were conducted to validate the method. The diffusion-velocity method simulating molecular diffusion without SGS model, in conjunction with the vortex-in-cell method has not yet been presented in previous literature. Therefore the method will be firstly validated by comparing with the experimental mixing layer data of Masutani and Bowman(1986) (M&B), because the two-dimensional flow was carefully maintained and verified, and also by comparing with a numerical experiment where molecular diffusion is simulated using random walk. Results obtained using the area-weighing scheme and the M_4' scheme are compared. Then LES results based on the diffusion-velocity method and both the Smagorinsky and Dynamic Eddy Viscosity SGS model were obtained. Several flow characteristics are reported and compared, vorticity contours, mean velocity profiles, root-mean-square (rms) longitudinal and lateral velocity fluctuations, Reynolds shear stress and rms vorticity fluctuations.

6.1 Flow Field and Numerical Parameters

The velocity ratio is $r = U_L/U_H = 0.5$ (ratio of the lower velocity side of the splitter plate to the higher velocity side) with the free stream velocity above the splitter plate U_H= 600 cm/s and below the splitter plate U_L = 300 cm/s, similar to the parameters used in the experiment of M&B. The spreading rate is σ=35 for r=0.5 (Spencer *et al.*, 1971). The coordinate y_{ov} in Eq. (39) is equal to 33cm and corresponds to the edge of the splitter plate in Figure 1. The reported results are for a viscous flow condition with $\nu = 14.5\times10^{-2}$ cm^2/s (the kinematic viscosity of air at 18 °C).

The computational domain for the base run consists in a 256×256 anisotropic grid with equidistant grid, δ_x= 0.5 cm and δ_y= 0.25 cm. The aspect ratio $a_{xy}=\delta_x/\delta_y$=2.0 is consistent with a_{xy}=2.0 used by Deardoff(1970) and a_{xy}=3.7 used by Shumann(1975) in LES of channel flow. Also Kaltenbach(1997) has reported that the representation of shear flows is most economical when anisotropic grid (i.e. a_{xy}>1) is used because it produces adequate values for ratios of Reynolds stresses. Also a numerical experiment using an isotropic grid, $\delta_x=\delta_y$=0.25 cm with 512×256 grid, and using the same computational domain size as the base run, is reported. The area-weighting scheme was used in the base run. For all LES, the filter sizes are set to twice the grid size in each direction, i.e. $\Delta_x= 2\delta_x$ and $\Delta_y =2\delta_y$.

At the level of the splitter plate, the shear layer is discretized into a layer of N_v =2560 equidistant vortex particles. Therefore, the circulation of each vortex is $\Gamma_i = 1.5\times10^{-3}$ m^2/s, and the time step $\Delta t= d/U_c = 11.1\times10^{-5}$ sec. N_v =2560 means that there are 10 vortices(10 = 2560 /256) in one grid. Sensitivity of the results to the number of vortices was tested using N_v =10240, i.e. 40 vortices per grid. No significant difference between N_v =2560 and N_v =10240 was found. In this study, the number of vortices is N_v =2560 for all the reported runs.

The flow is allowed to develop for two residence times (i.e., 2M time-steps) before the statistical calculations are started. Then the mean flow is obtained using time-averaging over the next twelve residence times, and the rms velocity fluctuations, the negative cross-stream correlation and the rms vorticity fluctuations are calculated using time-averaging over the next twenty eight residence times.

6.2 Diffusion Velocity Method Without SGS

The streamwise mean velocity normalized as $(U-U_L)/(U_H-U_L)$ is shown in Figure (3a) as a function of the similarity variable $\eta_v = (y-y_0)/(x-x_v)$ at four downstream locations, where U is the streamwise mean velocity, y_0 is the ordinate of the velocity centerline at location x, the virtual origin defined as the x-location at the intersection of the velocity centerline with the horizontal line at the level of the splitter plate is 4.01 cm. Figure (3a) shows that the agreement with the experiment of M&B (dark symbols) is adequate. The results of the numerical simulation are presented in the self-preserving region, which is from x= 51 cm to 77 cm, *i.e.* $0.4 \leq x/H \leq 0.6$. The self-preserving region corresponds to the region of linear growth of the momentum thickness θ as a function of x/H for several cases. For the case without SGS (symbol △), a region with a nearly linear growth is identified between $0.4 < x/H < 0.6$, where the slope is equal to about 0.0155. This value is close to the experimental value 0.0165 of M&B.

The rms longitudinal (rmsu') and lateral (rmsv') velocity fluctuations normalized with ΔU are shown in Figures (3b) and (3c), respectively, and the Reynolds shear stress ($-u'v'$) normalized with ΔU^2 is shown in Figure (3d). Adequate self-preserving profiles are obtained for $0.4 \leq x/H \leq 0.6$. The rmsu' is shown together with the data from the M&B(1986). The values for the rmsu' in the simulation slightly increase along the streamwise direction whereas it decreases in the experimental data. Similar behaviour is found in the numerical work of Ghoneim and Heidarinejad (1990),who argued that the experimental trend is caused by dissipation due to molecular diffusion. The rmsv' is consistent with previous 2D simulation (Abdolhosseini and Milane, 2000). the data for - $u'v'/\Delta U^2$ are not reported in M&B. However the peak values - $u'v'/\Delta U^2 = 0.014$ in Figure (3d) is comparable with the peak of 0.013 obtained in the experiment of Oster & Wygnanski (1982) for a velocity ratio of $r = 0.6$, which is slightly different than the value of $r = 0.5$ used in the present simulation.

Furthermore it is necessary to verify the sensitivity of the results to aspect ratio because results from LES are function of aspect ratios(Kaltenbach, 1997), particularly if they exhibit inhomogeneities of mean quantities as the mixing layer considered in this study where rmsu'/rmsv' ≈0.82. Figures (4a-4d) show that rmsu'/ΔU, rmsv'/ΔU, - $u'v'/\Delta U^2$ and rmsω', respectively, are quite insensitive to aspect ratios tested. The rms vorticity fluctuations (rmsω') has been reported in Figure (4d) because the effect of LES on this quantity will be discussed in section 6.6.

Figures (5a-5d) show the rmsu'/ΔU, rmsv'/ΔU, - $u'v'/\Delta U^2$ and rmsω' profiles for both the area-weighting scheme and the M_4' scheme. The peaks of the rmsu'/ΔU and rmsv'/ΔU are slightly lowered when the M_4' scheme is used as shown in Figures (5b-5c), respectively. The agreement for the mean in Figure (5a) is adequate. The negative cross-stream correlation - $u'v'/\Delta U^2$ in Figure (5d) indicates that there is a deviation at the peak. This can be explained by noting that the similarity has not been fully achieved when wither the M_4' scheme or the area weighting scheme is used. A longer computational run may be required. This will probably yield profiles that are close for both schemes. In summary the figures suggest that the sensitivity of the profiles to the smoothing function is quite small probably because the number of vortex particles used is high. Therefore the M_4' scheme was not used in evaluating the diffusion-velocity method with SGS model in the interest of reducing the computational time. The computational time is reduced by about 10% when the area-weighting scheme is used in comparison with the M_4'scheme. The test using the M_4'scheme was conducted with a view that a better representation of vorticity on the nodes would improve the calculations of the diffusion velocity.

However from a practical point of view and for the mixing layer tested, the area-weighting scheme is adequate for the qualitative assessment of the diffusion-velocity method and will be used in remaining numerical experiments.

6.3 Comparison of Diffusion Velocity Method with Random Walk

The results of the diffusion velocity method simulating the diffusion term is further validated by comparing with the results obtained using random walk. The virtual origin x_v = 2.55cm when random walk is used. Figures (6a-6d) show ($U - U_L$)/($U_H - U_L$), rmsu'/ΔU, rmsv'/ΔU and - u'v'/ΔU^2, respectively, at two downstream locations, x/H=0.5 and 0.6. The difference in profiles due to the different methods is quite small. This difference is attributed to the different numerical errors in the two methods. No further elaboration is made in this study. The agreement between the profiles of the two methods provides further validation that the diffusion velocity method is adequate.

6.4 LES Run withSmagorinsky SGS model

Figures (7a-7d) show ($U - U_L$)/($U_H - U_L$), rmsu'/ΔU, rmsv'/ΔU and - u'v'/ΔU^2, respectively, for LES with Smagorinsky SGS model and C_r=0.12. The mean in Figure (7a) indicates adequate self-similar profiles at four downstream locations between $0.4 \leq x/H \leq 0.6$. This is consistent with nearly linear development of momentum thickness in Figure (12b) and Figure (13) (symbol □). The rmsu'/ΔU, rmsv'/ΔU and - u'v'/ΔU^2 also show adequate similarity. It is noted that the profiles in Figures (7a-7d) are not fully self-similar. This is consistent with the investigation of Vreman *et al.*(1997), who conducted LES based on the filtered Navier-Stokes equations and where tests using six non-dynamic and dynamic SGS models showed that the profiles are not fully self-similar.

6.5 LES Run with Dynamic Eddy Viscosity SGS model

Figures (8a-8d) show the rmsu'/ΔU, rmsv'/ΔU, - u'v'/ΔU^2 and rmsω' profiles for both the Dynamic Eddy Viscosity SGS model. The mean, rmsu'/ΔU, rmsv'/ΔU and - u'v'/ΔU^2 indicate adequate self-similar profiles at four downstream locations between $0.4<x/H<0.6$. The self-similarity of rmsu'/ΔU and rmsv'/ΔU profiles are slightly better for Dynamic Eddy Viscosity model in Figures (8b-8c) than Smagorinsky SGS model in Figures (7b-7c) consistent with the results of Vreman *et al.* (1997)

The dynamic implementation requires calculating the dynamic constant C_r^2 at each node using [Eqs.(21-27)]. In Figures (9a-9f), C_r^2 is shown at six nodes which are around centre line and at downstream location (64 cm and x/H=0.5). The dynamic constant C_r^2 varies with time. Initially C_r^2 is zero then after about 500 timesteps, C_r^2 fluctuates with a value different with zero. Also Figures (9a-9f) show that the Smagorinsky constant C_r^2 is higher than the dynamic constant C_r^2 because it is more dissipative for Smagorinsky SGS model.

6.6 Comparison of LES Runs with Run without SGS

Comparison between five runs is made: without SGS, Dynamic Eddy Viscosity model, Smagorinsky SGS using C_r=0.12, Smagorinsky SGS using C_r=0.18 and Smagorinsky SGS with C_r=0.12 using an isotropic grid. The first four runs are conducted on an anisotropic grid. The case with Smagorinsky SGS using C_r=0.18 is more dissipative than the case with C_r=0.12 and therefore was chosen to verify whether the diffusion-velocity method predict the dissipative effect of SGS model. The isotropic case has finer grid in x-direction only and generates a lower eddy viscosity from SGS model. It is compared with the anisotropic case, with a view to verify whether a lower eddy viscosity leads to less dissipation and therefore validate further the dissipative nature of the diffusion-velocity method when used in conjunction with a SGS model. Figures (10a-10d) show the downstream evolution of the spanwise vorticity contours for the four cases with same anisotropic grid. The contours spread in the free stream as they develop from the edge of the splitter plate. The maximum contour level decreases as SGS model is applied consistent with its dissipate nature(see legend). It is 1800 for the case without SGS in Figure (10a), 1700 for the case with Dynamic Eddy Viscosity SGS model in Figure (10b), 1400 for the case with Smagorinsky using C_r=0.12 in Figure (10c), and 1200 using C_r=0.18 in Figure (10d). Close up of selected downstream location are shown in Figures (11a-11d) which are drawn using identical scale. Figure (11a) without SGS indicates that the contour peaks at 600, for Dynamic Eddy Viscosity SGS at 400 in Figure (11b) whereas it drops to 300 and 200 when the Smagorinsky SGS with C_r=0.12 and C_r=0.18 are used, respectively. The contour levels are further apart when SGS model is used. Therefore, in the context of the diffusion-velocity method, the SGS model is dissipative because it decreases the contour peaks and yields coarser contour lines.

The profiles of the various statistics are shown in Figure (12a) and Figures (14a-14d) at downstream location x/H=0.6 for the four cases discussed in the previous paragraph and the additional case with isotropic grid. In Figure (12b), the momentum thickness is less than zero when x/H is less than 0.3 due to the initial inlet boundary condition. The effect of initial inlet boundary condition on the flow will be discussed in section 7.8. For the anisotropic cases, the mean in Figure (12a) indicates that SGS model has a slight effect. This effect is clarified by the trend of momentum thickness in Figures (12b) and (13). In Figure (13), the position of the figure where the flow is self-similar is magnified. The momentum thickness growth is slightly slowed down as the dissipative effect of SGS is increased or equivalently as the eddy viscosity from SGS model is increased (see peak ν_{Tx}/ν for anisotropic cases in Table I). Comparison of the isotropic case (symbol ○) with the anisotropic case (symbol □) indicates that the growth of the momentum thickness is faster for the isotropic case because of lower eddy viscosity (see peak ν_{Tx}/ν in Table I). Furthermore, Table I show that the value rmsu'/rmsv' for LES using Dynamic Eddy Viscosity SGS model is closer to the case without SGS than the LES with Smagorinsky SGS model.

Figures (14a-14b) shows that the peaks and the profiles of rmsu'/ΔU and rmsv'/ΔU are lowered as the effect of SGS is increased by increasing eddy viscosity. The peaks of the rmsu'/ΔU, rmsv'/ΔU and - u'v'/ΔU^2 in Figures (14a-14c),respectively, is higher for Dynamic Eddy Viscosity SGS model in comparison with Smagorinsky model but lower than without SGS as excepted. This is consistent with the fact that the dynamic model is lower dissipative than Smagorinsky model (Vreman *et al.*, 1997). The quantity rmsω' in Figure (14d) is lowered as the effect SGS is increased, consistent with the lower contour level peaks in Figures (10a-10d) and (11a-11d). The Reynolds shear stress - u'v'/ΔU^2 is less affected by SGS, consistent with being linked to the mean in Figure (12a) by the mean momentum equation and the mean flow is slightly affected by SGS. Furthermore, Table I shows that the ratio rmsu'/rms v' for LES with anisotropic grid is closer to the cases without SGS than the LES with isotropic grid. This is one of the justification for using an anisotropic grid in LES (Kaltenbach, 1997).

Table I - Effect of SGS and grid on instantaneous peak ν_{Tx}/ν and rmsu'/rms v' at x/H=0.6

C_r	grid	peak ν_{Tx}/ν of last time-step	rmsu'/rmsv'
0 (without SGS)	isotropic (fine)	0	0.825
0 (without SGS)	anisotropic (coarse), △	0	0.812
Dynamic calculated	anisotropic (coarse), ▹	10	0.808
0.12	anisotropic (coarse), □	24	0.788
0.18	anisotropic (coarse), ▽	35	0.740
0.12	isotropic (fine), ○	12	0.735

Chapter 7

Scalar Field

The scalar field calculations are conducted on rectangular computational domain identical to the flow field computational domain. The number of particles is NP=36 which is within the range 20 to 200 (Jaberi *et al.*, 1999). The mean concentration, rms concentration fluctuations and PDFs are approximated at the nodes using particles located in rectangular boxes centred at nodes (Figure 2a). The boxes do not overlap, i.e. the box size is less than half of grid size. The approximation becomes more accurate as the box size is decreased and as the number of particles is increased. In this study, the box size is 0.4 of grid size. For each particle, at time $t = 0$ the concentration is initialized as $c_L = 1.0$ on the low speed stream and $c_U = 0.0$ on the high speed stream. Two SGS models, Smagorinsky and dynamic eddy viscosity models, are tested. Two inlet boundary conditions for scalar field are also tested, stepwise and error function with $y_{oc} = 31.8$ cm in Eq. (52). The run using dynamic eddy viscosity SGS model with error function as boundary condition for scalar is chosen as the base run.

The FDF solution requires specifying the constants S_{c_T} and C_ϕ, and the mixing model. For the base run, the Modified Curl model is used with $C_\phi = 3.0$ and $S_{c_T} = 0.7$ similar to the ones used in Zhou and Pereira (2000). Effects of Smagorinsky SGS model, S_{c_T}, C_ϕ and inlet boundary conditions on mean concentration, rms concentration fluctuations and probability density function will be discussed.

To achieve statistically stationary solutions, the Monte Carlo simulation is run for fourteen residence times. Firstly, the flow is allowed to develop in the first two residence times, then the mean concentration is computed over the next four residence times similar to the flow field. The rms concentration fluctuations and PDFs are computed over the next eight residence times.

7.1 Mean Concentration, RMS Concentration Fluctuations and Concentration Spread for Base Run

Figures (15a-15b) show the mean concentration ($\bar{\xi}$) plotted as a function of the similarity variable $\eta_c = (y-y_c)/(x-x_{vc})$, where y_c corresponds to the concentration centerline at stream-wise location x, and x_{vc} is the x-location of the virtual origin for concentration. Figures (15a-15b) show that the results of the simulation are close to the experiment of M&B (1986) and to the simulation of Zhou and Pereira (2000), respectively, for $0.5 \leq x/H \leq 0.6$. For x/H=0.4 the mean concentration profile is in the non self-preserving region unlike the mean velocity profile which is in the self-preserving region (see Figure 3(a)). Furthermore the free stream concentration extends further on the high speed side($\eta_c>0$) than on the low speed side($\eta_c<0$). This shows that the mixing layer entrains more particles from the high speed fluid. The mean concentration profiles exhibit triple inflection point for x/H= 0.5 and 0.6 similar to M&B(1986) and to Zhou and Pereira(2000). However for x/H=0.4, the triple inflection point profile is less pronounced, because the flow is still developing.

Figure (16a) shows the mean concentration profile and the mean velocity profile at x/H= 0.6. The scalar mixing region extends further into the free stream than does the momentum mixing region as found by M&B(1986). This result is consistent with Figure (16b), which indicates that the concentration spread is higher than the velocity spread.

The rms concentration fluctuations profiles (ξ_{rms}) are shown as a function of η_c at three downstream positions in Figures (17a-17b). The rms concentration fluctuations is indicative of the degree of homogeneity of the flow. If the two streams were composed of immiscible substances, then the rms concentration fluctuations would have a maximum value of 0.5. The calculated rms concentration fluctuations is lower than 0.5 but slightly higher than the measurements of M&B(1986) in Figure (17a) and close to the results of Zhou and Pereira (2000) in Figure (17b). The rms concentration fluctuation profiles exhibit bimodal shape and mixing asymmetry with respect to $\eta_c = 0$ with values on the high speed side ($\eta_c>0$) lower than the low speed side ($\eta_c<0$). This indicates that fluid mixing becomes faster as the high speed side is reached. In the simulation, the bimodal shape in the ξ_{rms} profiles together with the asymmetry with lower ξ_{rms} on the high speed side were obtained, when error function was used as inlet boundary condition for scalar field(see section 7.6).

In order to interpret the asymmetry with respect to $\eta_c = 0$ in the rms profiles, the instantaneous mixing frequency in the cross-stream location is shown in Figures (18a-18d) at several streamwise locations from x/H= 0.4 to 0.6. The mixing frequency is asymmetric about the concentration centerline with higher values biased toward the high speed side therefore leading to lower ξ_{rms} in Figures (17a-17b). Therefore the asymmetry in mixing frequency is responsible for the asymmetry of ξ_{rms} as shown also by Vanormelingen and Bulck(1999).

7.2 Mean and RMS Concentration Profiles for Smagorinsky SGS Model

Figures (19a-19b) and (20a-20b) show that the profiles of mean concentration and rms concentration fluctuations, using Smagorinsky SGS model with C_r=0.12 together with the experiment of M&B(1986) and simulation of Zhou and Pereira (2000), respectively. The profiles are similar to the results using Dynamic Eddy Viscosity SGS model. For x/H=0.4 the mean concentration profile in Figures (19a-19b) is closer to the self-preserving region unlike the results obtained using the Dynamic Eddy Viscosity SGS. This is probably due to the fact that the scalar field has developed because the more dissipative Smagorinsky SGS yields higher turbulent diffusivities and higher mixing frequency. Comparison of the results obtained using Smagorinsky SGS and Dynamic Eddy Viscosity SGS model will be discussed in next section.

7.3 Comparison of Dynamic SGS with Smagorinsky SGS Model

Figures (21a-21b) show the profiles of mean concentration and rms concentration fluctuations, using the Smagorinsky SGS model with C_r=0.12 and Dynamic Eddy Viscosity SGS model, respectively. In Figure (21a), the mean concentration exhibit triple inflection point for both Dynamic Eddy Viscosity SGS and Smagorinsky SGS in the high speed side region. The inflection point of Dynamic Eddy Viscosity SGS at about η_c=0.04 is slightly further to high speed side than that of Smagorinsky SGS. The profile of rms concentration fluctuations in Figure (21b) for Smagorinsky SGS is a slightly lower than the profile of Dynamic Eddy Viscosity SGS model, This is probably due to the fact that the Smagorinsky model is more dissipative and consequently yields higher mixing frequency than the one obtained using Dynamic Eddy Viscosity SGS.

7.4 Effect of Turbulent Schmidt Number

Numerical tests were performed to investigate the effects of varying scalar diffusion by varying S_{c_T}=0.3 and 1.0 with other parameters similar to base run. The range of S_{c_T} includes the value of 0.5

used for plane mixing layer(Launder, 1976) and the value of 0.35 for the scalar mixing layer experiment of Bilger *et al.*(1991). In Figure (21c), the mean concentration profile show that the position of inflection point of S_{c_T}=0.7 move further on high speed side than that of S_{c_T} =1.0 and that the triple inflection point profile is less pronounced for S_{c_T}=0.3. Figure (21d) shows that the profiles of rms concentration fluctuations are lowered as S_{c_T} is decreased from 1.0 to 0.3, because mixing frequency increase as S_{c_T} decreases. The profile spreads further into the free stream on high speed for S_{c_T}=0.7 and 1.0 as compared to S_{c_T}=0.3.

7.5 Effect of Constant in Mixing Frequency

The effect of constant mixing frequency was investigated by comparing the base run results C_ϕ=3.0 with the results obtained using C_ϕ=9.0 keeping all other parameters similar to base run. The mean concentration profiles in Figure (21e) exhibit triple inflection point for both C_ϕ=9.0 and C_ϕ=3.0. In Figure (21f) the profile of the rms concentration fluctuations with C_ϕ=9.0 is lower than the base run with C_ϕ=3.0. This result is expected because the mixing is enhanced as C_ϕ is increased. This causes the profile of rms concentration fluctuations to be lowered.

7.6 Effect of Inlet boundary condition

Several combination of inlet boundary conditions were tested: error function and laminar boundary layer for flow field and stepwise and error function for scalar field were tested, respectively, as shown in Table II - Inlet boundary condition test. Results are presented in Figures (22-23).

Figures (22a-22d) compare the flow field characteristics, $(U - U_L)/(U_H - U_L)$, rmsu'/ΔU, rmsv'/ΔU and $-u'v'/\Delta U^2$ profiles for both laminar boundary layer and error function as inlet boundary conditions, at x/H=0.5 and 0.6. The difference in profiles due to the different inlet boundary condition for flow field is quite small. Therefore the velocity characteristics are not significant affected by the inlet boundary conditions.

Figures (23a-23d) compare the runs using stepwise profile as inlet boundary condition for scalar field with laminar boundary layer (case 1) and error function (case 2) for flow field. Figures (23a) and (23c) show that the mean for case 1 and 2 spread less than the base run. Figures (23b) and (23d), show that the rms concentration fluctuations for case 1 and 2 results in higher peak value on the high speed side(η_c>0) as compared to the low speed side(η_c<0), which is the opposite of the results obtained using base run.

Figures (23e-23f) compare the runs using error function as inlet boundary condition for scalar field with laminar boundary layer (base run) and error function (case 3) for flow field. The mean concentration in Figure (23e) shows that the triple inflection point in case 3 is lower than the base run. Figure (23f) indicates that the trend in the rms concentration fluctuations is almost unaffected by inlet boundary condition for flow field (base run or case 3), however the profile for case 3 spreads further on both the high speed side(η_c>0) and low speed side(η_c<0).

Table II - Inlet boundary condition test

Flow field Scalar field	Laminar Boundary layer	Error Function
Error Function	Figures (23a-23f) (Base Run)	Figures (23e-23f)(Case 3)
Stepwise	Figures (23a-23b)(Case 1)	Figures (23c-23d)(Case 2)

7.7 Probability Density Function

Each particle of the ensemble N (total number of particles in the box centred at each node) is identified by a value of the concentration $0 \leq c \leq 1$. In order to obtain the probability, the range of c (0 to 1) is subdivided into 100 windows, so that any one of the particles belongs in an interval based on its value of c. The probability of finding a particle having concentration c within an interval $\xi \leq c \prec \xi + \Delta\xi$ is written as,

$$p(\xi)\ \Delta\xi = \frac{n}{N}$$

where n is the number of elements in the interval and $p(\xi)$ is the PDF. The behaviour of the ensemble of PDFs can be characterized as marching and non-marching. For marching PDFs, the most probable value on each side of the layer is closer to the free stream value of that side, whereas for the non-marching PDFs, the most probable value of the scalar is substantially independent of the position in the layer.

The PDFs of passive scalar for Dynamic Eddy Viscosity SGS model (base run), for x/H=0.4, 0.5 and 0.6, are shown in Figures (24a), (24c) and (24e) and mean concentration profiles are shown in Figures (24b), (24d) and (24f), respectively. At x/H=0.40, the PDFs in Figure (24a) have U shape in qualitative agreement with the experiment of Pickett and Ghandhi (2001). The mean concentration profile in Figure (24b) shows that there is a single inflection point at about $\eta_c=0$. In Figures (24c) and (24e), for x/H $\geq$0.5, the PDFs have intermediate peaks on high speed side ($\xi<0.5$). The PDFs are non-marching. This indicates that the mixing layer entrains and subsequently mixes more particles from the high speed side, i.e. at $\eta_c>0$, and is in agreement with the investigations of Koochesfahani and Dimotakis (1986) and Pickett and Ghandhi (2001). In Figures (24d) and (24f), on the high speed side the concentration profiles at x/H=0.6 exhibit a triple inflection point but is more pronounced than at x/H=0.5, i.e. as the flow develops.

In Figures (25a-25d), comparison of probability density function at $\eta_c>0$ for four cases: effect of downstream location, x/H=0.5 and x/H=0.6; effect of SGS model; effect of C_ϕ at x/H=0.6 and effect of S_{c_T} at x/H=0.6.

Figure (25a) for base run shows the peak on high speed side moves from $\xi=0.18$ for x/H= 0.5 to $\xi=0.23$ for x/H= 0.6. Also the peak value is higher for x/H=0.6 than for x/H= 0.5 in agreement with M&B(1986). Figure (25b) compares PDFs obtained using Smagorinsky SGS model with base run using Dynamic Eddy Viscosity SGS model. For Smagorinsky SGS model, the peak is higher than the base run. And also the position of the peak on high speed side is closer to the mean value ($\xi=0.5$) than the one obtained for base run. This is probably due to the fact that Smagorinsky SGS model is more dissipative and consequently results in higher mixing frequency than Dynamic Eddy Viscosity SGS model. Higher mixing results in higher probabilities at peaks and also peak positions closer to the mean value ($\xi=0.5$). Figure (25c) compares PDFs obtained using $C_\phi=9.0$ in mixing frequency with base run using $C_\phi=3.0$. The peak is higher than the one obtained using base run and the peak value get close to the mean value ($\xi=0.5$). This results is expected because as mixing is enhanced. The effect of varying S_{c_T} is shown in Figure (25d). As S_{c_T} is decreased, the peak values are higher and the locations of peak move to the mean value ($\xi=0.5$). It indicates the mixing is enhanced by decreasing S_{c_T} leading to higher mixing frequency.

The behaviour of the PDFs is sensitive to the inlet boundary conditions. Figures (26a-26f) show the PDFs profiles with different inlet boundary conditions for flow and scalar field, respectively. The run using stepwise profile as inflow boundary layer for scalar field with laminar boundary layer (case 1) and error function (case 2) for flow field are shown in Figures (26a-26d). For case 1 in Figure (26a), the PDFs at x/H=0.6 for stepwise profile show peak at about $\xi=0.5$ on low speed side for $\eta_c<0$ and the PDFs at x/H=0.5 have U shape without peak. In Figure (26b) on high speed side for η_c>0, the PDFs have U shape for both x/H=0.5 and x/H=0.6. For case 2 in Figures (26c) and (26d), the PDFs trends are similar to case 1 in Figures (26a-26b). The runs using error function as inflow boundary layer for scalar field with laminar boundary layer(Base Run) and error function (case 3) for flow field are shown in Figures (25a) and (26e-26f), respectively. The peaks are higher for case 3 in Figure 26(f) compared to base run in Figure 18(a), and in Figure (26e) on low speed side for η_c <0, the results are similar to high speed side η_c>0.

Chapter 8

Conclusions and Recommendations

8.1 Conclusions

A LES based on the diffusion-velocity method for the vorticity equation in conjunction with an eddy viscosity SGS model has been developed. The methodology was tested using a spatially developing mixing layer. In the context of the vortex method, the SGS terms in the vorticity equation produce convection of vortex particles governed by the diffusion velocity. The two-dimensional vortex-in-cell in conjunction with the Smagorinsky SGS model and Dynamic Eddy Viscosity SGS model has been used to calculate the flow characteristics. The diffusion velocity requires one constraint, i.e., nullifying it in regions of small vorticity and non-zero vorticity gradients.

Without SGS model, the results using the diffusion velocity method are in agreement with those using the random walk, a fundamentally different approach. The dissipative effect of the SGS model produced by the diffusion velocity was demonstrated by the slower momentum thickness development, lower contour values and cross-stream profiles for spanwise vorticity, lower cross-stream profiles for rms longitudinal and lateral velocity fluctuations as the eddy viscosity from SGS model is increased. The Smagorinsky SGS model is more dissipative than the Dynamic Eddy Viscosity SGS model due to the bigger constant C_r^2 in Smagorinsky SGS compared to Dynamic Eddy Viscosity SGS. The self-similarity of rms velocity fluctuation using Dynamic Eddy Viscosity SGS model are better than those using Smagorinsky SGS model and is consistent with previous numerical simulation when the SGS model is used. The effect of anisotropic and isotropic computational grids is in agreement with previous numerical simulations.

A two-dimensional LES based on the filtered density function(FDF) for concentration (or scalar) has been used to predict the scalar field of spatially growing mixing layer together with the LES based Vortex-In-Cell(VIC) for flow field. Subgrid Convective terms in FDF are modelled using the conventional gradient diffusion model following the eddy diffusivity concept for an anisotropic flow. The FDF transport equation has been solved using Langrangian Monte Carlo scheme. The development of the boundary layers from the splitter plate is included in the calculations by assuming an error function for scalar field at inflow. The mean and rms concentration fluctuation profiles in the self-preserving region are in good agreement with the previous experimental measurements and numerical simulations. The simulation predicts that the scalar mixing region extends further into the free stream than does the momentum mixing region, indicating enhanced transport of scalar over momentum. As mixing is enhanced, the PDFs peak are higher and closer to mean value ($\xi = 0.5$) and the rms are lowered. The rms concentration obtained using Dynamic Eddy Viscosity SGS model is lower than Smagorinsky SGS because of less dissipation. The mean concentration profiles have an inflection point on high speed stream side. The rms concentration profiles exhibit mixing asymmetry with bimodal shape, with the high speed fluid mixing at a faster rate than the low speed fluid. The bimodal shape and asymmetry in rms concentration fluctuation profiles are sensitive to the inlet boundary condition and mixing frequency, with the combination of inflow laminar boundary layer for flow field and error function for scalar field giving profiles close to experiments and previous simulations. As the flow develops in the downstream direction, the PDFs develop from an initial U shape to PDFs exhibiting peaks biased toward the high speed side and non-marching behave. This indicates that the mixing layer entrains and subsequently mixes larger quantities of high speed fluid.

8.2 Recommendations

From this study, there are aspects that could be investigated to improve the methodology: (1) The linear mean square estimation (LMSE) or the interaction by exchange with mean (IEM) could be used as molecular mixing model and the effect shall be investigated; (2) In the Lagrangian approach, the mean is first calculated as the arithmetic average over the particles in a box centred at the node, then the mean is transferred from node to the particles at the particles' location using area-weighting scheme. Another approach suggested by Möbus *et al.*(2001) does not require to calculate the mean at the nodes but estimates the mean at each particle's location as the value obtained from a least-square fit of particles within a box. This needs further investigation; (3) To investigate the spatially developing chemical reacting flows with the method.

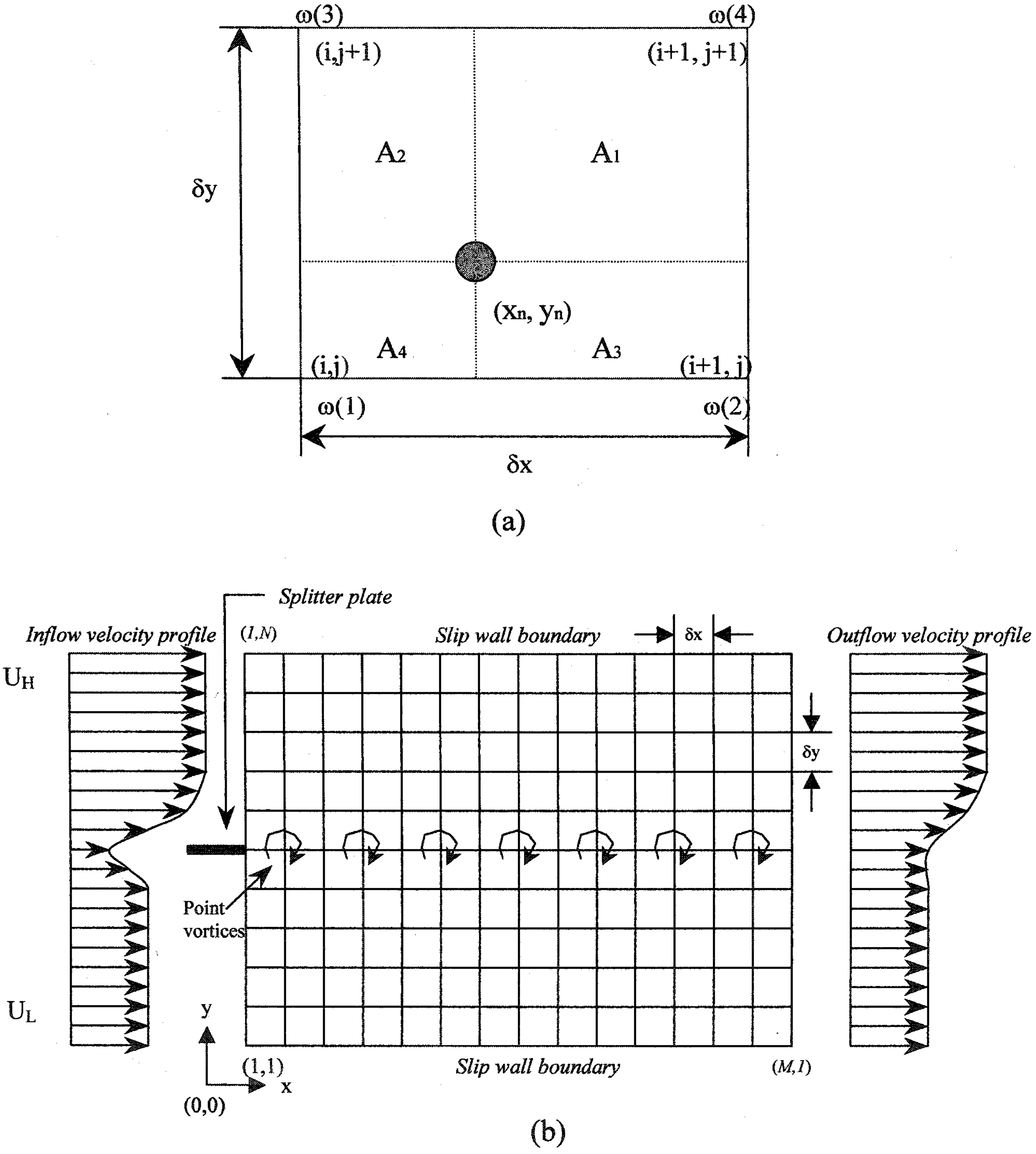

Figure 1. (a) Two-dimensional area-weighting scheme in the VIC method. (b) Computational domain, rectangular grid, initial position of the vortices, and boundary conditions.

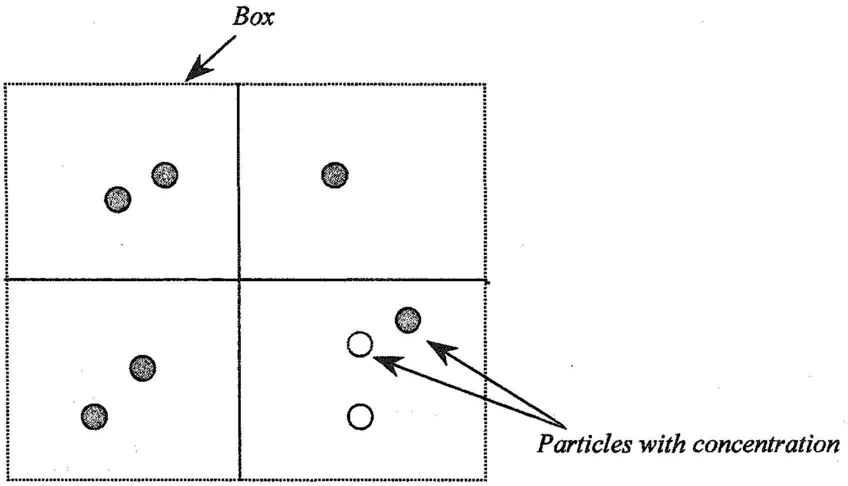

(a)

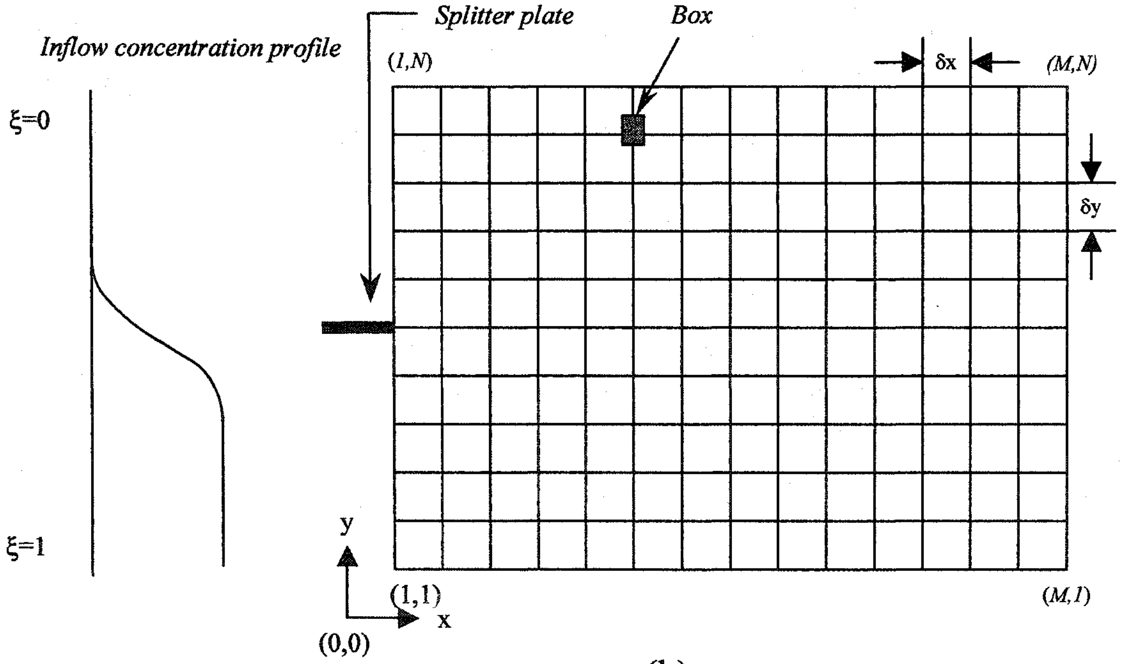

(b)

Figure 2. (a) Box centered at node and particles with concentration distribution.
(b) Computational domain, rectangular grid, box and boundary condition for scalar field.

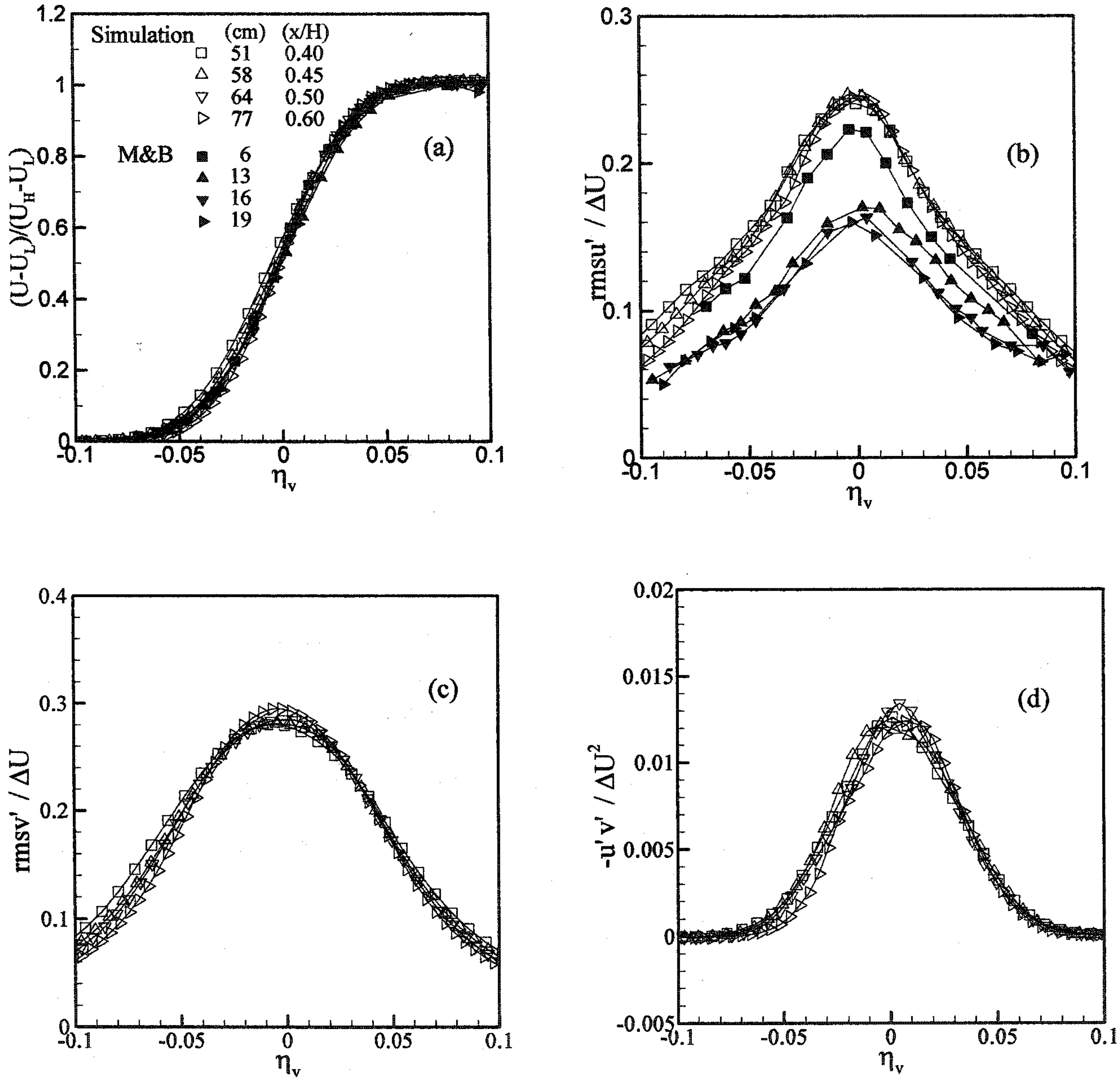

Figure 3. Normalized velocity profiles at four downstream locations for case without SGS: (a) streamwise mean velocity, (b) rms longitudinal velocity fluctuations, (c) rms lateral velocity fluctuations, (d) negative cross-stream correlation. The mesh lines connecting the open symbols show the predicted profiles; the dark symbols correspond to the data from the experiment of M&B.

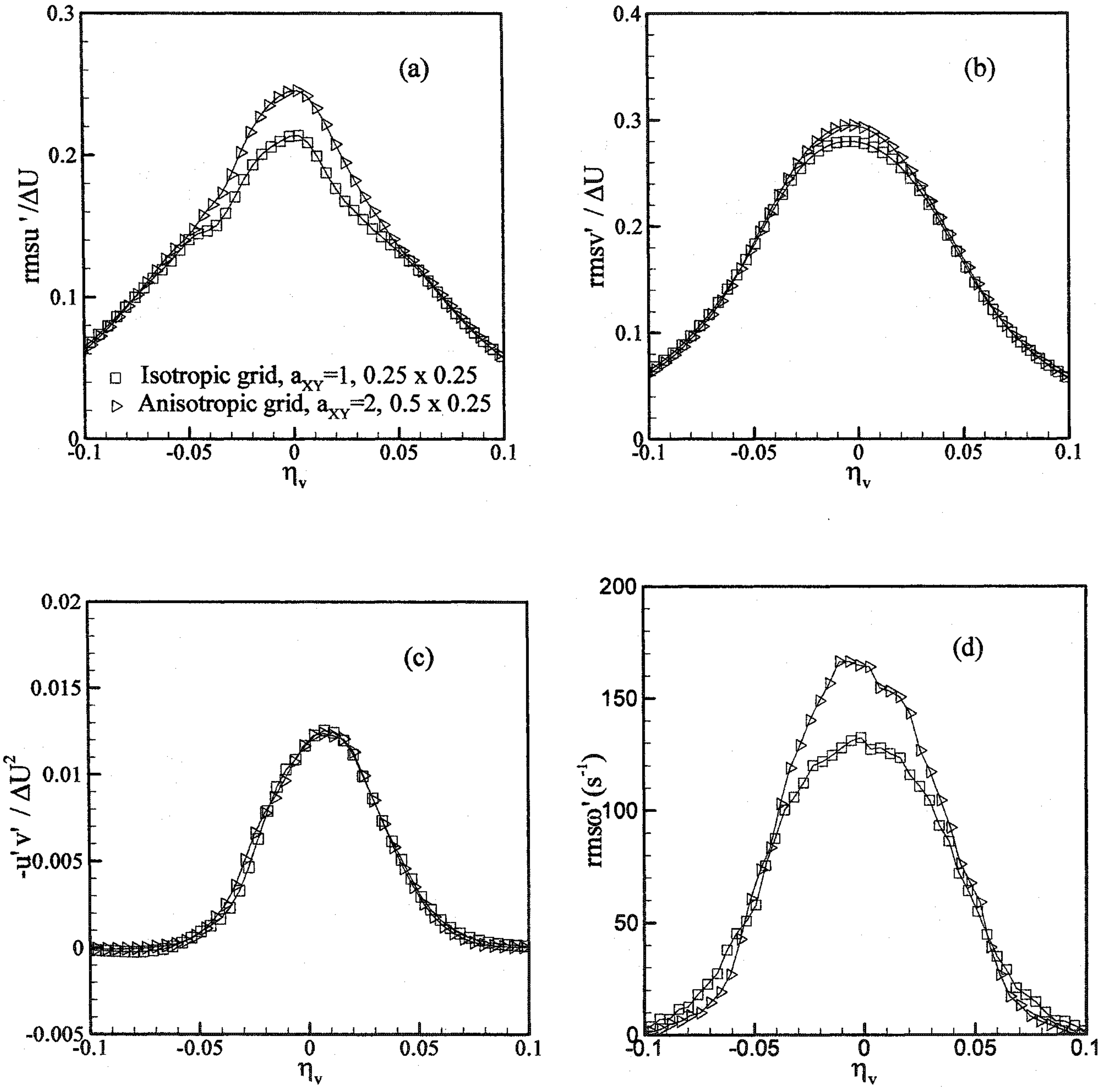

Figure 4. Sensitivity to aspect ratios (a) rms longitudinal velocity fluctuations, (b) rms lateral velocity fluctuations, (c) negative cross-stream correlation, and (d) rms vorticity fluctuations for case without SGS at x/H=0.6.

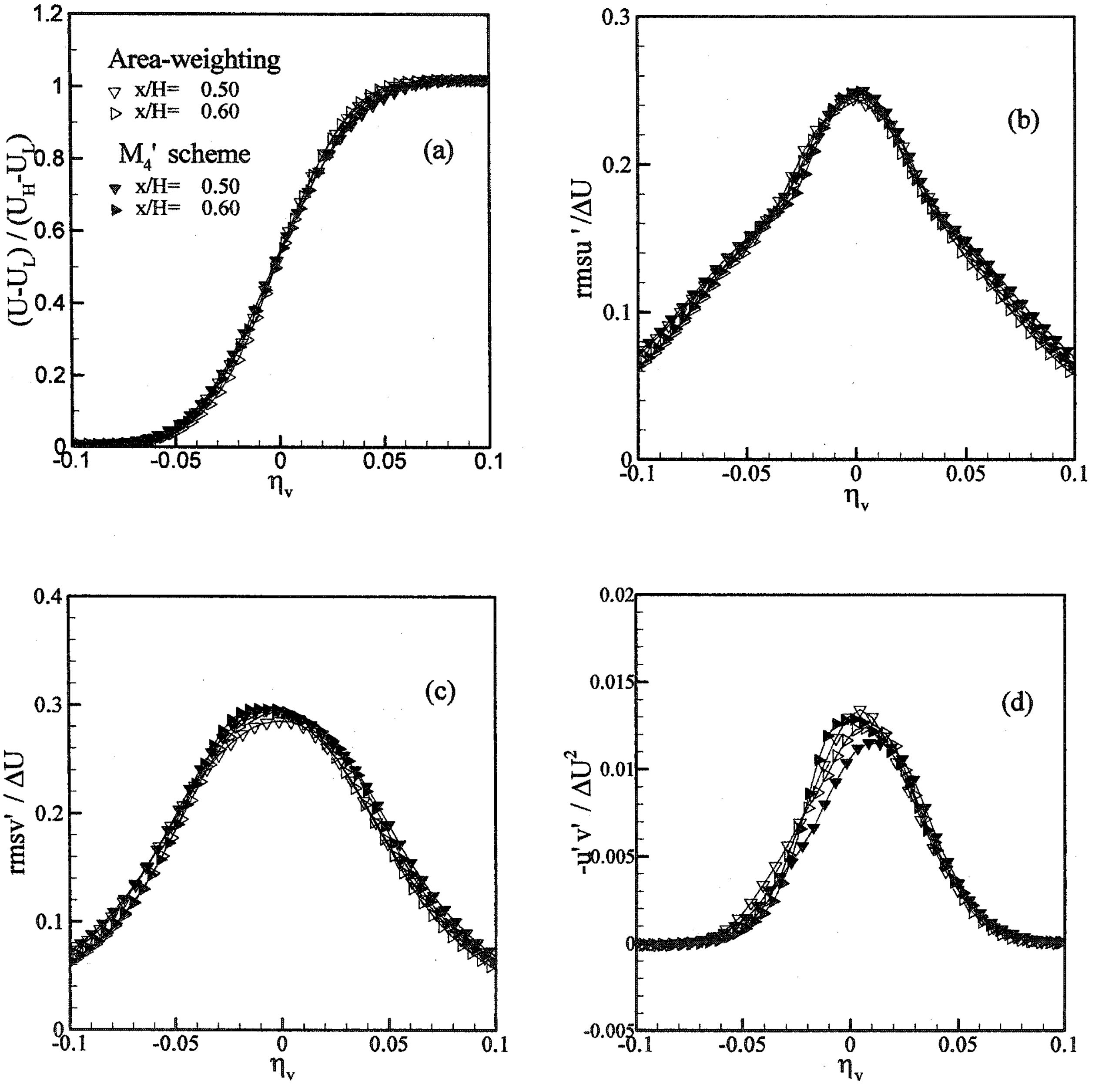

Figure 5. Comparison of area-weighting scheme with M$_4$' scheme using diffusion velocity method without SGS model at two downstream locations: (a) streamwise mean velocity, (b) rms longitudinal velocity fluctuations, (c) rms lateral velocity fluctuations, (d) negative cross-stream correlation. Dark symbols, M$_4$' scheme; open symbols, area-weighting scheme.

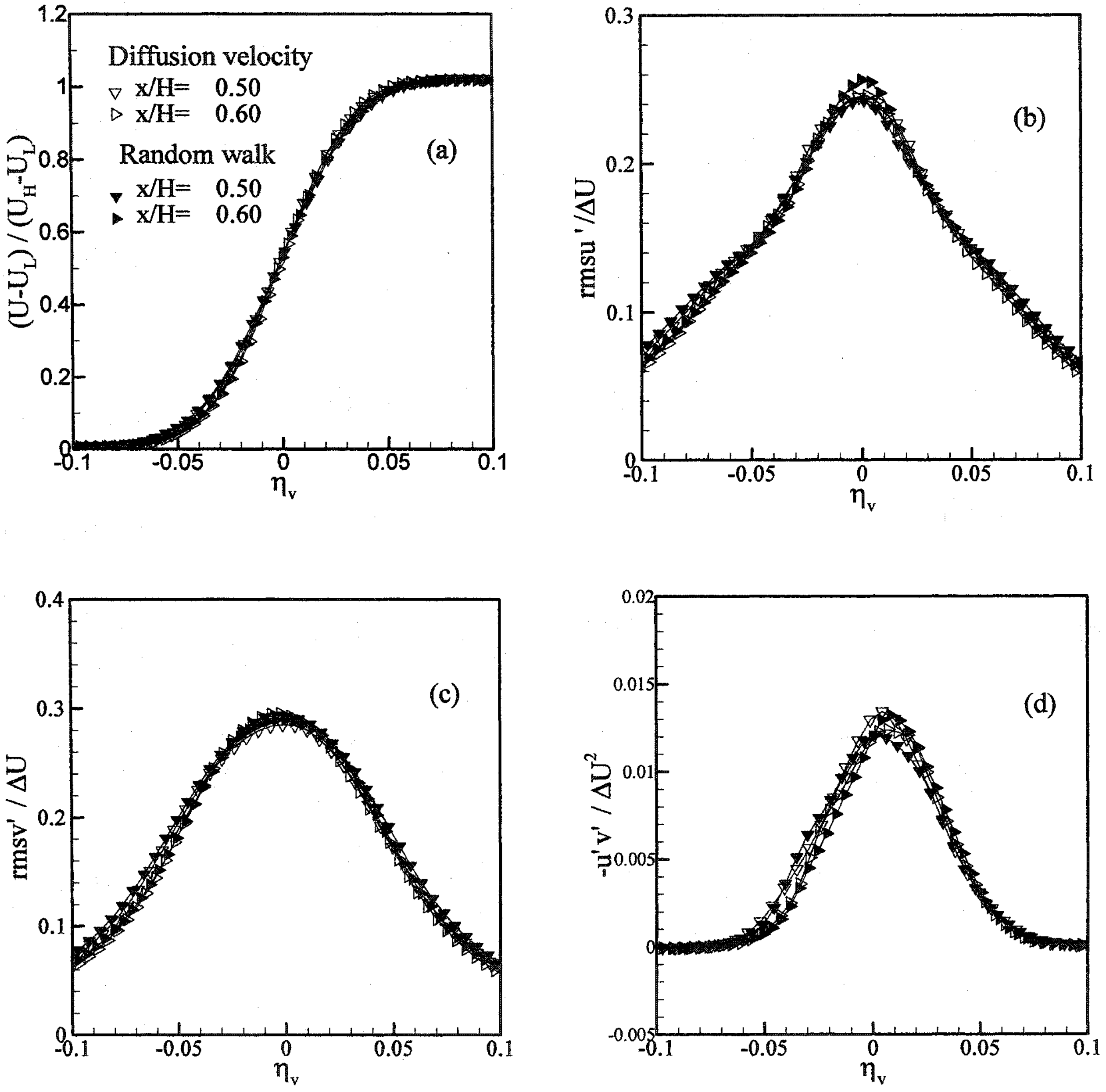

Figure 6. Comparison of diffusion velocity method with random walk at two downstream locations: (a) streamwise mean velocity, (b) rms longitudinal velocity fluctuations, (c) rms lateral velocity fluctuations, (d) negative cross-stream correlation. Open symbols, diffusion velocity method; dark symbols, random walk.

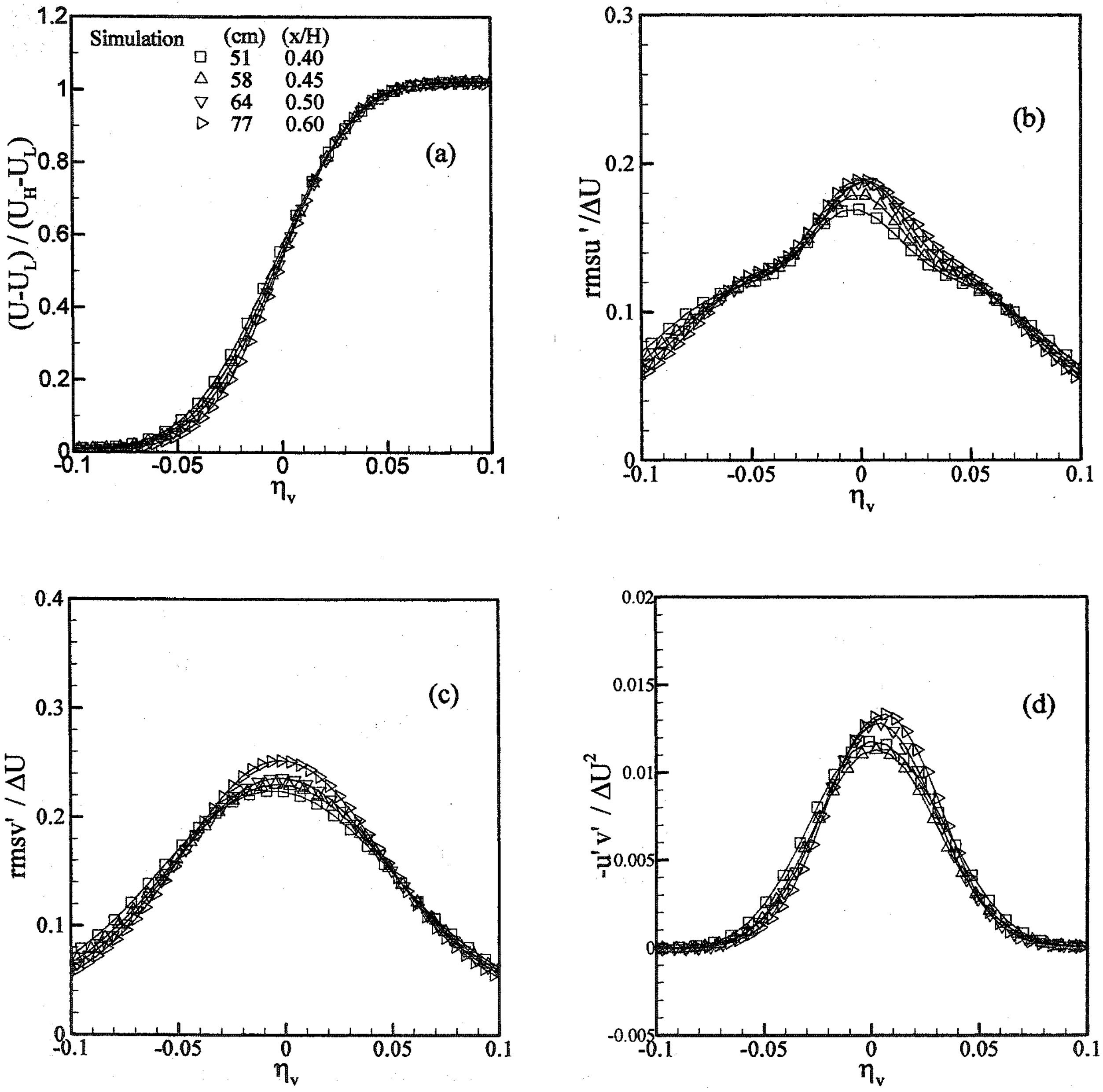

Figure 7. Normalized velocity profiles at four downstream locations for case with Smagorinsky SGS(C_r=0.12): (a) streamwise mean velocity, (b) rms longitudinal velocity fluctuations, (c) rms lateral velocity fluctuations, (d) negative cross-stream correlation.

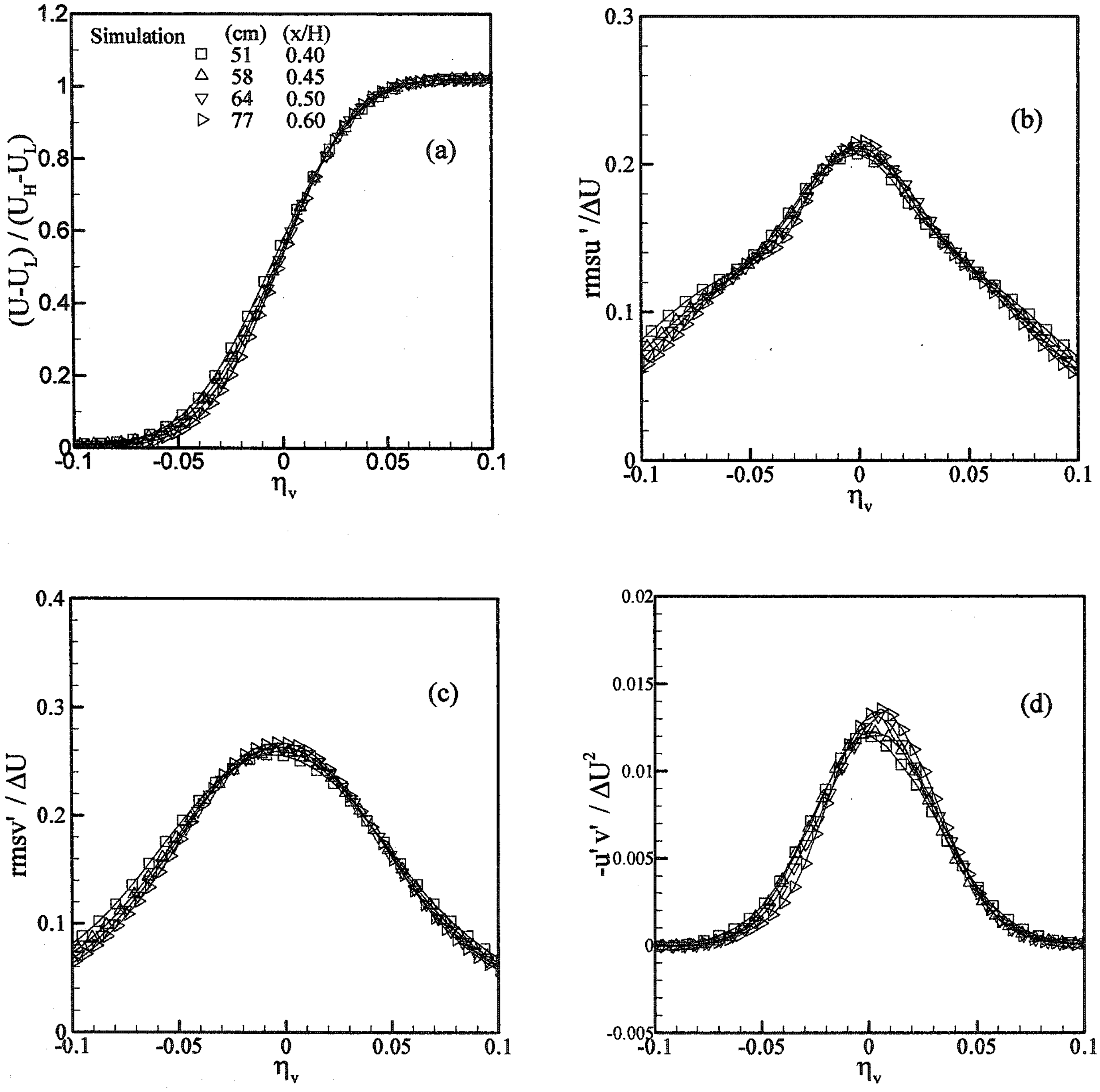

Figure 8. Normalized velocity profiles at four downstream locations for case with Dynamic Eddy Viscosity SGS: (a) streamwise mean velocity, (b) rms longitudinal velocity fluctuations, (c) rms lateral velocity fluctuations, (d) negative cross-stream correlation.

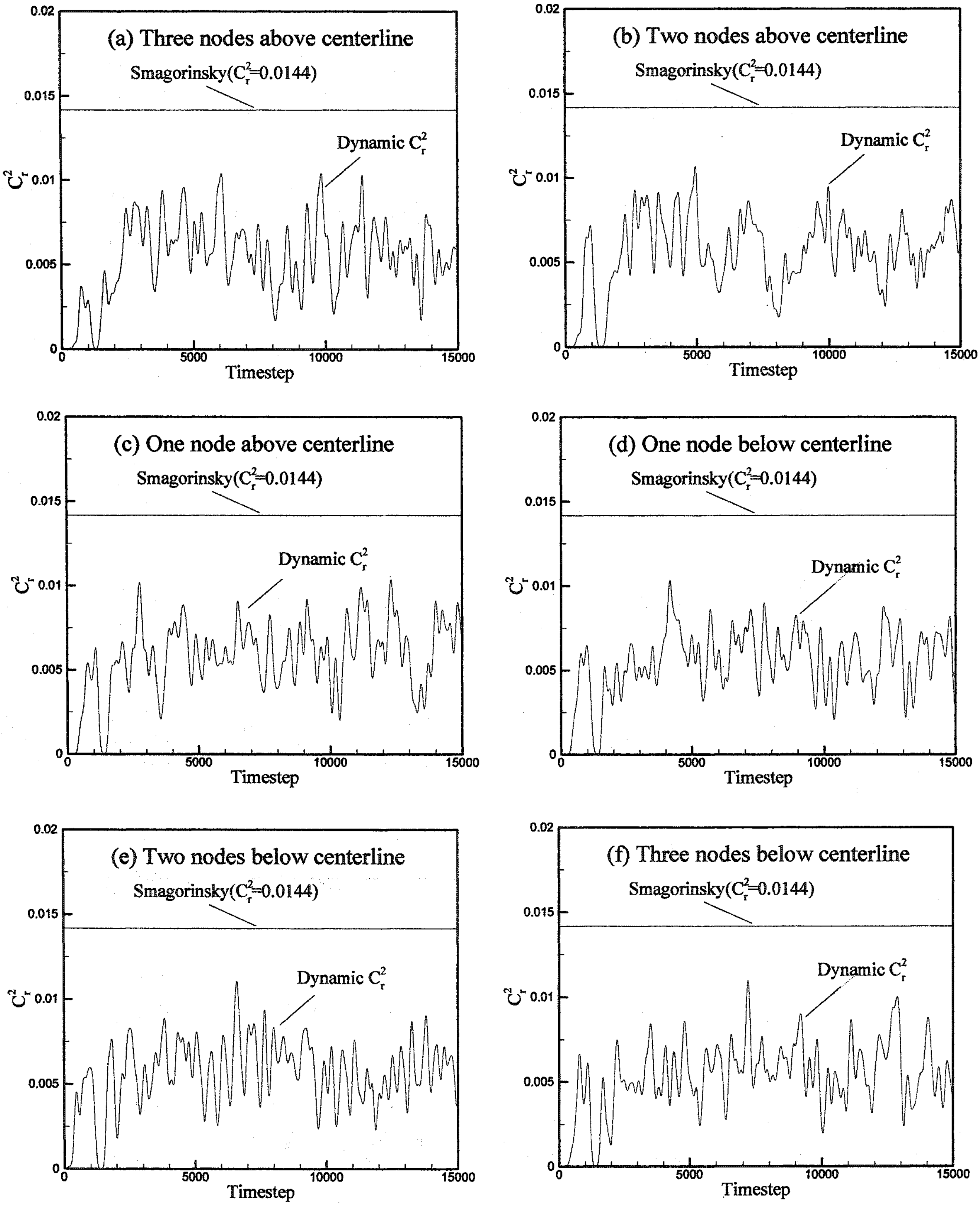

Figure 9. Dynamic constant C_r^2 calculated at six nodes around centerline at x/H=0.6

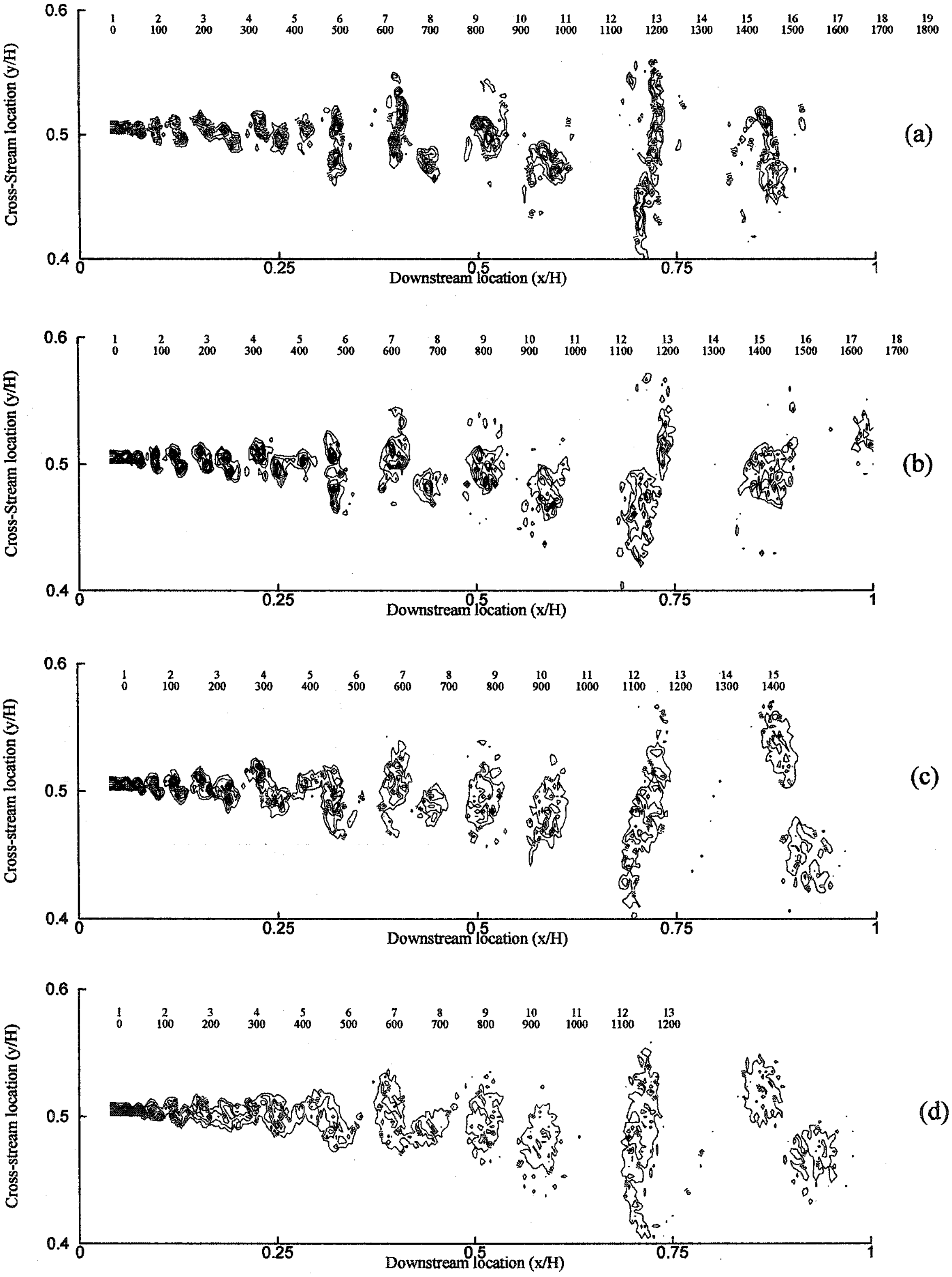

Figure 10. Vorticity contours for cases (a) without SGS, (b) with Dynamic Eddy Viscosity SGS, (c) with Smagorinsky SGS using C_r=0.12, (d) with Smagorinsky SGS using C_r=0.18. Contour level increment is 100.

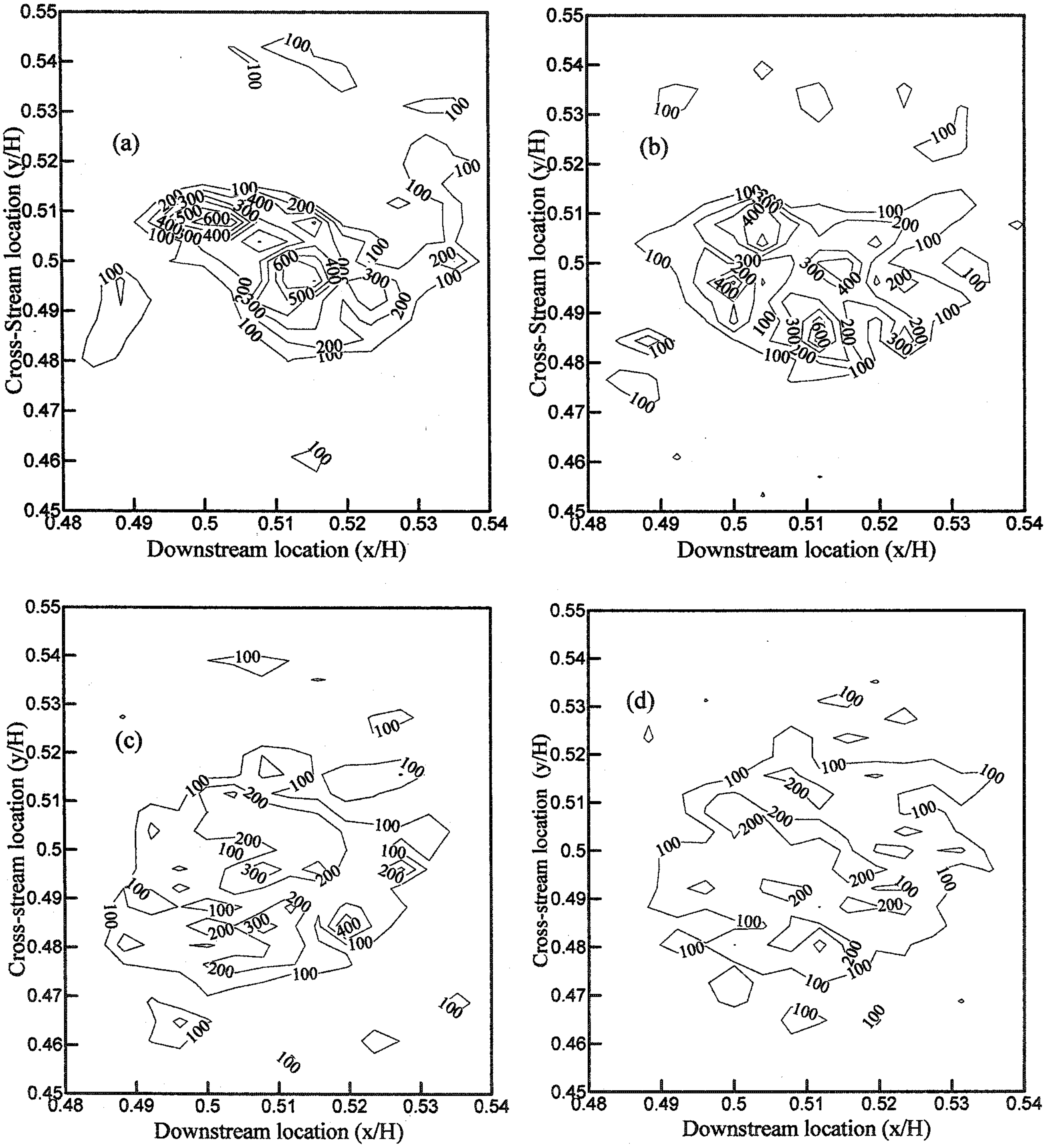

Figure 11. Vorticity contours at selected downstream location for cases (a) without SGS, (b) with Dynamic Eddy Viscosity SGS, (c) with Smagorinsky SGS using C_r=0.12, (d) with Smagorinsky SGS using C_r=0.18. Contour level increment is 100.

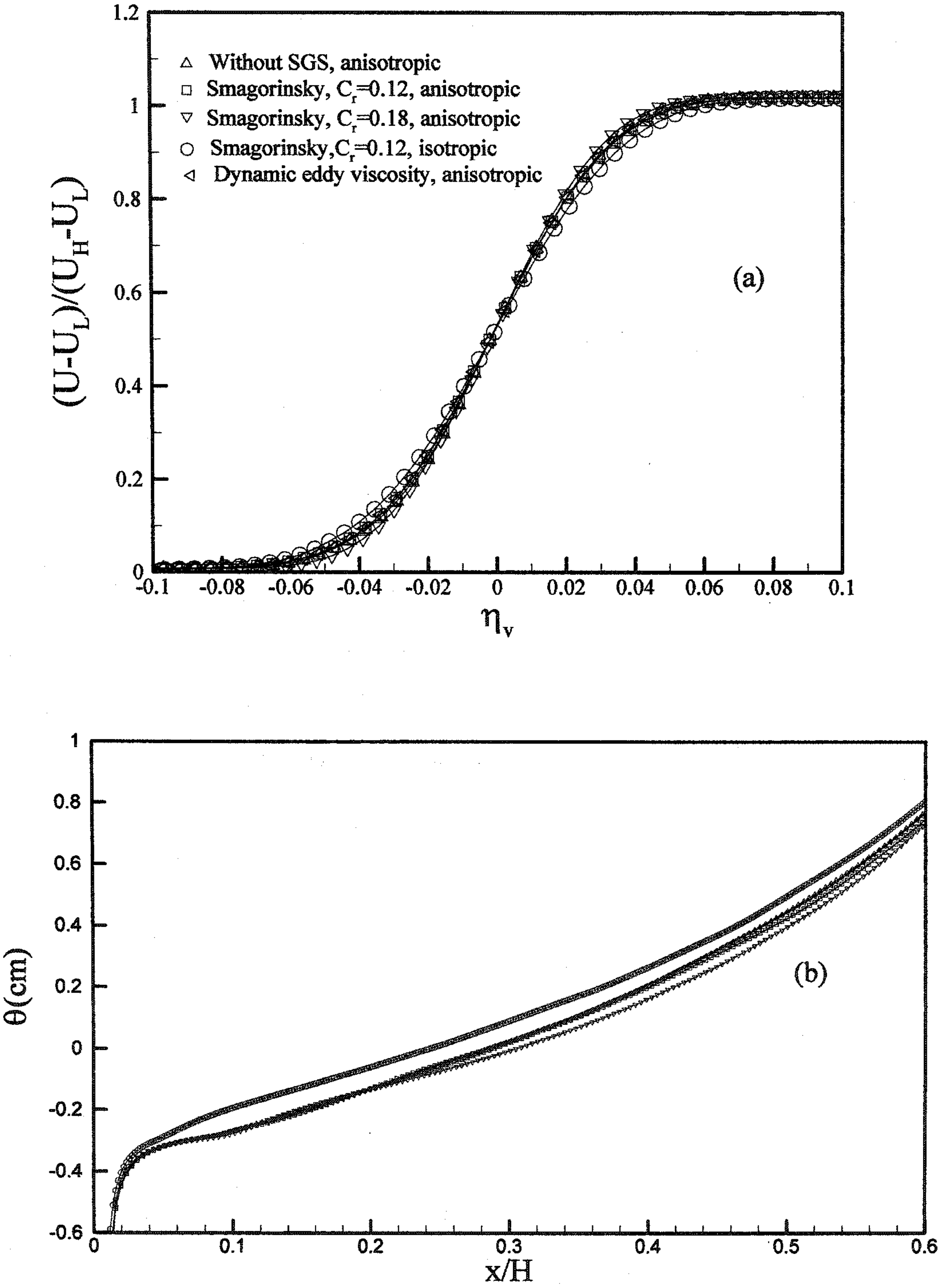

Figure 12. Comparison of profiles with and without SGS: (a) streamwise mean velocity at x/H=0.6, (b) downstream evolution of momentum thickness.

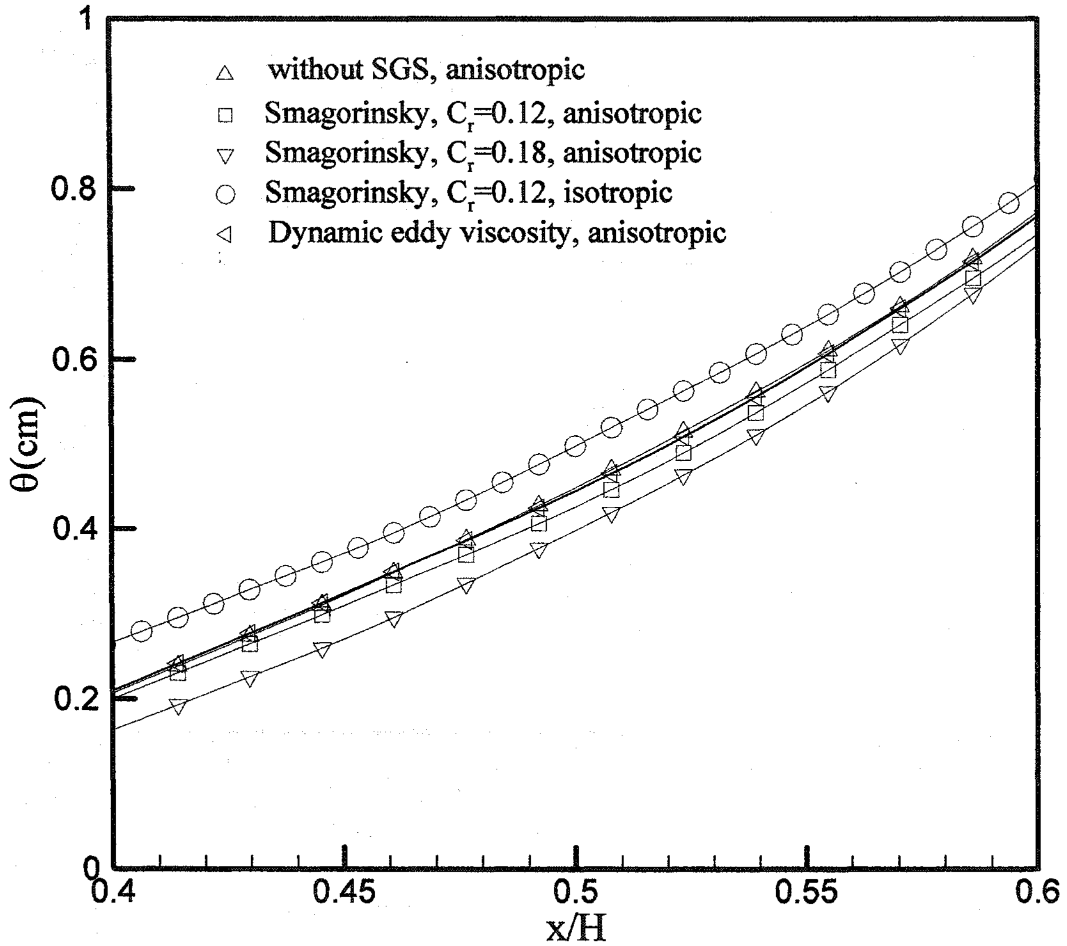

Figure 13. Comparison of profiles with and without SGS, downstream evolution of momentum thickness for $0.4 \le x/H \le 0.6$.

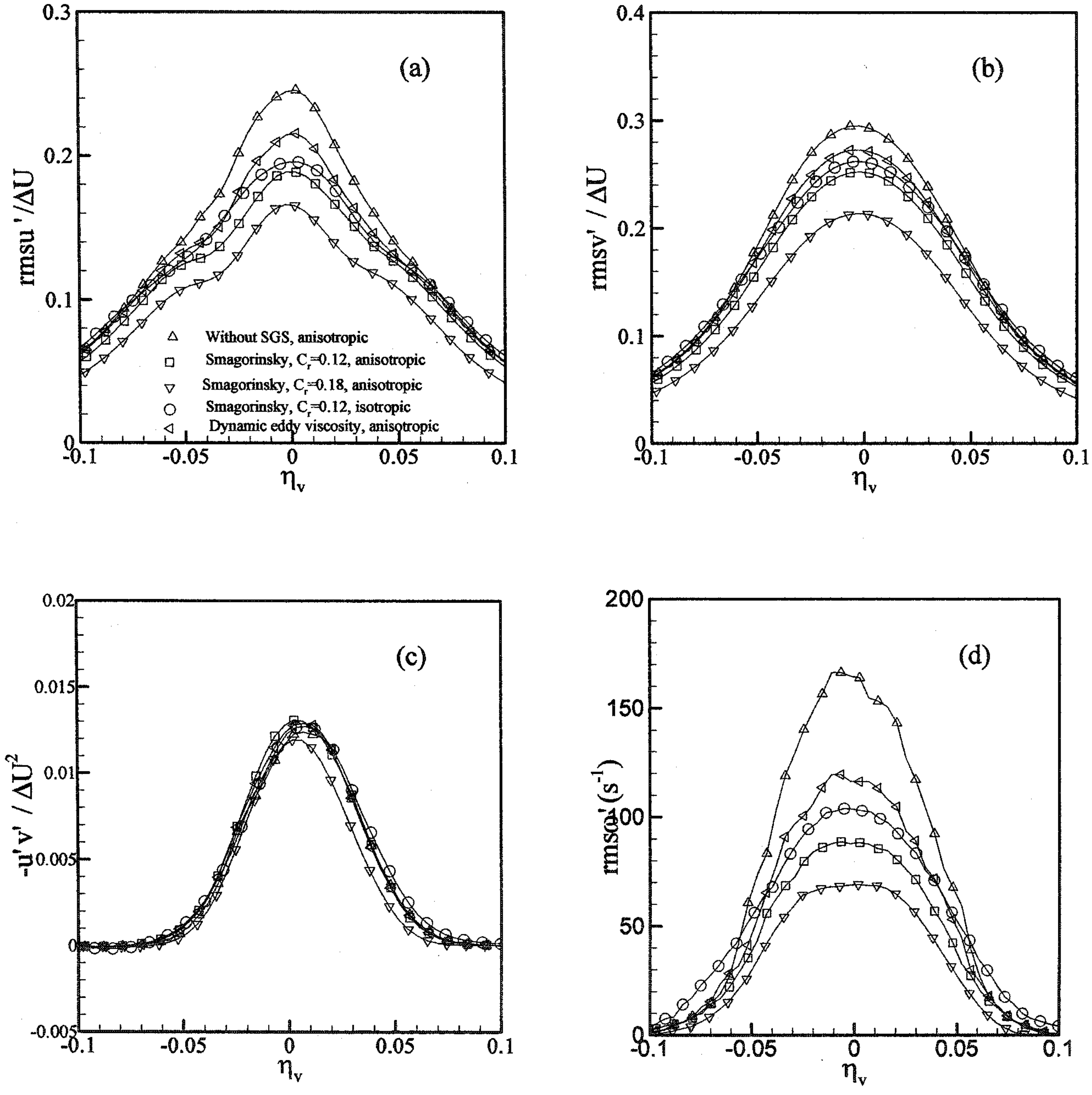

Figure 14. Effect of constant in SGS model and grid on: (a) rms longitudinal velocity fluctuations, (b) rms lateral velocity fluctuations, (c) negative cross-stream correlation, (d) rms vorticity fluctuations at x/H=0.6.

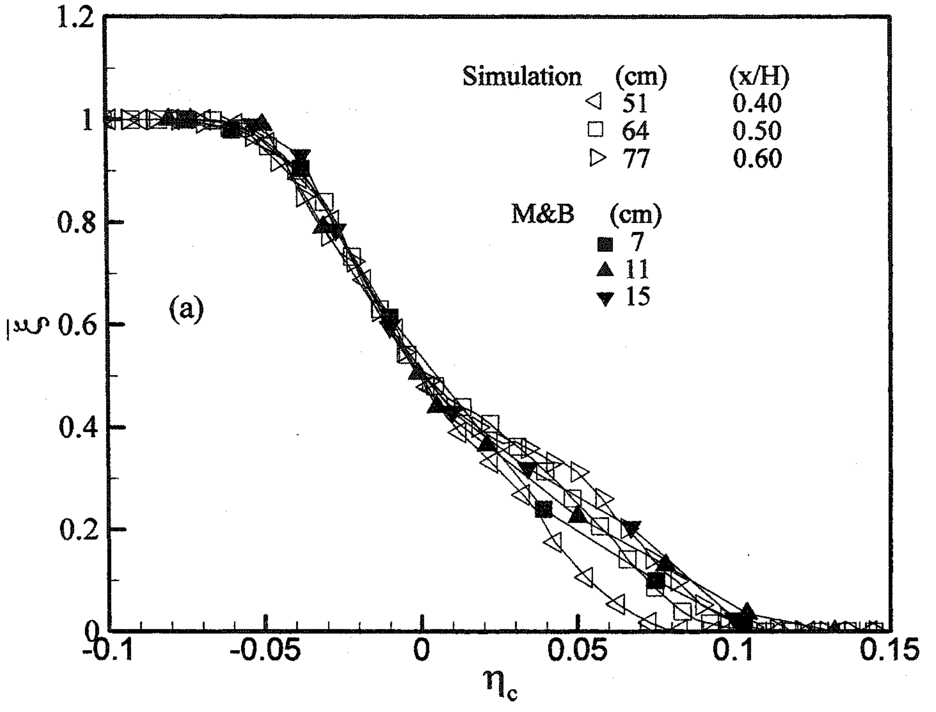

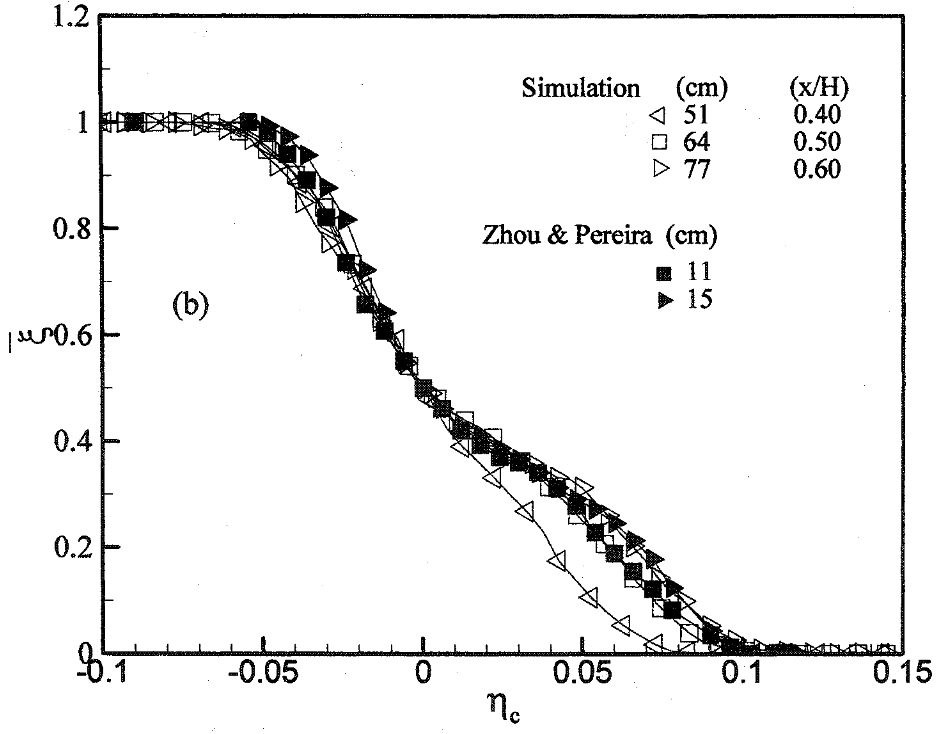

Figure 15. Mean concentration profiles at three downstream locations for base run: (a) comparison with the data from the experiment of M&B(1986), (b) comparison with the numerical simulation of Zhou and Pereira (2000).

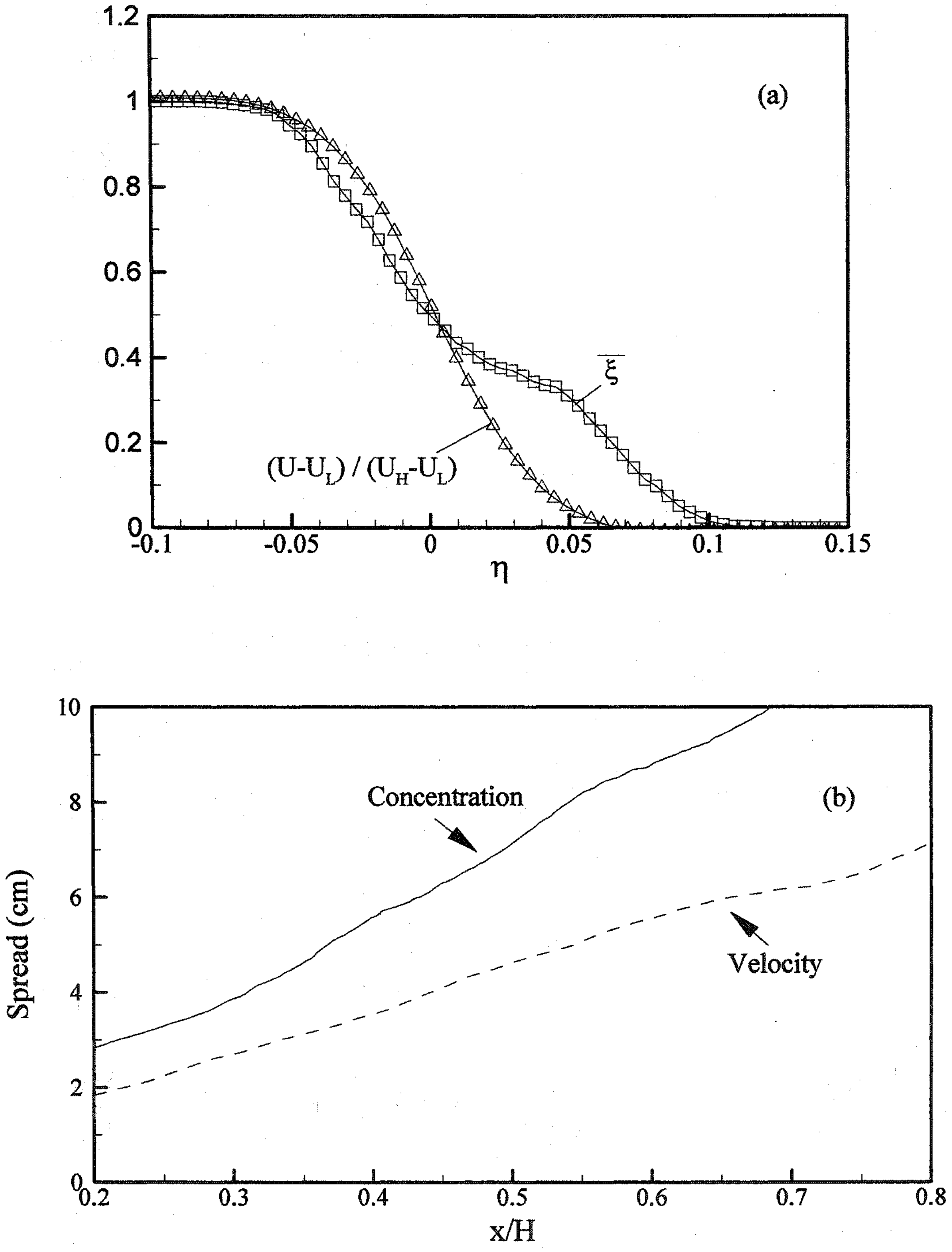

Figure 16. (a) Mean concentration profile and normalized mean velocity profile at x/H=0.6 for base run, (b) spread of concentration and velocity for base run.

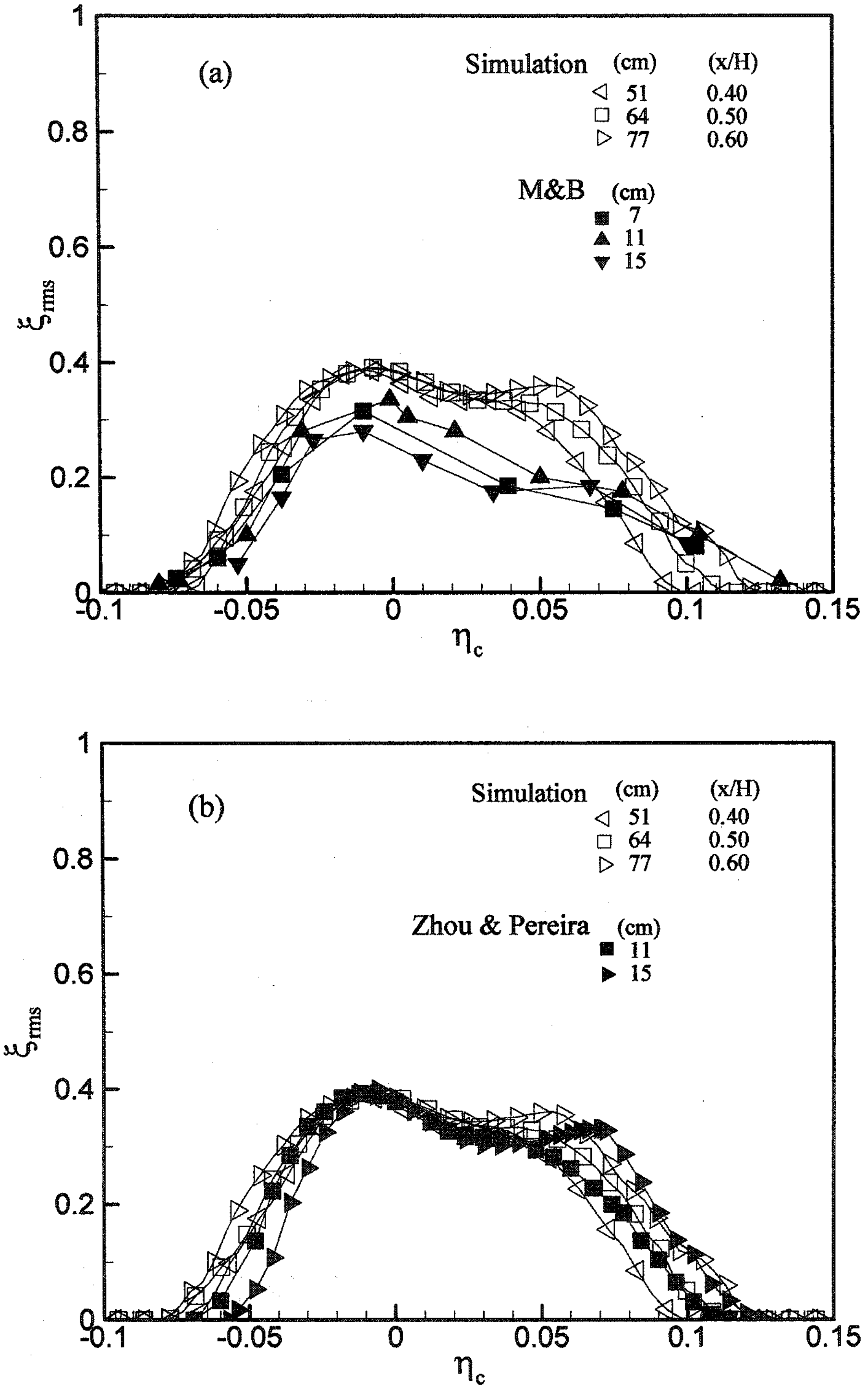

Figure 17. RMS concentration fluctuations profiles at three downstream locations for base run: (a) comparison with the data from the experiment of M&B(1986), (b) comparison with the numerical simulation of Zhou and Pereira(2000).

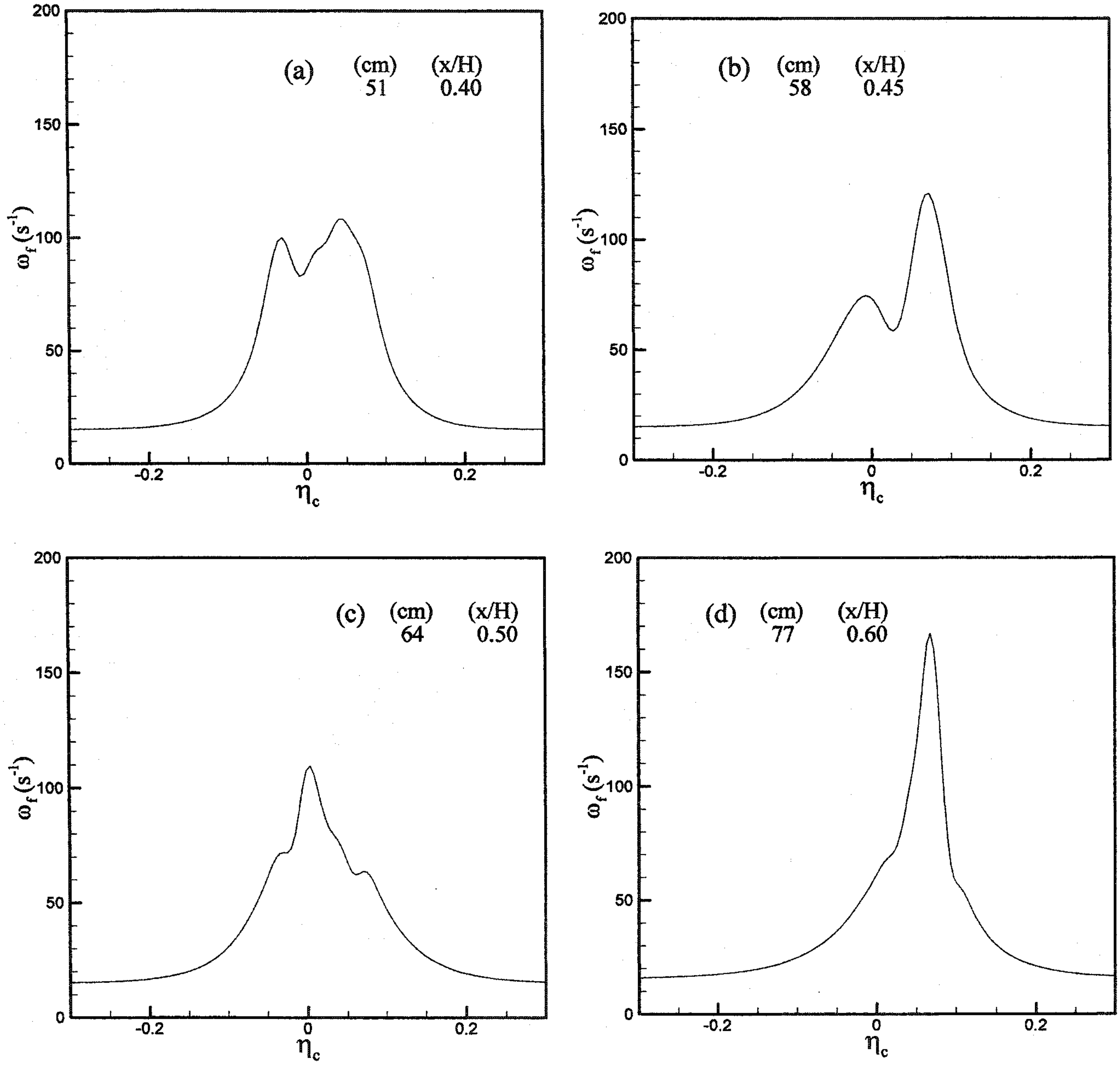

Figure 18. Profiles of mixing frequency versus η_c at several downstream locations: (a) x/H=0.40, (b) x/H=0.45, (c) x/H=0.50, (d) x/H=0.60.

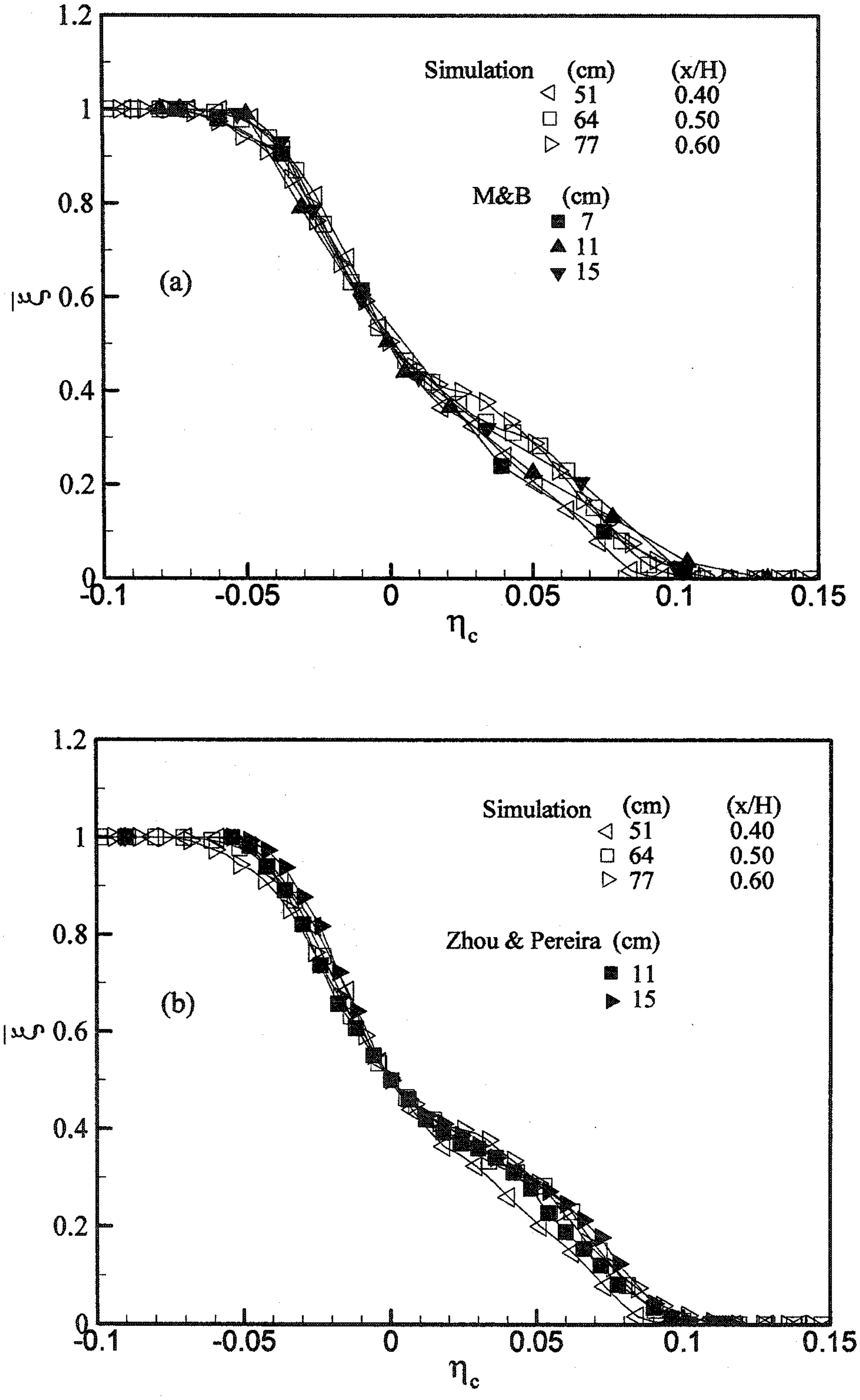

Figure 19. Mean concentration profiles at three downstream locations using Smagorinsky SGS (C_r=0.12): (a) comparison with the data from the experiment of M&B(1986), (b) comparison with numerical simulation of Zhou and Pereira (2000).

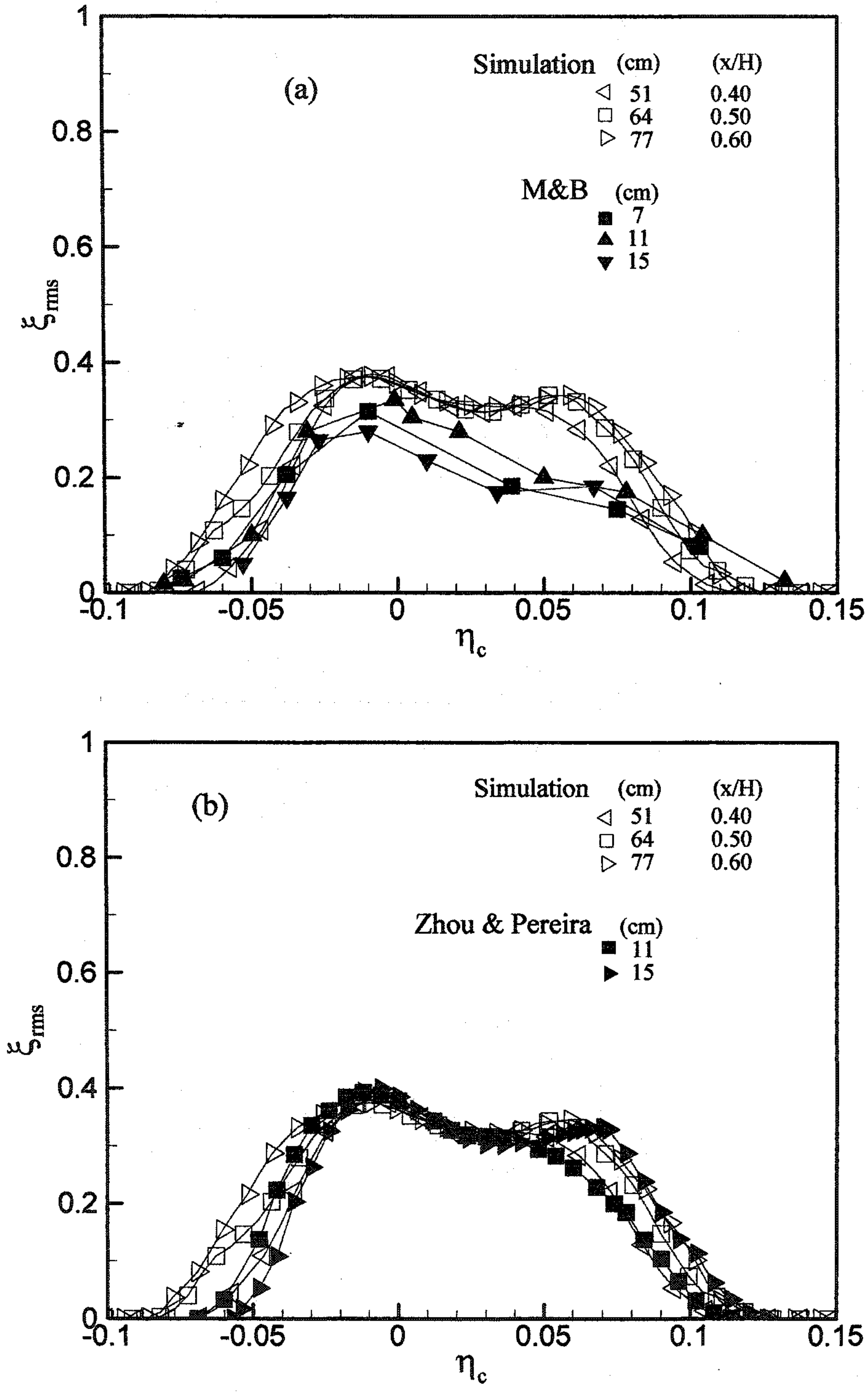

Figure 20. RMS concentration fluctuations profiles at three downstream locations using Smagorinsky SGS (C_r=0.12): (a) comparison with the data from the experiment of M&B(1986), (b) comparison with the numerical simulation of Zhou and Pereira(2000).

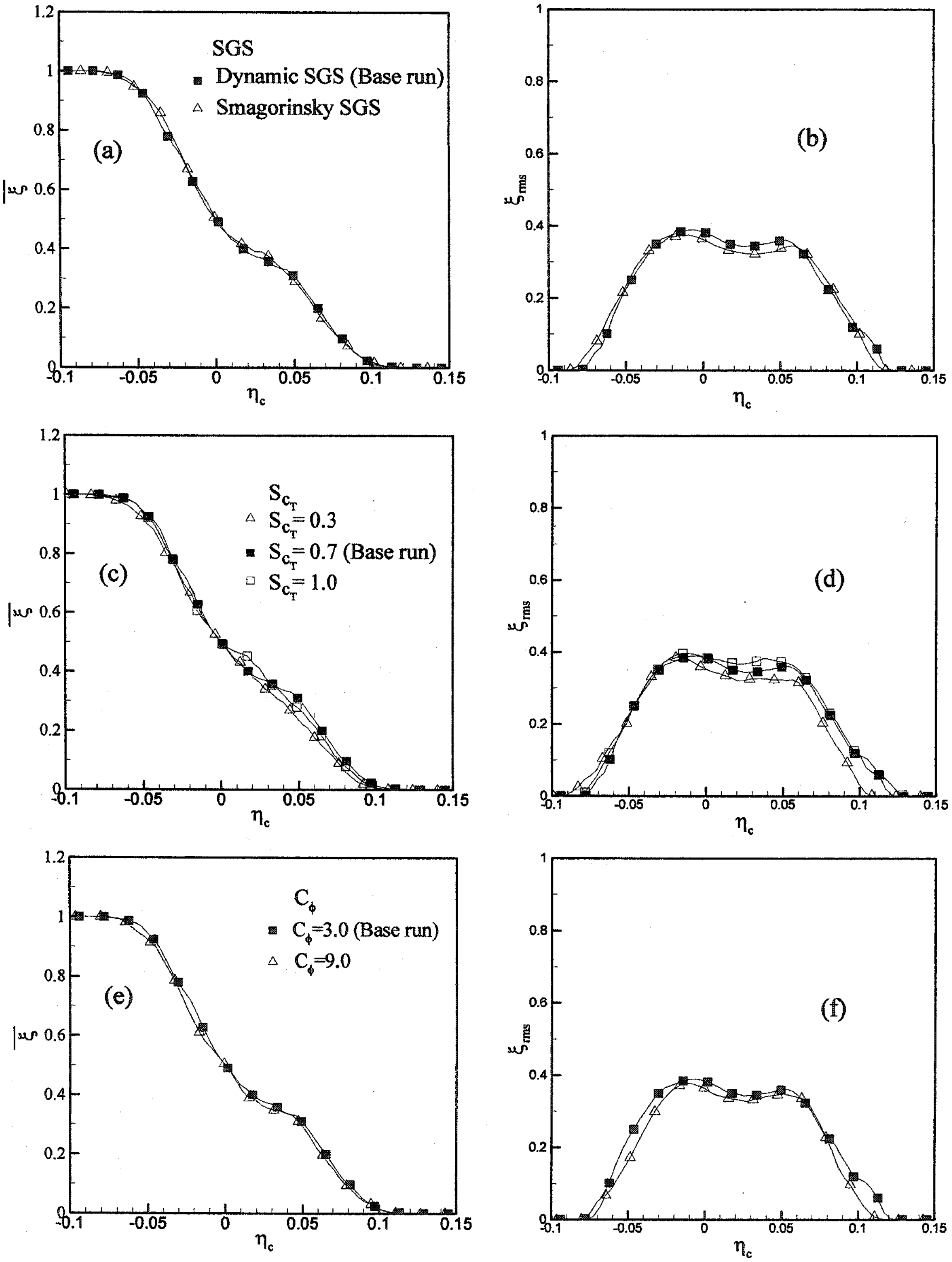

Figure 21. Comparison of mean concentration profiles: (a) effect of SGS; (c) effect of Schmidt number (S_{c_T}), (e) effect of constant (C_ϕ) in mixing frequency, at x/H=0.60. Comparison of rms concentration fluctuations profiles: (b) effect of SGS; (d) effect of Schmidt number (S_{c_T}), (f) effect of constant (C_ϕ) in mixing frequency, at x/H=0.60.

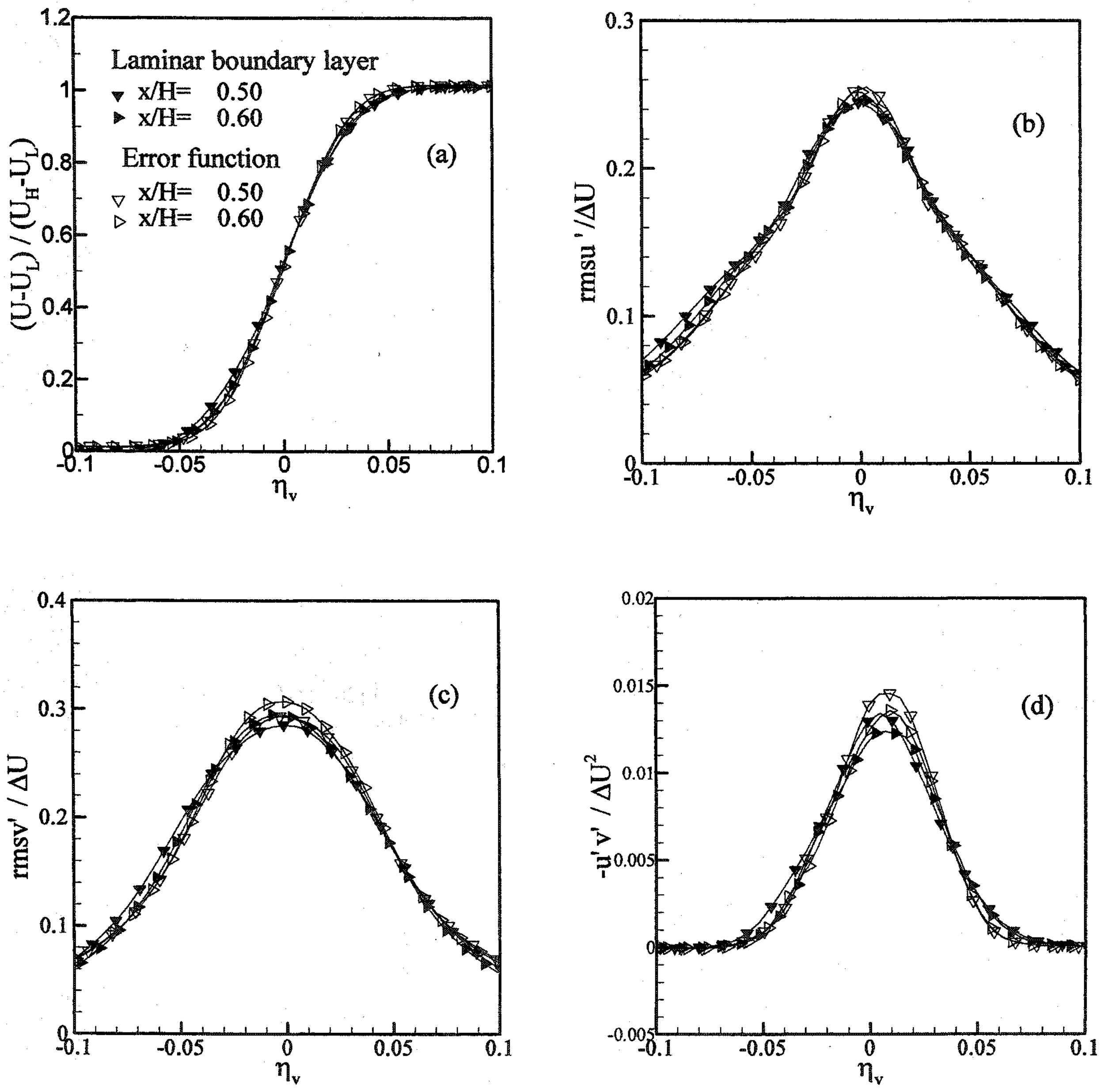

Figure 22. Effect of inlet boundary conditions on flow field, laminar boundary layer versus error function at two downstream locations: (a) streamwise mean velocity, (b) rms longitudinal velocity fluctuations, (c) rms lateral velocity fluctuations, (d) negative cross-stream correlation. Open symbols, error function; dark symbols, laminar boundary layer.

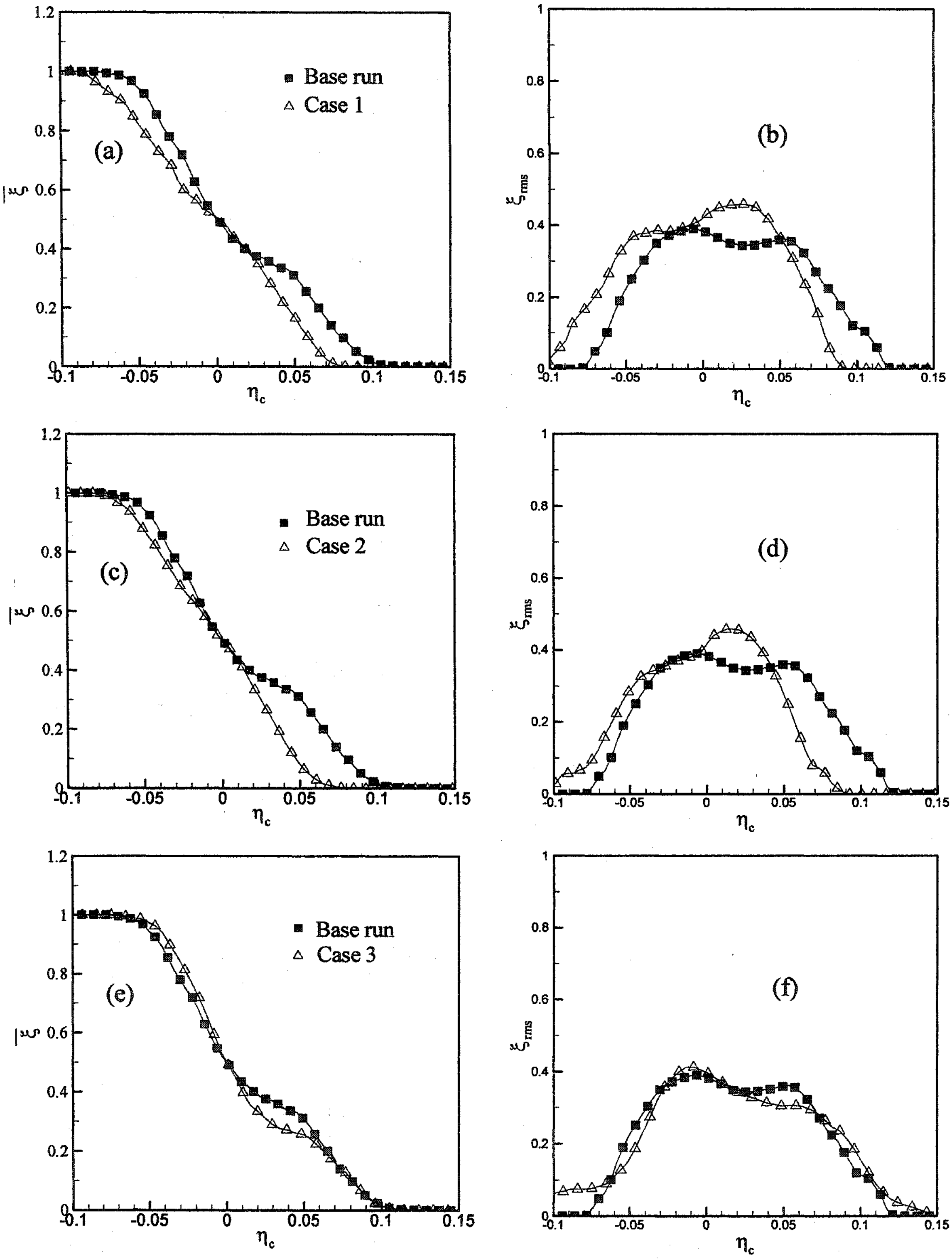

Figure 23. Effect of inlet boundary conditions: (a,c,e) mean concentration profiles, (b,d,f) rms concentration fluctuations profiles, at x/H=0.60.
Base run: Laminar boundary layer flow field and error function scalar field.
Case 1: Laminar boundary layer flow field and stepwise scalar field.
Case 2: Error function flow field and stepwise scalar field.
Case 3: Error function flow field and error function scalar field.

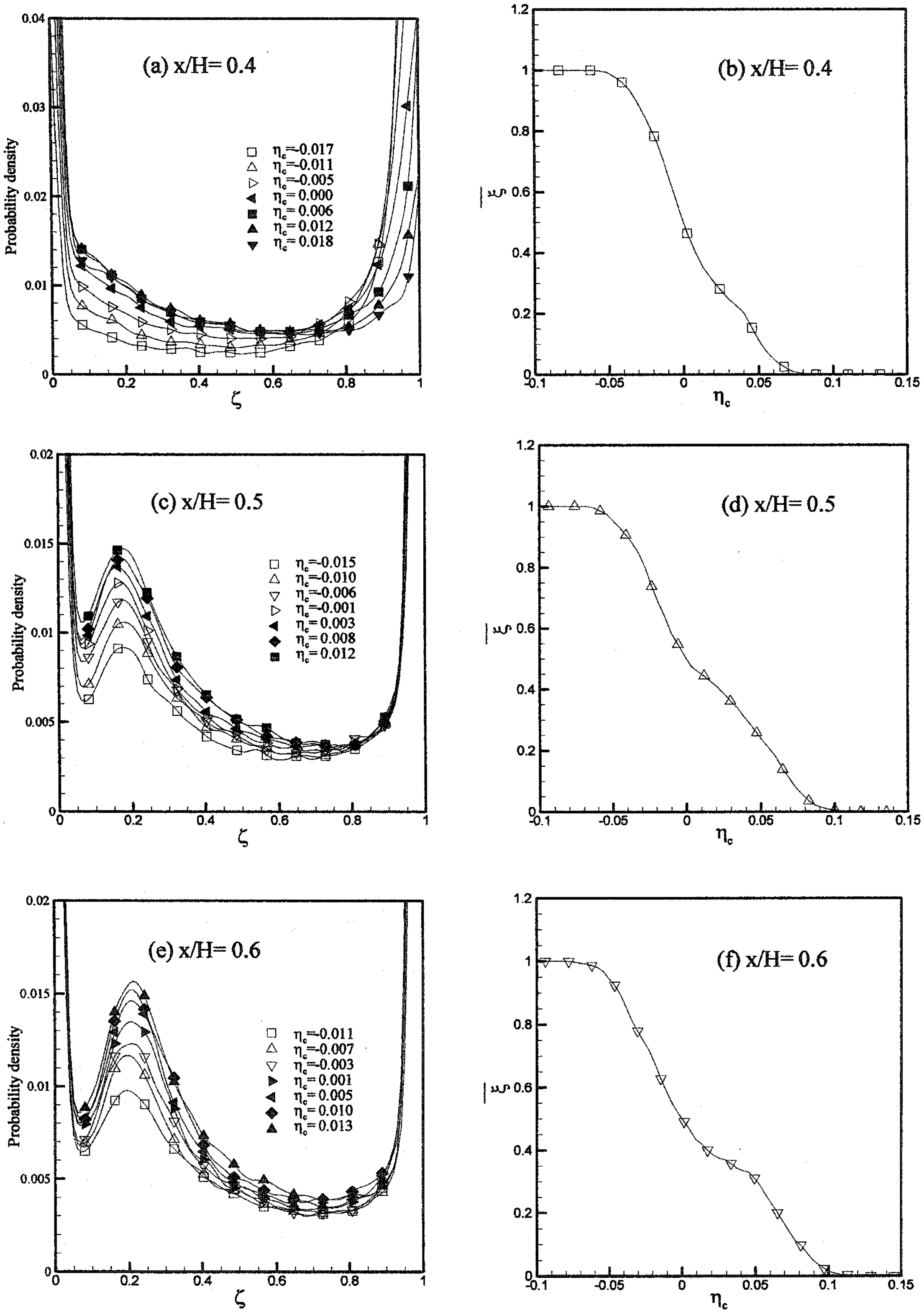

Figure 24. Probability density functions at several cross-stream locations for base run: (a) x/H=0.4, (c) x/H=0.5, (e) x/H=0.6. Mean concentration profile for base run: (b) x/H=0.4, (d) x/H=0.5, (f) x/H=0.6.

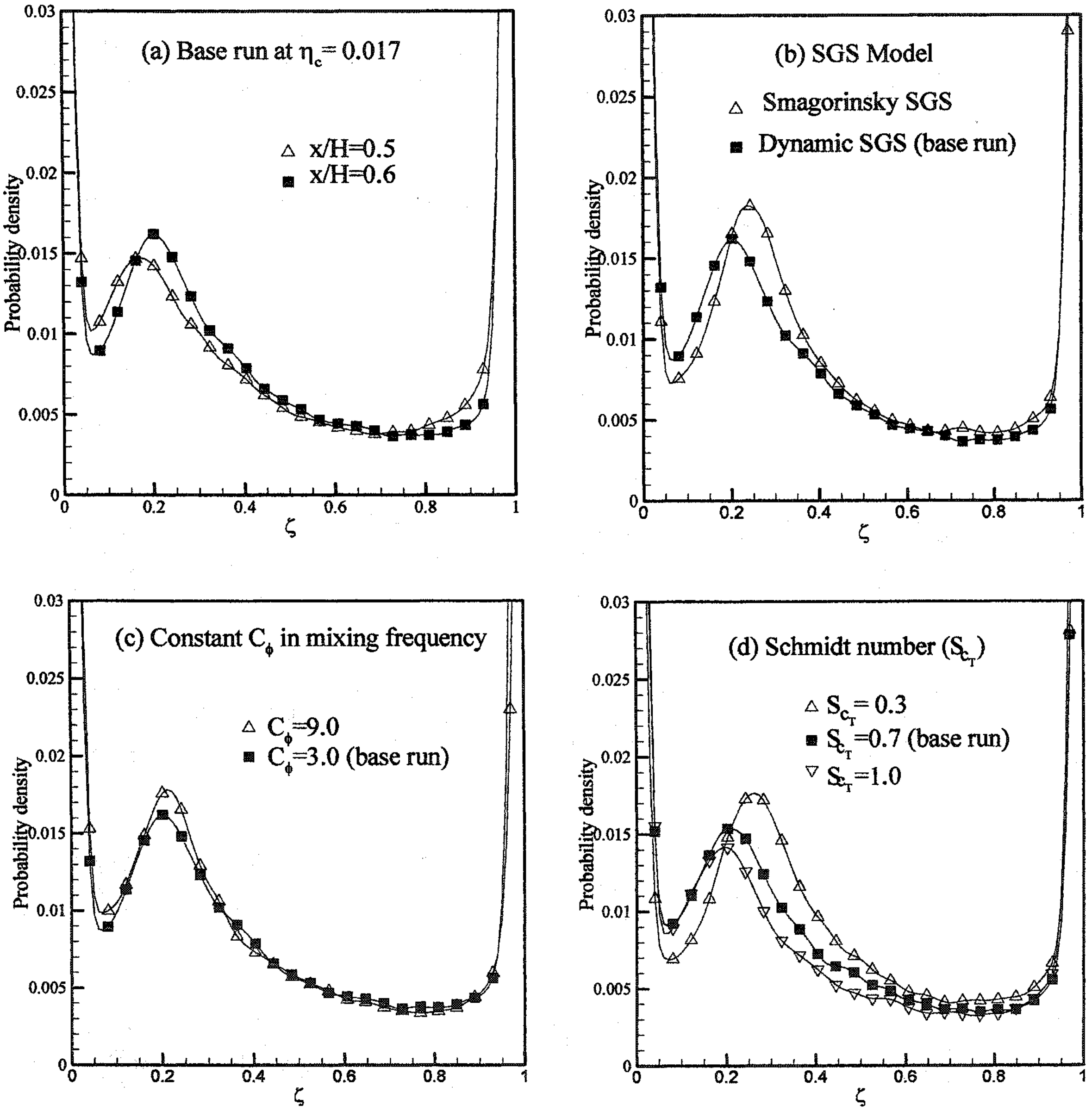

Figure 25. Comparison of probability density functions: (a) effect of downstream location, x/H=0.5 and x/H=0.6; (b) effect of SGS at x/H=0.6; (c) effect of C_ϕ at x/H=0.6; (d) effect of S_{c_T} at x/H=0.6.

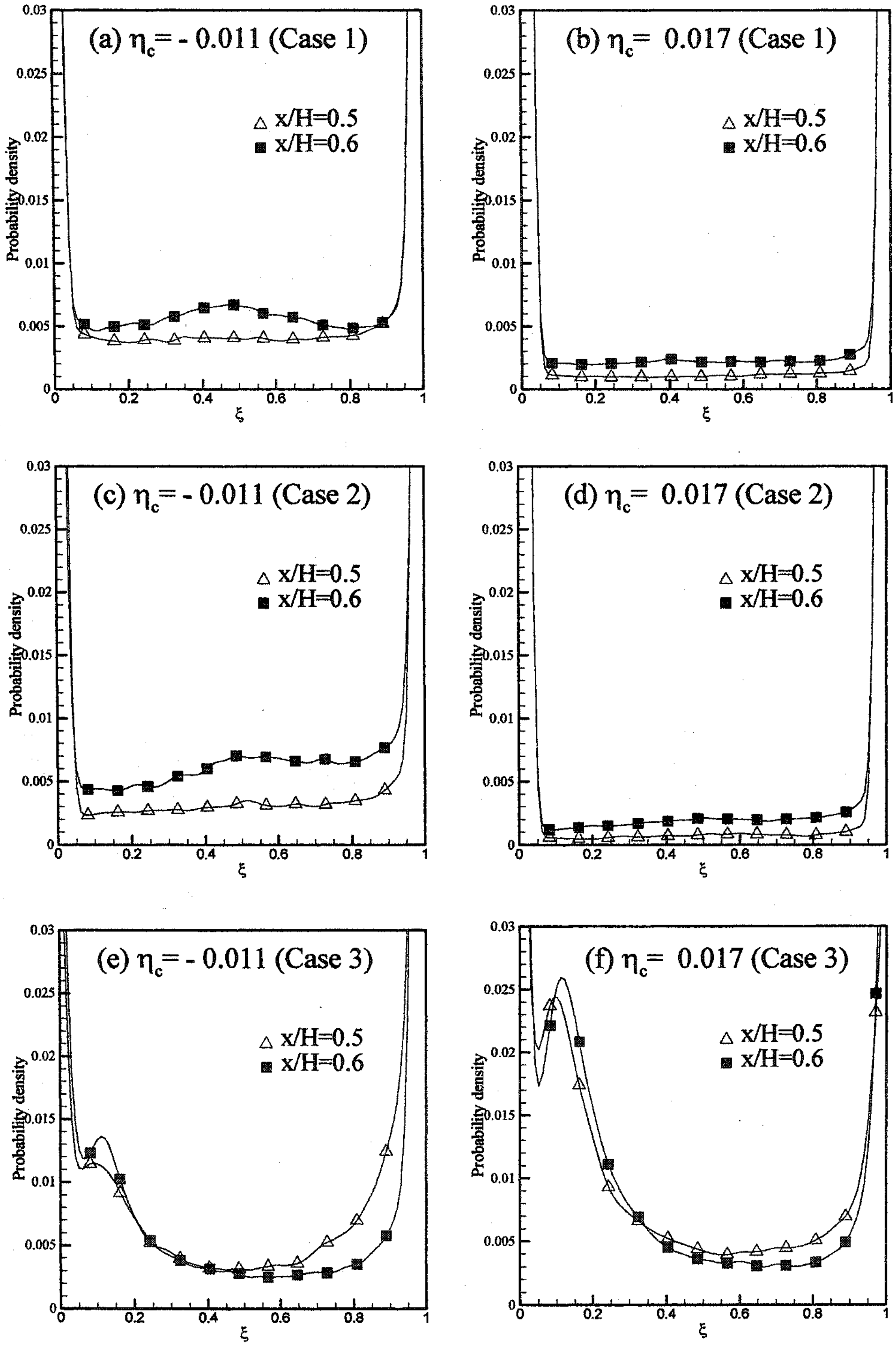

Figure 26. Effect of inlet boundary conditions on probability density functions:
(a, c, e) pdf below centerline at η_c= -0.011; (b, d, f) pdf above centerline at η_c= 0.017.
Case 1: Laminar boundary layer flow field and stepwise scalar field.
Case 2: Error function flow field and stepwise scalar field.
Case 3: Error function flow field and error function scalar field.

References

Abdolhosseini R, Milane RE. On the effect of Vortex Grid Density in the Vortex-in-Cell Simulation of Mixing Layer. International Journal of Fluid Dynamics 2000; v. 13, pp. 161-183.

Abernathy, F. H. and Kronauer, R. E. The Formation of Vortex Sheets, J. Fluid Mech.1962, v.13, pp. 1-20.

Aref, H. and Siggia, E. D. Vortex Dynamics of the Two Dimensional Turbulent Shear Layer, J. Fluid Mech.1980, 100, pp.705-737.

Ashurst, W. T. Numerical simulation of Turbulent Mixing Layer Via Vortex Dynamics, Turbulent Shear Flows I, (Ed.) Durst et al., Springer-Verlag, New York 1979, 402-413.

Baig, A. M. and Milane, R. E. Vortex-In-Cell and Probability Density Function Approach for a Passive Scalar Field in a Mixing Layer, J. Computational Fluid Dynamic. 2004, v.18(3), pp. 247-263.

Baker, G. R. The Cloud-in-Cell Technique Applied to the Roll-Up of the vortex Sheets. J. Comp. Phys.1979, vol.31, pp. 76-95.

Bardina J, Ferziger JH, Reynolds WC. Improved subgrid models for large eddy simulation. AIAA, 1980; 80-1357.

Batchelor GK. An introduction to Fluid Dynamics. Cambridge University Press 1967.

Beaudoin A, Huberson S, Rivoalen E. Simulation of anisotropic diffusion by means of a diffusion velocity method. Journal of Computational Physics 2003; 186:122-135.

Bilger, R.W., Saetran, L.R. and Krishnamoorthy, L.V. Reaction in a Scalar Mixing Layer, J. Fluid. Mech. 1991, vol. 233, pp. 211-242.

Bray, K. N. C. Equations of Turbulent Combustion I. Fundamental Equations of Reacting Turbulent Flows 1973. AASU report 330.

BRITE-EURAM project, PDF/CFD-based methods: Development and validation for low emission combustor technology. AERO-2018-P 1993-1996.

Brown, G. L. and Roshko, A. On Density Effects and Large Structure in Turbulent Mixing Layers, J. Fluid Mech. 1974, vol 57, pp. 785-796.

Chorin, A. J. Numerical Study of Slightly Viscous Flow, J. Fluid Mech. 1973, vol. 57, pp.785-796.

Chorin A.J. and Marsden, J.E. A Mathematical Introduction to Fluid Mechanics, Springer (New York) 1979.

Clarke NR, Tutty O.R. Construction and Validation of a Discrete Vortex Method for the Two-Dimensional Incompressible Navier-Stokes Equations. Computers & Fluids 1994; Vol.23, No. 6, pp. 751-783.

Colucci, P.J., Jaberi,F.A., Givi,P. and Pope, S.B. Filtered Density Function for Large Eddy Simulation of Turbulent Reacting Flows, Phys. Fluids 1998, 10(2):499-515.

Cottet GH. Artificial Viscosity Models for Vortex and Particle Methods. Journal of Computational Physics 1996; 127: 299-308.

Cottet GH, Koumoutsakos PD. Vortex methods: theory and practice. Cambridge University 2000.

Deardoff J. A numerical study of three-dimensional turbulent channel flow at large Reynolds numbers. Journal of Fluid Mechanics 1970; 41 2: 453-480.

Degond, P. and Mas-Gallic, S. The Weighted Particle Method for Convection-Diffusion Equations. Part 1: The Case of Isotropic Viscosity. Mathematics of Computation 1989, Volume 53, Issue 188, 485-507.

Dopazo C. Recent Developments in PDF Methods. Turbulent Reactive Flows 1994, Chapter 7, pp. 375-474, Academic Press.

Ghoneim AF, Givi P. Vortex-Scalar Element Calculations of a Diffusion Flame Stabilized on a Plane Mixing Layer. NASA Tech. Memo 1987. 100133 ICOMP-87-4.

Ghoneim AF, Heidarinejad G, Krishnan A. Numerical simulation of a thermally stratified shear layer using the vortex element method. Journal of Computational Physics 1988; 79: 135.

Ghoneim A F, Heidarinejad G. Effect of Two-Dimensional Shear Layer Dynamics on Mixing and Combustion at Low Heat Release. Combustion Science and Technology 1990; 72: 79-99.

Greengard C. The core spreading vortex method approximates the wrong equation. Journal of Computational Physics 1985; 61: 345-348.

Gao, F and O'Brien, E.E., A Large-Eddy Simulation Scheme for Turbulent Reacting Flows, Phys. Fluids A, 5(6), 1993; pp1282-1284

Hsu, A.T., Tsai, Y.L.P. and Raju, M.S. Probability Density Function Approach for Compressible Turbulent Reacting Flows, AIAA 1994, Vol. 32(7).

Inoue, O. and Leonard, A. Vortex Simulation of Forced/Unforced Mixing Layers, AIAA J 1987. vol. 26(11), p.1417.

Inoue, O. Double-frequency forcing on spatially growing mixing layers, J. Fluid Mech. 1992, 234, pp. 553-581.

Jaberi,F.A., Colucci, P.J., James,S., Givi,P. and Pope, S.B. Filtered Mass Density Function for Large Eddy Simulation of Turbulent Flows, J. Fluid Mech.1999, vol. 401, pp. 85-121.

Kaltenbach H-J. Cell Aspect Ratio Dependence of Anisotropy Measures for Resolved and Subgrid Scale Stresses. Journal of Computational Physics 1997; 136: 399-410.

Koochesfahani M. M., Dimotakis P.E. Mixing and Chemical Reactions in a Turbulent Liquid Mixing Layer, J.Fluid Mech. 1986, Vol. 170.83-112.

Lacombe G. and Mas-Gallic S. Presentation and analysis of a Diffusion-Velocity Method. ESAIM Proceedings 1999; Vol.7: 225-233.

Launder, B.E. Heat and Mass Transport in Turbulence (ed. P. Bradshaw), Springer 1976.

Leonard, A.Energy Cascade in Large Eddy Simulation of Turbulent Fluid Flows, Advances in Geophys 1974, 18A, pp. 237-248.

Leonard, A. Vortex methods for flow simulation, J. Comp. Phys.1980, 37, pp.289-335.

Lilly, D. K. The Representation of Small-Scale Turbulence in Numerical Simulation Experiments, Proc. IBM Sci. Comput. Symp. Environ. Sci., IBM Data Process. Div., White Plain, N.Y 1967, pp. 195-210.

Lin, P. and Pratt, D. T. Numerical Simulation of a Plane Turbulent Mixing Layer, with Applications to Isothermal, Rapid Reactions 1987, AIAA Pap. 87-0224.

Lundgren, T. S. Phys. Fluids 1969, vol12, p.485.

Mansfield JR, Knio OM, Meneveau C. A Dynamic LES Scheme for the Vorticity Transport Equation: Formulation and a Priori Tests. Journal of Computational Physics 1998; 145: 693-730.

Mansour NN, Moin P, Reynolds WC, Ferziger JH. Improved Method for Turbulence. Turb. Shear Flow I 1979; 386-401.

Masutani SM, Bowman CT. The structure of a chemically reacting plane mixing layer. Journal of Fluid Mechanics 1986; 172: 93-126.

Milane RE, Nourazar, S. On the Turbulent Diffusion Velocity in Mixing Layer Simulated Using the Vortex Method and the Subgrid Scale Vorticity Model. Mechanics Research Communication 1995; 22 4; 327-333.

Milane RE, Nourazar S. Large-Eddy Simulation of Mixing Layer using Vortex Method: Effect of Subgrid-Scale Models on early Development. Mechanics Research Communication 1997; 24 2; 215-221.

Monkewitz PA, Huerre P. Influence of the velocity ratio on the spatial instability of mixing layer. Physics of Fluids 1982; 25:7.

Möbus, H., Gerlinger, P. and Brüggeman, D. Comparison of Eulerian and Lagrangian Monte Carlo PDF Methods for Turbulent Diffusion Flame, Combustion and Flame 2001, 124:519-534.

Ogami, Y. and Akamatsu. Viscous Flow Simulation Using the Discrete Vortex Model-The Diffusion Velocity Method. Computers & Fluids 1991, Vol. 19, No. 3/4, pp. 433-441.

Ogami Y. A vortex Method for Heat-Vortex Interaction and Fast Summation Technique. First International Conference on Vortex Methods (Kobo) World Scientific 1999: 145:152.

Oster, D. and Wygnanski, I. The forced Mixing Layer Between Parallel Streams. Journal of Fluid Mechanics 1982; vol. 123, pp. 91-130.

Pickett, L.M. and Ghandhi, J.B. Passive Scalar Measurements in a planar mixing layer by PLIF of Acetone, Experiments in Fluids 2001, v. 31, pp. 309-318.

Pope, S. B. Combust. Flame 1976, vol 27, p. 299.

Pope, S. B. MIT Report EL-80-012 1980.

Pope, S. B. A Monte Carlo Method for the PDF Equations of turbulent reactive flow, Combust. Sci. Technol. 1981, v. 25, pp.159-174

Pope, S. B. PDF Methods for Turbulent Reactive Flows. Prog. Energ. Combust. Sci.1985, v.11, pp.119-192.

Pope, S.B Lagrangian PDF methods for turbulent flows, Annu. Rev. Fluid Mech. 1994, 26: 23-63.

Pope, S. B. Turbulent Flows, Cambridge Univ Press 2000.

Richardson, L.F. Weather Prediction by Numerical Process. Cambridge Univ Press (1922).

Rosenhead, L. The Formation of Vortices From Surface of Discontinuity, Proc. Roy. Soc. 1931, Series A, v.134, pp. 170-192.

Sagaut P. Large Eddy Simulation for Incompressible Flows. Scientific Computation, Springer 2002.

Sarpkaya, E. Vortex Element Methods for Flow Simulation. Advances in Applied Mathematics 1994, v.31, pp. 113-247.

Shumann U. Subgrid Scale Model for Finite Difference Simulations of Turbulent Flows in Plane Channels and Annuli. Journal of Computational Physics 1975; 18: 376-404.

Smagorinski, J., General Circulation Experiment with the Primitive Equations I, The Basic Experiment, Mon.Wether 1963, Rev. 91, pp. 99-164.

Soteriou Marios C. and Ghoniem Ahmed F., On the Effects of the Inlet Boundary Condition on the Mixing and Burning in Reacting Shear Flows, Combustion and Flame, 1998, 112: 404-417

Spencer, B.W. and Jones, B.G.. Statistical Investigation of Pressure and velocity Fields in the Turbulent Two-Stream Mixing Layer. AIAA 4th Fluid and Plasma Conf. 1971, no. 71-613.

Vanormelingen, J. and den Bulck, E. Van., 1999, Scalar Transport in plane mixing layers, Heat & Mass Transfer, v.35 n.5, pp. 383-390.

Vreman B, Geurts B, Kuerten H. Large-eddy simulation of the turbulent mixing layer. Journal of Fluid Mechanics 1997; 339: 357-390.

Zhou, X.Y. and Pereira, J.C.F. Large Eddy Simulation (2D) of a Reacting Plane Mixing Layer Using Filtered Density Function, Flow, Turbulence and Combustion 2000, 64:279-300.

Appendix

This simulation work uses one main program and two post processing programs given below:
1) **VIC_PDF.f:** This main program solves the instantaneous velocity and vorticity field using the VIC and diffusion velocity. Then the spatially resolved time averaged fields will be calculated and used as input to solve the FDF transport equation with modelled Subgrid Convective term and Mixing term using the Monte-Carlo method. Every two-residence time to write scalar statistics to new data files rms {step number}.dat, pdf {step number}.dat for scalar field.The output data files for flow field are: vorticity contours: (P4830238.dat); momentum data: (P482508.dat); rms of velocity fluctuation: (P483022B.dat); rms vorticity fluctuations:(eddy.dat) with variables U, V, ν_T, ε/k, Ω, θ, u', v', $u'v'$, $\partial U/\partial y$ and will be written out at the end of the program running.

2) **VICPP.f90:** A post-processing program for the flow field after VIC_PDF.f finishes running. It reads the flow field output data files of VIC_PDF.f, computes the similarity variable η_v, vorticity thickness, velocity spread, filters ν_T and writes data for plotting vs. η_v. The output is written to files named:(eddyC.dat), (momThickness.dat), (momSlope.dat), (MeanVel.dat), (statA.dat), (stats.dat) and (velSpread.dat).

3) **SCALAR.f90:** Post processing of the Monte-Carlo simulation for scalar field after running VICPP.f90. The program reads output data files of VIC_PDF.f and VICPP.f90, computes the similarity variable η_c, concentration spread and writes scalar statistics for plotting vs. η_c. The output is written to files named:(MeanConc.dat), (RMSConc.dat), (Mixfrequence.dat), (concSpread.dat) and (scalarPdf.dat).

Running programs in the following order.

VIC_PDF.f : To solve the instantaneous velocity and vorticity field using the VIC and diffusion velocity. Then the spatially resolved time averaged fields will be calculated and used as input to solve the FDF transport equation with modelled Subgrid Convective term and Mixing term using the Monte-Carlo method. Every two-residence time to write scalar statistics to new data files rms {step number}.dat, pdf {step number}.dat for scalar field.The output data files for flow field are: **vorticity contours**: (P4830238.dat); **momentum data**: (P482508.dat); **rms of velocity fluctuation**: (P483022B.dat); **rms vorticity fluctuations**: (eddy.dat) with variables U, V, ν_T, ε/k, Ω, θ, u', v', $u'v'$, $\partial U/\partial y$ and will be written out at the end of the program running.

VICPP.f90: To read output data files of VIC_PDF.f, computes the similarity variable η_v, vorticity thickness, velocity spread, filters ν_T and write data for plotting vs. η_v. The output is written to files named: (eddyC.dat), (momThickness.dat), (momSlope.dat), (MeanVel.dat), (stats.dat), (statsA.dat), (vortTh2.dat) and (velSpread.dat).

SCALAR.f90: To read data files of VIC_PDF.f and VICPP.f90, compute the similarity variable η_c, concentration spread and write scalar statistics for plotting vs. η_c. The output is written to files: (MeanConc.dat), (RMSConc.dat), (Mean_Flow.dat), (Mean_Scalar.dat), (concSpread.dat) and (scalarPdf.dat).

VIC PDF.f:
The main program is a numerical similarity of flow field and scalar field. (Setting for Base Run)

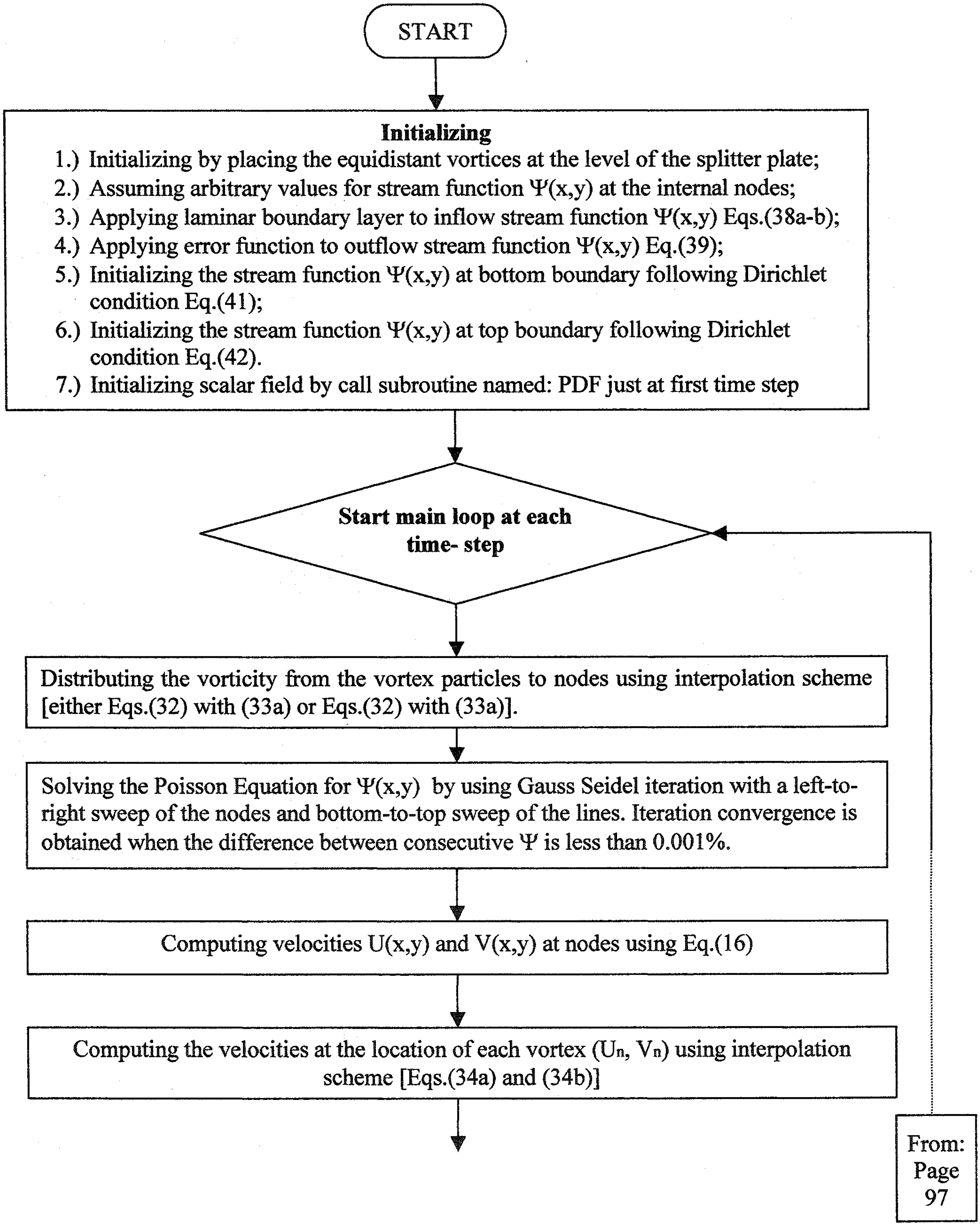

Initializing

1.) Initializing by placing the equidistant vortices at the level of the splitter plate;
2.) Assuming arbitrary values for stream function Ψ(x,y) at the internal nodes;
3.) Applying laminar boundary layer to inflow stream function Ψ(x,y) Eqs.(38a-b);
4.) Applying error function to outflow stream function Ψ(x,y) Eq.(39);
5.) Initializing the stream function Ψ(x,y) at bottom boundary following Dirichlet condition Eq.(41);
6.) Initializing the stream function Ψ(x,y) at top boundary following Dirichlet condition Eq.(42).
7.) Initializing scalar field by call subroutine named: PDF just at first time step

Start main loop at each time- step

Distributing the vorticity from the vortex particles to nodes using interpolation scheme [either Eqs.(32) with (33a) or Eqs.(32) with (33a)].

Solving the Poisson Equation for Ψ(x,y) by using Gauss Seidel iteration with a left-to-right sweep of the nodes and bottom-to-top sweep of the lines. Iteration convergence is obtained when the difference between consecutive Ψ is less than 0.001%.

Computing velocities U(x,y) and V(x,y) at nodes using Eq.(16)

Computing the velocities at the location of each vortex (U_n, V_n) using interpolation scheme [Eqs.(34a) and (34b)]

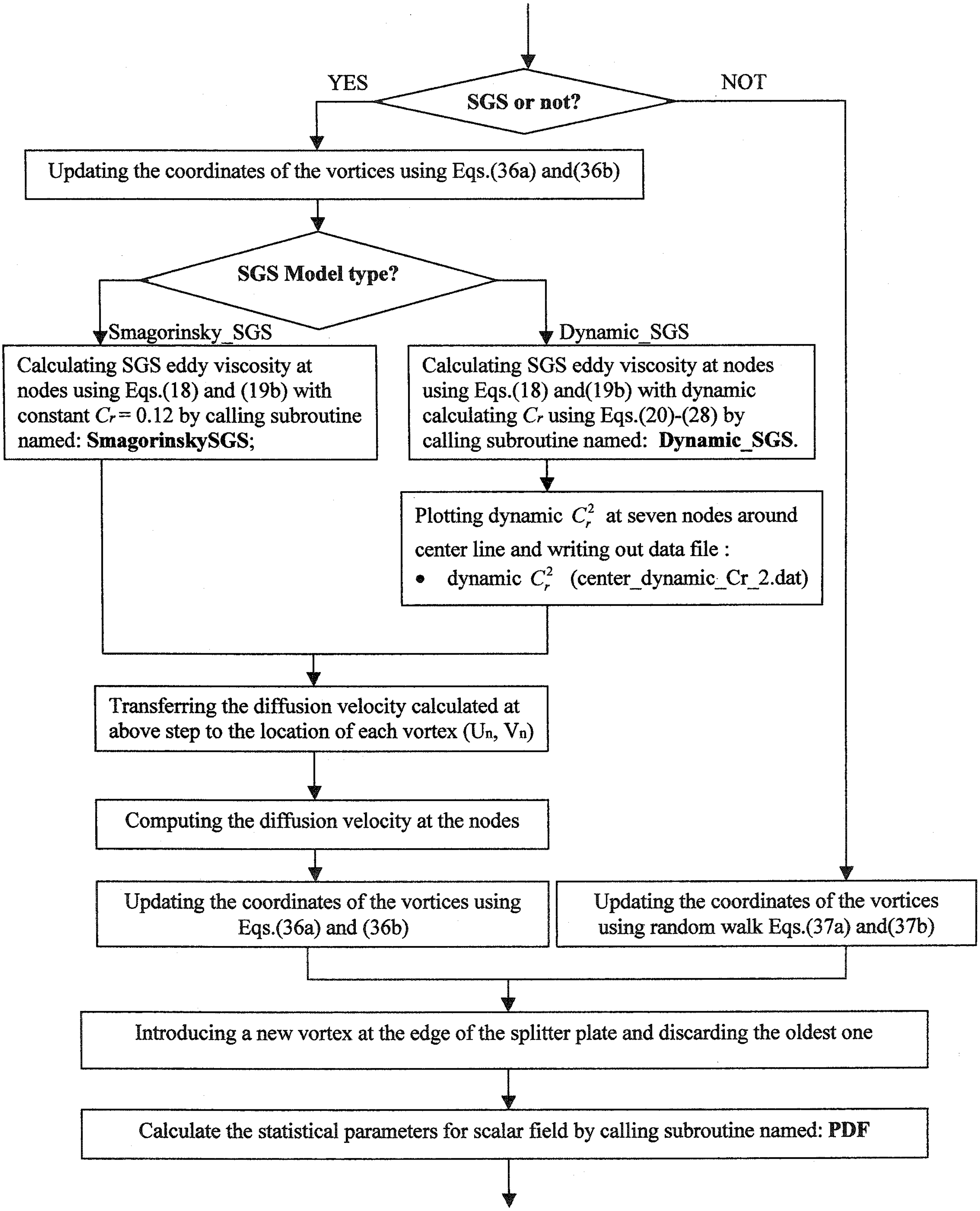
YES
SGS or not?
NOT
Updating the coordinates of the vortices using Eqs.(36a) and(36b)
SGS Model type?
Smagorinsky_SGS
Dynamic_SGS
Calculating SGS eddy viscosity at nodes using Eqs.(18) and (19b) with constant C_r = 0.12 by calling subroutine named: **SmagorinskySGS**;
Calculating SGS eddy viscosity at nodes using Eqs.(18) and(19b) with dynamic calculating C_r using Eqs.(20)-(28) by calling subroutine named: **Dynamic_SGS**.
Plotting dynamic C_r^2 at seven nodes around center line and writing out data file :
• dynamic C_r^2 (center_dynamic_Cr_2.dat)
Transferring the diffusion velocity calculated at above step to the location of each vortex (U_n, V_n)
Computing the diffusion velocity at the nodes
Updating the coordinates of the vortices using Eqs.(36a) and (36b)
Updating the coordinates of the vortices using random walk Eqs.(37a) and(37b)
Introducing a new vortex at the edge of the splitter plate and discarding the oldest one
Calculate the statistical parameters for scalar field by calling subroutine named: **PDF**

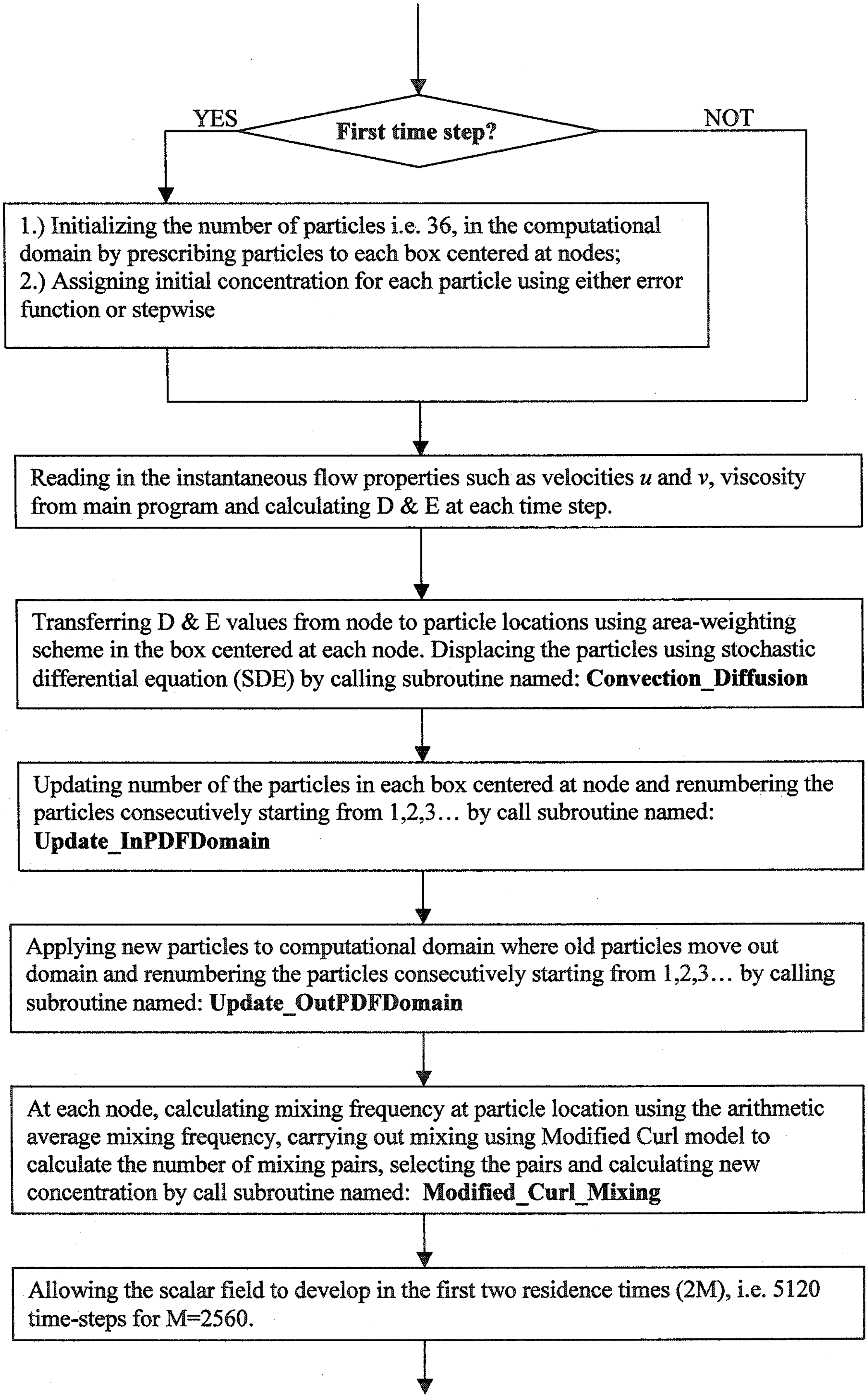

1.) Initializing the number of particles i.e. 36, in the computational domain by prescribing particles to each box centered at nodes;
2.) Assigning initial concentration for each particle using either error function or stepwise

Reading in the instantaneous flow properties such as velocities *u* and *v*, viscosity from main program and calculating D & E at each time step.

Transferring D & E values from node to particle locations using area-weighting scheme in the box centered at each node. Displacing the particles using stochastic differential equation (SDE) by calling subroutine named: **Convection_Diffusion**

Updating number of the particles in each box centered at node and renumbering the particles consecutively starting from 1,2,3… by call subroutine named: **Update_InPDFDomain**

Applying new particles to computational domain where old particles move out domain and renumbering the particles consecutively starting from 1,2,3… by calling subroutine named: **Update_OutPDFDomain**

At each node, calculating mixing frequency at particle location using the arithmetic average mixing frequency, carrying out mixing using Modified Curl model to calculate the number of mixing pairs, selecting the pairs and calculating new concentration by call subroutine named: **Modified_Curl_Mixing**

Allowing the scalar field to develop in the first two residence times (2M), i.e. 5120 time-steps for M=2560.

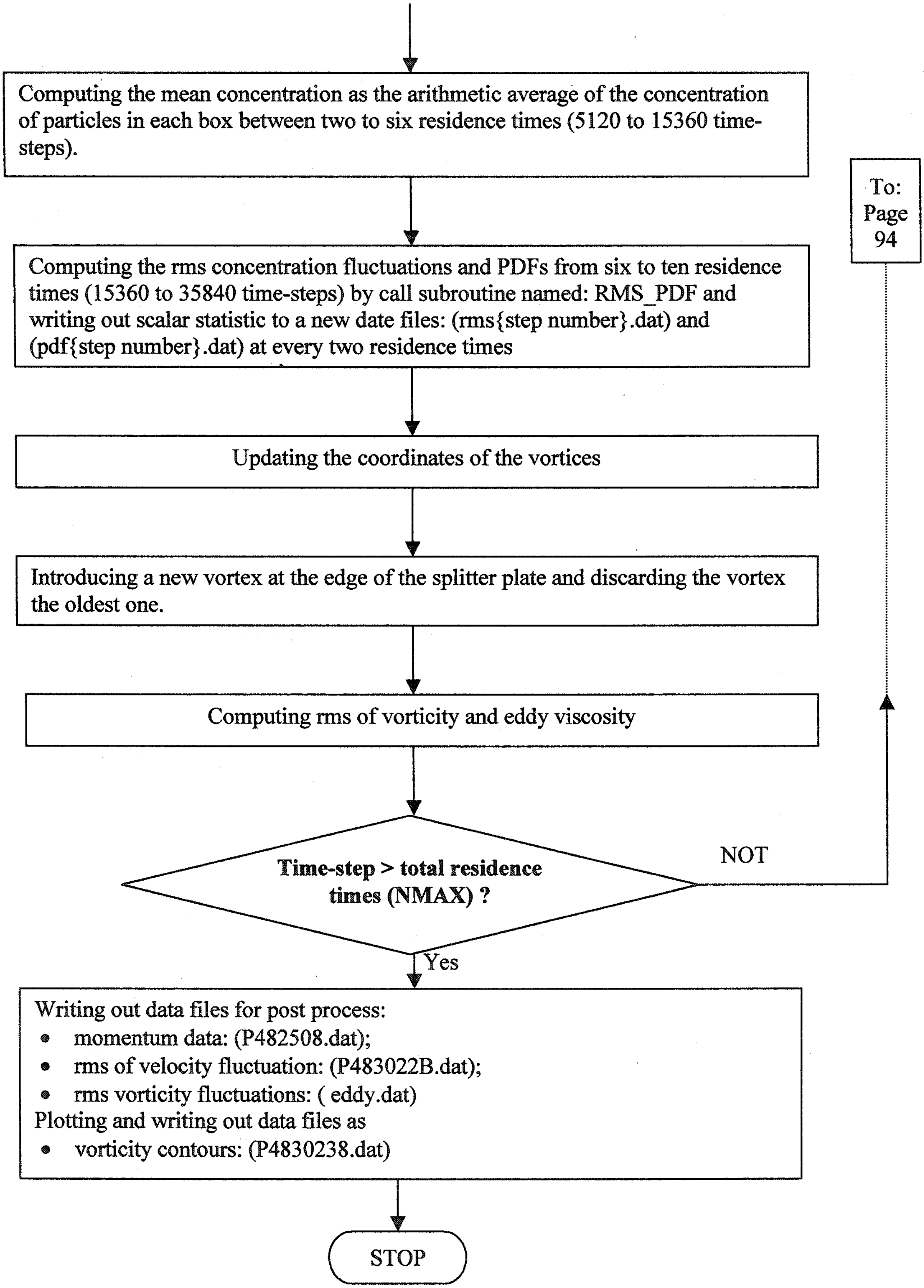

Computing the mean concentration as the arithmetic average of the concentration of particles in each box between two to six residence times (5120 to 15360 time-steps).

Computing the rms concentration fluctuations and PDFs from six to ten residence times (15360 to 35840 time-steps) by call subroutine named: RMS_PDF and writing out scalar statistic to a new date files: (rms{step number}.dat) and (pdf{step number}.dat) at every two residence times

Updating the coordinates of the vortices

Introducing a new vortex at the edge of the splitter plate and discarding the vortex the oldest one.

Computing rms of vorticity and eddy viscosity

Time-step > total residence times (NMAX) ?

Writing out data files for post process:
- momentum data: (P482508.dat);
- rms of velocity fluctuation: (P483022B.dat);
- rms vorticity fluctuations: (eddy.dat)

Plotting and writing out data files as
- vorticity contours: (P4830238.dat)

VICPP.f90:
The program post processes the output data from program VIC_PDF.f for flow field, calculates the similarity variable η_v and vorticity thickness and writes out data for plot.

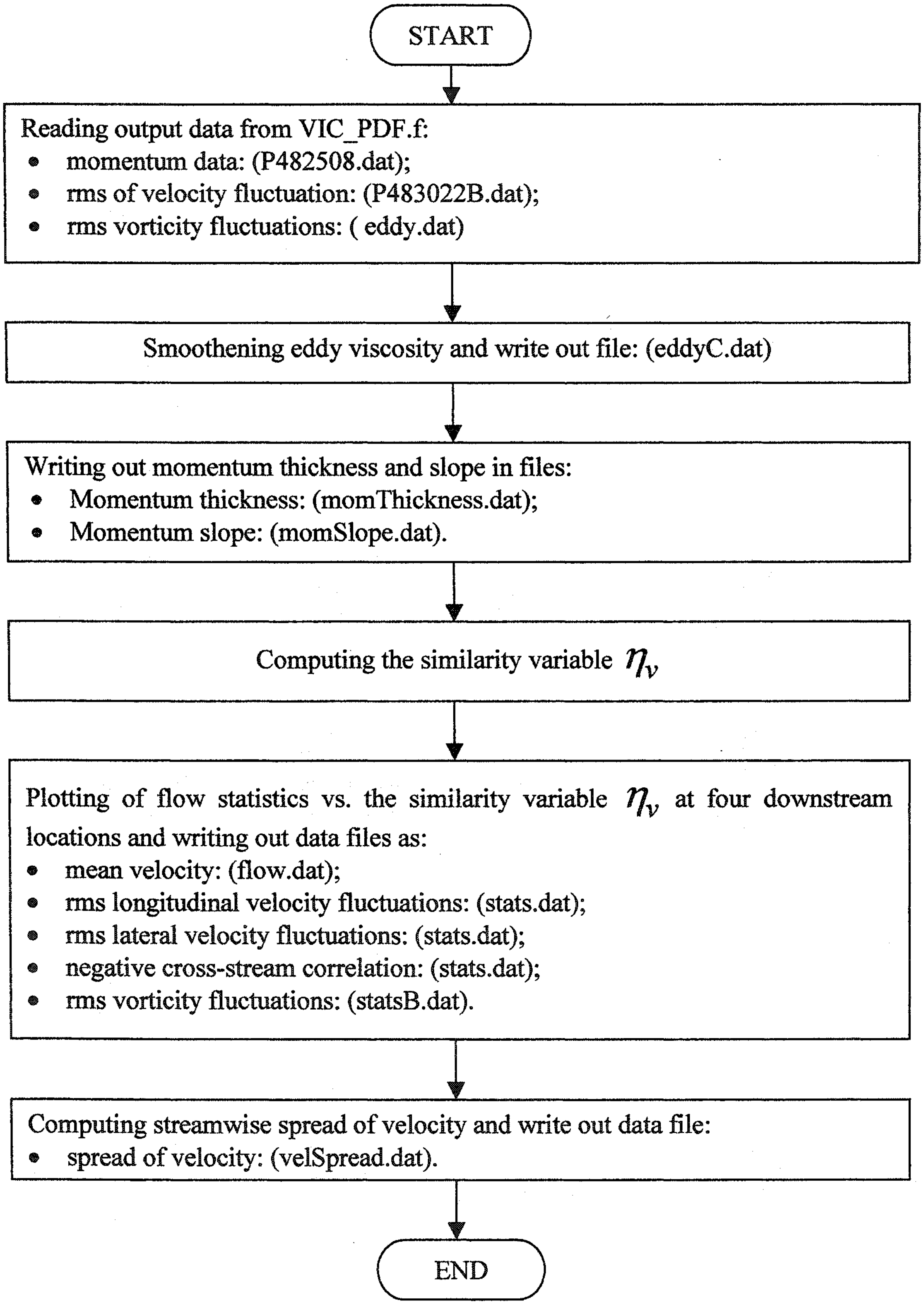

Reading output data from VIC_PDF.f:

- momentum data: (P482508.dat);
- rms of velocity fluctuation: (P483022B.dat);
- rms vorticity fluctuations: (eddy.dat)

Smoothening eddy viscosity and write out file: (eddyC.dat)

Writing out momentum thickness and slope in files:

- Momentum thickness: (momThickness.dat);
- Momentum slope: (momSlope.dat).

Computing the similarity variable η_v

Plotting of flow statistics vs. the similarity variable η_v at four downstream locations and writing out data files as:

- mean velocity: (flow.dat);
- rms longitudinal velocity fluctuations: (stats.dat);
- rms lateral velocity fluctuations: (stats.dat);
- negative cross-stream correlation: (stats.dat);
- rms vorticity fluctuations: (statsB.dat).

Computing streamwise spread of velocity and write out data file:

- spread of velocity: (velSpread.dat).

SCALARPP.f90:

The program post processes the output data from program VIC_PDF.f for scalar field, calculates the similarity variable η_c and writes out data for plot.

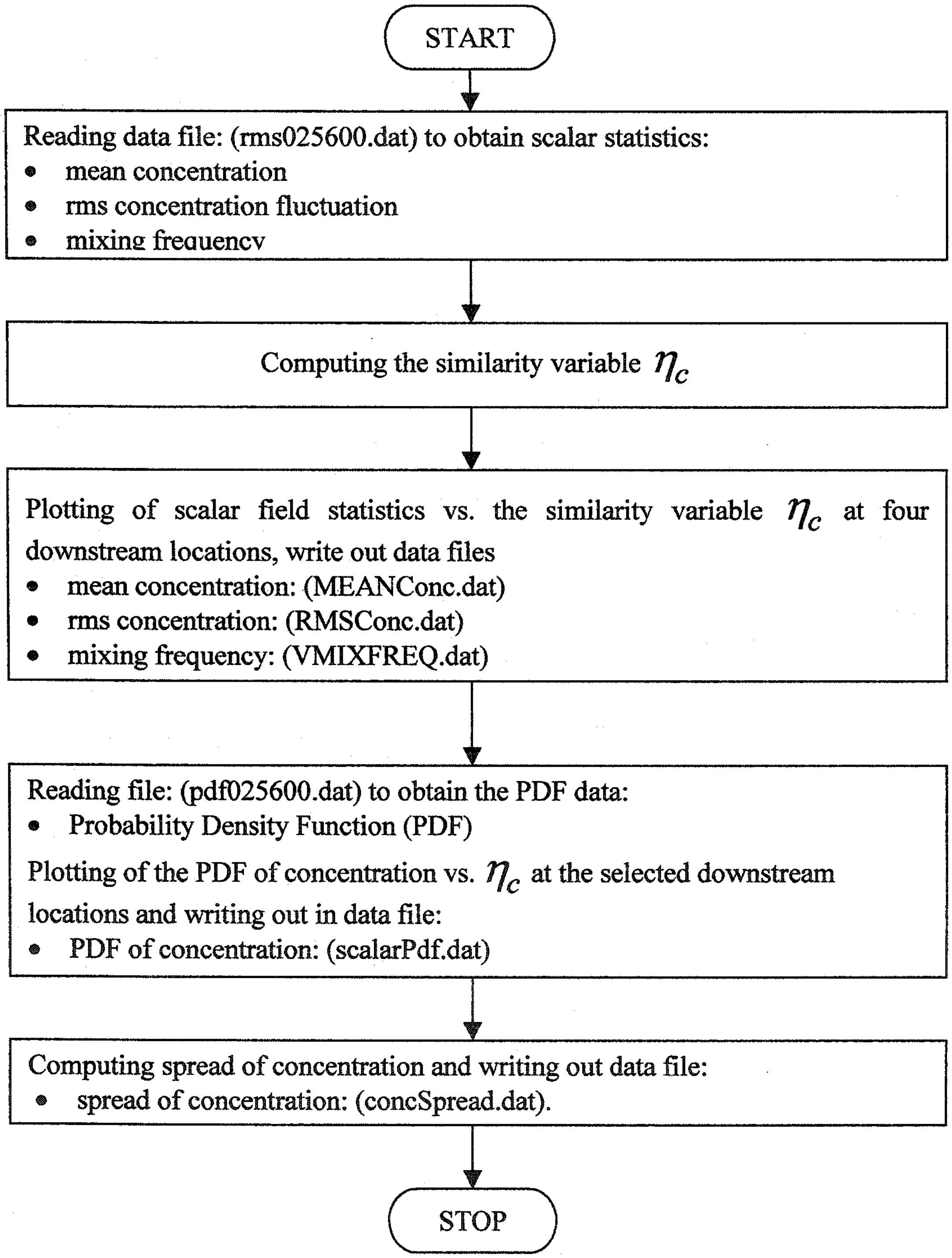

START

Reading data file: (rms025600.dat) to obtain scalar statistics:
- mean concentration
- rms concentration fluctuation
- mixing frequency

Computing the similarity variable η_c

Plotting of scalar field statistics vs. the similarity variable η_c at four downstream locations, write out data files
- mean concentration: (MEANConc.dat)
- rms concentration: (RMSConc.dat)
- mixing frequency: (VMIXFREQ.dat)

Reading file: (pdf025600.dat) to obtain the PDF data:
- Probability Density Function (PDF)

Plotting of the PDF of concentration vs. η_c at the selected downstream locations and writing out in data file:
- PDF of concentration: (scalarPdf.dat)

Computing spread of concentration and writing out data file:
- spread of concentration: (concSpread.dat).

STOP